Mathematical modelling of the cardiovascular system to study the effects of respiratory sinus arrhythmia and heart failure

Shumaila Noreen

School of Natural and Computational Sciences
Massey University

This dissertation is submitted for the degree of
Doctor of Philosophy

November 2021

I would like to dedicate this thesis to my loving family: my mother, my husband, Khadija, Hania and Abubakar.

Acknowledgements

In the name of Allah, the Most Gracious, the Most Merciful.
This project would not have been possible without the help and support of many people. Here I want to acknowledge them appreciatively.

First and foremost I would like to thank my research supervisor, Associate Professor Alona Ben-Tal for her four years of support, thoughtful guidance and cooperation. Her dedication to work, honesty and integrity are truly inspiring. Her expertise was invaluable in formulating the research questions and methodology. Her brilliant comments, scholarly advice and scientific approach have helped me to a very great extent through all stages of writing this thesis. I must also pay tribute to her high quality of supervision. I can remember many times when I felt discouraged and unsure about the worth of my own work, it was she who never failed to offer advice and encouragement.

Also, I greatly appreciate my co-supervisors Associate Professor Winston Sweatman and Rohit Ramchandra for their great feedback, excellent encouragement and guidance. Winston has helped me throughout this research project. I am extremely grateful to him for his constructive remarks, analytical approach and providing advice regarding analysis and formulation during our meetings. Thanks to Rohit for responding to my questions and queries so promptly, for providing experimental data and giving valuable suggestions from a physiology perspective. Thanks a lot to you both.

I gratefully acknowledge the New Zealand research health council and Massey University for awarding me an excellent opportunity to do this wonderful PhD project, providing me with financial means to complete this degree. My sincere thanks also goes to Professor Dianne Brunton, Head of School of Natural and Computational Sciences, for providing access to facilities that ensured successful completion of my work.

I am grateful to Maja Elstad, Associate Professor, Institute of Basic Medical Sciences, University of Oslo, for making her experimental data available to us and for providing feedback on our work along the way.

I owe my gratitude to my office-mates in the laboratory, it was a wonderful experience to share an office with such collaborative and helpful people. Satwinder's computer's skills are outstanding and invaluable. He never tired of answering my programming questions,

and he never hesitated to assist and guide me whenever I needed. Preeti Cowan's tenure in our laboratory had many lasting effects. Appreciatively, I continue to seek her advice on technical and non-technical matters.

I would like to pay my special regards to Annette Warbrooke, Linh Mills and Freda Mickisch for their administrative support over the years. I also wish to show my gratitude to Anil Malhotra, System Manager, School of Natural and Computational Sciences, Massey University, for his immense support and huge help during this project.

I would like to express my special thanks to my friends Rahila Umar, Ayesha Shaukat, Amna Farrukh, Sidra Zafar, Neelum Bashir, Faheem Zaidi and Nabila Zaidi for their boundless support and help over the years. Without their presence my life in New Zealand would have been difficult as they were the best advisors and counsellors for me. The good time spent with them can never be erased from my memories.

I would like to express my gratitude to the Principal and staff members of the Albany Primary School who continued their services during covid-19 period for the children of the essential workers. Due to this coordination, I managed to complete a large fraction of my work during this "Stay home Stay Safe" period.

Last but not least, my biggest thanks to my family: my mother, my husband and my kids; Khadija, Hania and Abubakar for supporting me spiritually throughout writing this thesis and my life in general.

Abstract

This thesis presents the development of lumped parameter models of the cardiovascular system with a specific aim of simulating the system dynamics over a range of heart rates. The models contain several new modelling features that have been introduced progressively throughout the thesis starting with isolated models and continuing with closed loop models of the circulation. Specifically, the contraction of the cardiac chambers is modelled using a time-dependent muscle force with constant elasticity instead of time dependent elasticity. A new hypothesis about the mechanical contraction of the atria generates realistic pressure volume loops. The inter-ventricular interaction is modelled as well. Additionally, hysteresis is incorporated in the aortic valve to produce an end-systolic reverse (negative) flow. Most of the model parameters were taken from the literature and experimental data. Sensitivity analysis was performed on one of the models outputs by changing one parameter at a time; this analysis indicated that the total blood volume is the most influential parameter in the model.

The developed models were used to study the effects of Respiratory Sinus Arrhythmia (RSA), a variability in heart rate at the frequency of breathing. RSA is an indicator of good health but the mechanism that gives rise to RSA and its function are still debatable. Two potential sources of RSA were incorporated: periodic heart rate that mimics the central regulation of heart rate which originates in the brainstem, and periodic systemic veins resistance that mimics one possible effect of the pleural pressure which drives breathing. The effects of RSA on cardiac output were then studied. The simulations suggest that the mean cardiac output does not change significantly due to RSA at either low or high heart rates.

Two types of heart failure were simulated using the new models by changing certain model parameters: systolic and diastolic. Both the systolic and diastolic heart failures caused an accumulation of blood in the lungs. The ejection fraction for diastolic heart failure remained within the normal physiological range while in the case of systolic heart failure the ejection fraction reduced rapidly. These results are consistent with physiological observations.

Table of contents

List of figures

List of tables

List of Abbreviations

AV node	Atrio-ventricular node
BF	Breathing frequency
bpm	beats per minute
breaths/m	Breaths per minute
DHF	Diastolic heart failure
ECG	Electrocardiogram
EDV	End diastolic volume
EF	Ejection fraction
ET	Ejection time
HF	Heart failure
HR	Heart rate
L/min	Liter per minute
ml	Milliliter
mmHg	millimeters of mercury
PV	Pressure volume
RSA	Respiratory sinus arrhythmia
SA node	Sinoatrial node
sec	Seconds

SHF	Systolic heart failure
SV	Stroke volume

Chapter 1

Introduction

The mathematical modelling and numerical simulations of the cardiovascular system have been the focus of many investigations in the past. Respiratory sinus arrhythmia (RSA) is a beneficial oscillation of heart rate at the frequency of breathing. There are a number of hypotheses related to the effects of RSA that are still under consideration. A model that can simulate the dynamics of the cardiovascular system over a range of heart rates is needed to study the functions and mechanism of this phenomenon.

In this chapter, we first provide some physiological background of the cardiovascular system, blood circulation and electrocardiogram (ECG). Then we review the current literature on the mathematical modelling of the cardiovascular system.

1.1 Physiological background

The basic tasks of the cardiovascular system are to provide oxygen and other nutrients to the body and, at the same time, remove the metabolic wastes. In order to fulfill these tasks the blood is pumped by the heart through two vascular circuits: the pulmonary circulation that transfers blood through the lungs and the systemic circulation that transports blood through the rest of the body (Batzel et al., 2007).

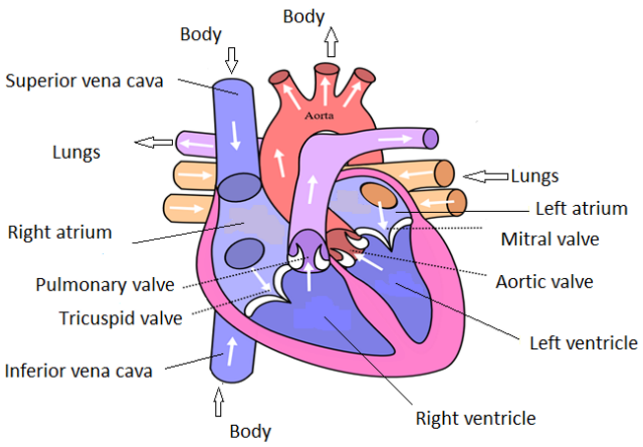

Fig. 1.1 Heart chambers, valves and heart vessels. White arrows represent the direction of blood flow. https://en.wikipedia.org/wiki/Heart (Re-used under a creative commons Attribution-ShareAlike License).

The heart consists of four chambers and all four chambers are connected to the circulatory system: the left ventricle through the aorta, the right ventricle through the pulmonary artery, the left atrium through the pulmonary veins and the right atrium through the superior and inferior vena cavae. The heart acts as a pump in the circulatory system to pump blood continuously throughout the body. The left atrium receives oxygenated blood from the lungs and transports it into the left ventricle through the mitral valve. The left ventricle pumps the blood into the aorta, the largest vessel of the arterial tree which distributes the blood flow to the whole body. The aorta further splits into many branches, arteries, arterioles and ultimately capillaries. In the capillaries, the oxygen and other nutrients in the blood are delivered to body cells and are exchanged with carbon dioxide and other waste products. This de-oxygenated blood now travels from the capillary region and enters into venules, veins and finally reaches the right atrium. From the right atrium it goes to the right ventricle through the tricuspid valve. The right ventricle pumps the blood into the pulmonary artery, which further splits into smaller arteries throughout the lungs, until it reaches the capillary region. In the capillaries, CO_2 is exchanged with O_2 by diffusion. The blood, now, enriched with O_2 flows through the pulmonary veins to the left atrium. This is how the blood completes one cycle of its journey (Formaggia et al., 2010, Batzel et al., 2007). Besides the mitral and tricuspid valves, there are two other valves at the end of each ventricle; the pulmonary valve is located at the base of the pulmonary artery and the aortic valve is at the base of the aorta. The mechanisms of these valves are similar to that of the mitral and tricuspid valves,

that is, they open when the pressure in the ventricles is higher than in the associated artery (Formaggia et al., 2010).

There are two phases of the heart cycle, systole (contraction) and diastole (relaxation), see Figure 1.2. A systole starts with the contraction of the heart muscle. As a result the pressure in the left ventricle rises and the tricuspid valve is closed. As long as the pressure in the left ventricle is lower than the pressure in the aorta the aortic valve is closed. Since during this phase the volume in the left ventricle is not changing, this phase is called isovolumetric contraction. When the left ventricle pressure exceeds the pressure in the artery (about 80 mmHg) the aortic valve opens and ejection starts. The pressure in the ventricle starts to increase during the ejection phase (up to 120 mmHg). When systole is ended the heart muscle starts to relax and that results in a rapid decrease in the left ventricle pressure. When the left ventricular pressure is lower than the arterial pressure, the aortic valve closes and diastole starts.

The first phase of the diastole is the isovolumetric relaxation of the heart muscle. The pressure in the left ventricle decreases until it reaches the pressure in the atria (about 5 mmHg) and the mitral valve opens. While the pressure in the left ventricle is lower than the pressure in the left atrium, blood flows into the left ventricle. When the heart muscle starts to contract the diastole is ended and the pressure in the left ventricle increases and becomes higher than the pressure in the left atrium and the mitral valve closes. All these occur in the right heart too, but the pressure values in the right heart are smaller (Batzel et al., 2007).

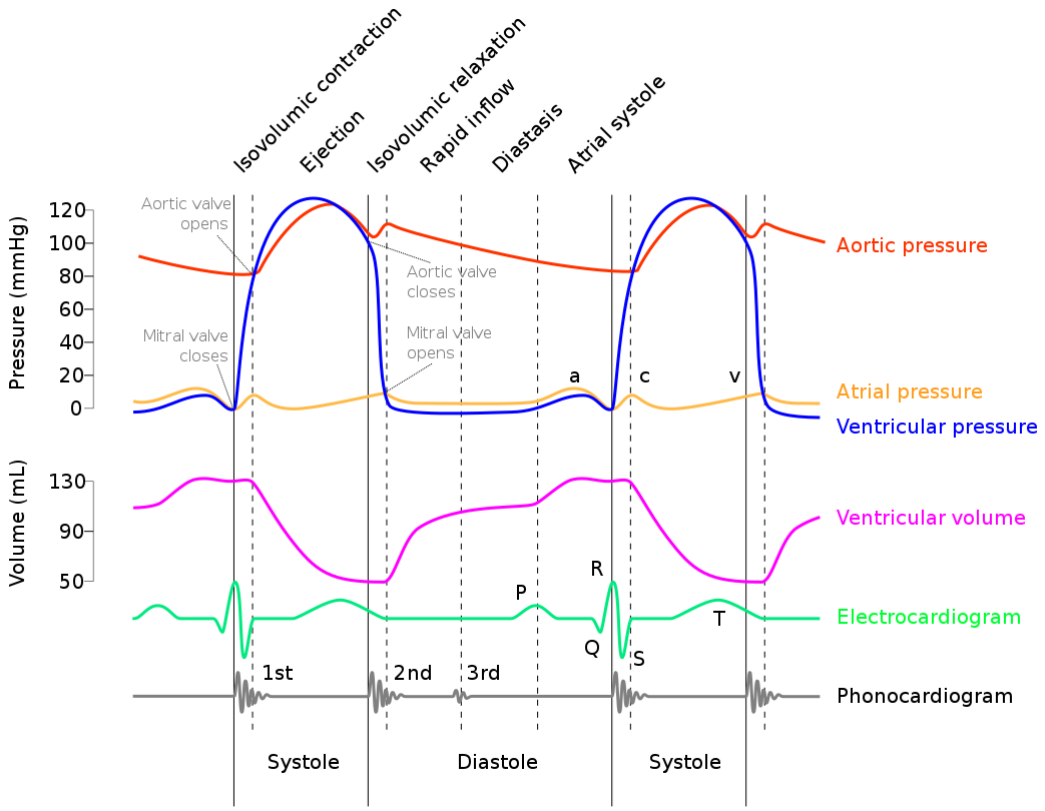

Fig. 1.2 Events of the cardiac cycle, showing changes in pressures for the left ventricle, left atrium and in the aorta, the ventricular volume, the ECG, and the phonocardiogram (Hall, 2015). ©2016 Elsevier, Inc. Re-used with permission from Elsevier by "automatic process".

We next discuss the electrical activation of the heart.

1.2 Electrocardiogram (ECG)

An electrocardiogram (ECG or EKG) is the electrical visual activity of the heart. With each beat, an electric impulse travels through the heart. This wave squeezes the heart muscles and pumps blood from the heart. A normal heartbeat on ECG shows the timings of the electrical activity of the atria and the ventricles. To record this activity different electrodes are placed on the body. Depending on the positioning of these electrodes different recordings of ECG are obtained. A normal ECG of a sheep for two beats is shown in Figure 1.3.

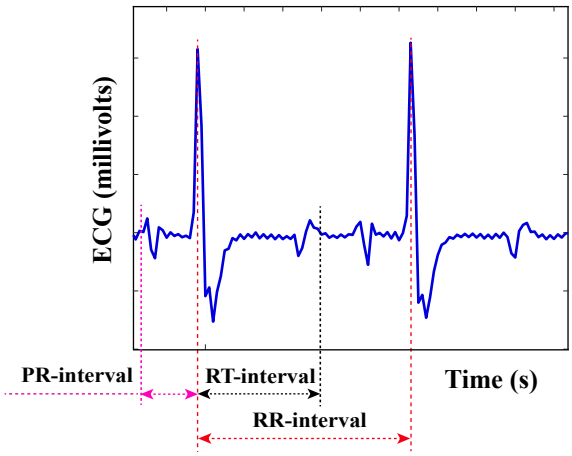

Fig. 1.3 ECG of a sheep showing two heart periods. The RR-interval is marked between two consecutive peaks of R-waves and the RT-interval starts from the beginning of the R-wave and finishes at the end of the T-wave. The PR-interval starts from the beginning of the P-wave and ends at the R-wave.

A normal ECG consists of a P-wave, QRS-complex and T-wave. The QRS-complex often, but not always, contains three separate waves: the Q, the R and the S. The electrical signals are initiated from the Sinoatrial node or SA node, which is a group of cells located in the wall of the right atrium of the heart. Unlike other cells of the body, these cells are unique as they have the ability to generate an electric impulse all by themselves, that travels through the heart. The SA node is known as the natural pacemaker of the heart. The electrical impulse from the SA node first reaches the atria and causes them to contract, this event can be seen in the ECG by the first positive deflection and it is denoted as a P-wave. From the atria, the signal goes down to another node called the Atrioventricular node or AV node. The AV node is located at the base of the left atrium close to the start of the ventricle tissue. It briefly slows down the electric signal, giving the ventricles time to receive blood from the atria. This delay can be seen by the PR-interval on the ECG. Thus, the PR-interval is the time from the onset of the P-wave to the start of the QRS-complex. From the AV node the signal moves to the Bundle of HIS, this Bundle then splits into left and right Bundle branches which run along the inter ventricular septum. The left bundle branch further splits into tiny fibers known as Pukinje fibers. Purkinje fibers spread the electric signal in all directions through the ventricles, causing the ventricles to contract. This event is recorded in the ECG by the length of the QRS-complex which is the time from the start of the Q wave to the end of the S wave and it represents the spread of electrical activity in the heart. This is followed by contraction. During this time, the atria also begin to relax, however the ECG signals of atrial relaxation are lost because the QRS-complex dominates. The time when ventricles begin to

relax is recorded on the ECG by the T-wave - the positive deflection after the QRS-complex (Hall, 2015).

In this thesis, we need ECG measurements to extract timings of the atrial and ventricular contraction and delay to use as our model inputs. We will use values of the RT-interval (the time from start of the R-wave to end of the T-wave) and PR-interval in our models. We will describe in detail in Chapter 4 how we extract the key time intervals from the ECG measurements. These timings are important when we simulate RSA in which the R-R interval on an ECG is shortened during inspiration and prolonged during expiration. We next discuss RSA and review its current literature.

1.3 Respiratory Sinus Arrhythmia (RSA)

An optimally-functioning heart is of primary importance for the well-being of the entire organism. Factors affecting the heart rate have been studied by many researchers but many questions are still unanswered. RSA is a variability in HR at the frequency of respiration, where the heart rate increases during inspiration and decreases during expiration. The presence of strong RSA corresponds to a healthy cardiac system. While RSA is very much weaker in individuals whose conditions have been complicated by various cardiovascular diseases.

The physiological functions of RSA and its mechanism have been studied previously (Paton et al., 2006, Taha et al., 1995, Anrep et al., 1936) but the physiological significance of RSA is still debatable. Ben-Tal et al. (2012) conducted a theoretical study of the physiological significance of RSA by formulating an optimization problem and by numerical simulations of simplified models of gas exchange. This study supported the hypothesis that RSA minimizes the work done by the heart while maintaining a desired average partial pressure of CO_2. This study also tested a previous hypothesis suggested by Hayano et al. (1996) that RSA improves gas exchange efficiency but found that although gas exchange efficiency improved with slow and deep breathing, this was unrelated to RSA. However, this model did not include any feedback mechanism of the cardio-respiratory system, and numerical simulations were performed by pre-setting the heart rate variations.

In further studies (Ben-Tal et al., 2014), a model of autonomic heart-rate control was presented, resulting in the natural appearance of RSA. This model was capable of reproducing a wide range of physiological observations and provided several predictions. It confirmed the hypothesis that RSA minimizes the work done by the heart while maintaining arterial CO_2. But this new hypothesis still needs more verification by mathematical models that take more detailed models of the heart into account, as well as by further animal experimental studies.

Another suggested physiological function of RSA is that it stabilizes the arterial blood pressure. Toska and Eriksen (1993) showed that RSA reduces fluctuations in the mean arterial blood pressure. Another study (Taylor and Eckberg, 1996) suggested that elimination of RSA reduces fluctuations in the systolic blood pressure while supine, but not during head-up tilt. Another study by Tan and Taylor (2010) has shown that RSA can dampen oscillations in mean arterial blood pressure but not in the systolic or diastolic blood pressure. Stabilization of the systemic blood flow is another benefit of RSA that has been proposed. The irregular breathing creates large pressure changes intrathoracically, which are transmitted to the heart and affect the ventricular filling and ejection. If there is no stabilizing factor, these fluctuations can transfer to the systemic blood flow and may cause end organ damage. Elstad et al. (2018) stated two hypotheses, that RSA has the capacity to dampen the variability in the systemic blood flow as well as reduce the work done by the heart while maintaining physiological levels of CO_2, are more convincing. However, more mathematical and computational models are needed for better understanding of the presumed role of RSA.

1.4 Mathematical modelling of the cardiovascular system

The cardiovascular system can be modelled using different approaches. The selection of the appropriate model dimension, from 0D to 3D, depends on the modelling goals and assumptions of the research study. Three-dimensional models are needed if detailed information on blood flow in a particular region is required (see for example, Aoki et al. (1987), Freudenberg et al. (2000) and Trunk et al. (2007)). The main disadvantage of these models is the high computational cost and time-consuming numerical simulations. On the other hand, most of the two-dimensional models are homogeneous models aiming at modelling activation propagation in a small patch of cardiac tissue (see for example, Azzayani (2020) and Zimik and Pandit (2017)). One-dimensional models are well balanced between complexity and computational cost, thus they are very suitable for many biomedical applications (see for example, Yin et al. (2019) and Abdullateef et al. (2018)). In 0-D or lumped parameter models, different parts of the system are lumped into compartments. The 0-D models are governed by systems of ordinary differential equations and are suitable for the assessment of the global distribution of pressures, blood volumes and blood flows (Malatos et al., 2016, Balakrishnan et al., 2014, Shi et al., 2011).

Pioneering work in modelling the cardiovascular and the respiratory systems was done by Grodins (1959) and Guyton et al. (1972). Many of the cardiovascular system models that have been developed since are modifications or extensions of the Grodin's compartment model (Williams et al., 2013, Jung and Lee, 2006, Olufsen et al., 2004, Kappel and Peer,

1993).

Many mathematical models have been developed to see the reaction of the ergometric workload (a short cycle test on an apparatus to predict maximal workload and maximal oxygen uptake) imposed on the cardiovascular / cardio-respiratory system. Kappel and Peer (1993) developed a model for the response of the cardiovascular system to a short term workload. The ergometric situation assumed that the baroreceptor loop (a mechanism that helps to maintain blood pressure at nearly constant levels) is the essential control loop. However, the components of the baroreceptor loop were not modelled in detail but they obtained a linear time-constant feedback law by solving a linear-quadratic regulator problem for the system. This model provided a satisfactory description of data obtained in bicycle ergometer tests and attracted many researchers to work on modelling issues, parameter estimation and simulations with this model. Batzel et al. (2007) presented a technique for applying optimal control theory and parameter estimation to the analysis of regulation processes in the cardiovascular and the respiratory systems. Models introduced in (Batzel et al., 2007) were derived from the principles of the physiological mechanisms rather than descriptions of input-output relationships. Therefore, the state variables in these models usually possess physiological meaning, which is useful in broader applications in medicine. Further studies on control aspects of the human cardiovascular system in response to workload have been done by Calderon et al. (2017), Vovkodav and Pasichnyk (2014) and Timischl (1998).

Reaction of the cardiovascular system to orthostatic stress refers to the effect of gravity or other forces on the distribution of blood volume in different parts of the cardiovascular system. Various mathematical models investigate the reaction of the cardiovascular / cardio-respiratory system to different postural changes such as, sit-to-stand, head-up-tilt and the lower-body-negative-pressure. Olufsen et al. (2004) developed a six-compartment mathematical model that can predict blood flow and pressure during posture change from sitting to standing. In advance study, Olufsen et al. (2005) presented a mathematical model of 11 compartments to describe blood pressure, blood flow, compliance and resistance in the heart and the systemic circulation. This model can predict cerebral blood flow velocity and finger blood pressure and provide a physiological description of the dynamics in response to hydrostatic pressure changes during postural change from sitting to standing.

Heldt et al. (2002) developed a closed-loop lumped parameter model of the cardiovascular system that can simulate the short term transient and steady state hemodynamics response to head-up tilt. The entire model was described by 12 compartments, the peripheral circulation was divided into upper body, renal, splanchnic, and legs compartments; the superior, inferior, abdominal vena cavae, left and right ventricles were identified separately. To describe the

pumping action of the heart they used the time varying elasticity function for the ventricles, but they did not include atria in this model, which are considered important to ventricular filling at high heart rates. The model output was in good agreement with sets of population-averaged hemodynamics data reported in the literature. In later study, Artiles et al. (2016) developed a 21-compartmental model to simulate the short term hemodynamics response to artificial gravity. More studies that investigate the effect of orthostatic stress to head-up tilt or lower body negative pressure are Lim et al. (2013), Batzel et al. (2009), van Heusden et al. (2006) and Melchior et al. (1994).

For clinical application it is good to adapt the models to individual patients. But it is in general difficult to find all parameters for an individual patient which makes validation of such models considerably more difficult. Some studies have successfully developed patient-specific models of the cardiovascular system (Williams et al., 2013, Batzel et al., 2009, Van de Vooren et al., 2007, Fink et al., 2004). Williams et al. (2013) presented a patient-specific model that used the heart rate as an input to fit the dynamic changes in arterial blood pressure during head-up tilt. The model consists of five compartments representing arteries and veins in the upper and lower body of the systemic circulation, and left ventricle to describe the pumping action of the heart. The model used a time-varying elastance function and the heart valves were modelled using pressure dependent smooth sigmoidal function. The model was successfully able to fit experimental and calculated values of carotid blood pressure in the supine position (natural position of the supine when all three curves of the supine, neck, middle and the lower are in good alignment) and during head-up tilt. Moreover, it was also capable of estimating physiologically reasonable values for arterial and venous blood pressures, blood volumes and cardiac output for which data were not available.

The first part of this thesis focuses on developing a mathematical model of the cardiovascular system that can be used reliably under conditions when the heart rate changes significantly. The model we present combines together volumes and pressures into 8 compartments. As mentioned earlier, such compartmental models have been developed previously (Grodins, 1959, Olufsen et al., 2004, Williams et al., 2013, Jung and Lee, 2006). However, these models were used for studies with a different focus than ours. Furthermore, none of the models mentioned above are suitable for the study of RSA because either the timings of the heart contractility when the heart beats remain constant or they do not vary enough when the heart rate changes. The models we present in this thesis adjust the timings of heart contractility with heart rate and are valid for a large range of heart rates. Our models introduces several other new modelling features which we regard as important for the study of RSA. We described the pressure created by muscle contraction as a function of time with constant elasticity. This is in contrast to previous models which generated muscle contraction

by taking elasticity as a function of time (see for example, Williams et al. (2013), Olufsen et al. (2004) and Heldt et al. (2002)). A model of the ventricle is coupled with a model of the atrium to create realistic PV loops for the atria using a new hypothesis about the mechanical contraction of the atria. Also, the interaction between the ventricles is taken into account and a non-linear volume of the shared wall is used to model this interdependence. The ventricular interaction has been included in other models (see for example, Santamore and Burkhoff (1991), Smith et al. (2004)) but we use a different approach to model this interaction.

The model we present in this study represents the cardiovascular system of a sheep. Sheep are considered to be a good animal model for the human cardiovascular system (DiVincenti Jr et al., 2014, Genain et al., 2018). Some studies that considered sheep cardiovascular models are (Olansen et al., 2000, Segers et al., 2001, Qian et al., 2002). Qian et al. (2002) developed a closed loop mathematical model of the ovine cardiovascular system, he adopted the heart model describing the hemodynamic behaviour of the left and right ventricles including the effects of preload and afterload, direct ventricular interaction and the influence of pericardium (the membrane enclosing the heart) on pump performance. He also developed a lumped model for the coronary circulation and generated a model output in terms of pressures in the heart chambers and flow in the aorta, large pulmonary artery and coronary artery. This model was capable of generating virtual measurements of sheep with cardiovascular disease by changing some of the model parameters and comparing the model-generated dynamics of blood flow with the baseline output. Later on, by using the same model presented in Qian et al. (2002), a study of cardiovascular adaptation to orthostatic stress was performed in Ha et al. (2004). As mentioned earlier in relation to cardiovascular models that represent humans, the modelling study in this thesis differ from previous modelling studies of sheep by its focus on RSA and the new modelling features introduced to the models.

1.5 Thesis structure

The thesis is structured in three main parts. The first part (Chapter 2, 3 and 4) is related to the mathematical modelling of the cardiovascular system of a sheep. In this part, we develop isolated and fully integrated mathematical models that include several new features. The model outputs are compared with the literature and experimental values. Parameters assignment and sensitivity analysis are also included in this part. The first part of the thesis has already been submitted for publication in the journal of Mathematical Biosciences. In the second part (Chapter 5), we investigate the effects and benefits of RSA on cardiac output and stroke volume in a healthy cardiovascular system of a sheep by using the models developed in the first part of the thesis. In part 3 (Chapter 6), we turn our focus to heart failure conditions.

We model two types of heart failure: diastolic and systolic by changing the model parameters. A physiological background and relevant literature review is provided at the beginning of the chapter.

Chapter 2

Isolated Models of the Cardiovascular System

In this chapter, we introduce isolated models of the cardiovascular system and give details of important characteristics of the system progressively. We start with an isolated model of the ventricle. We then construct a mathematical model of the atrium and the ventricle. Finally, we model an inter-ventricular dependence.

2.1 Isolated model of the ventricle

In this section, we describe a single compartment model that can represent either the left or right ventricle (see Figure 2.1 for a schematic of the left ventricle). The compartment contains a moving plate attached to a spring. We distinguish between the force exerted by the muscle when it gets externally excited and passive elasticity (represented by the spring).

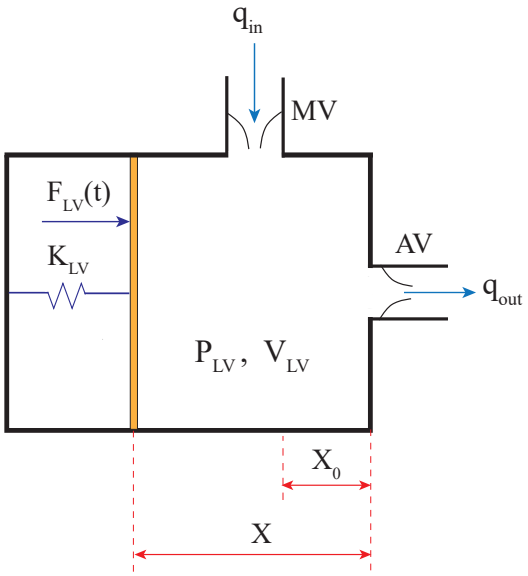

Fig. 2.1 Schematic model of the left ventricle. Blood flows through the mitral valve (MV) into a compartment with pressure P_{LV} and volume V_{LV}. It flows out of the compartment through the aortic valve (AV). The compartment has a moving plate attached to a spring K_{LV}, representing the elasticity of the ventricular muscle. Spring compression represents muscle expansion. The plate is at X_0 when there are no passive elastic forces acting on it. The force exerted by the muscle when it gets externally excited is depicted by $F_{LV}(t)$. $q_{in} = (P_{LA} - P_{LV})/R_{mv}$ is the flow into the compartment and $q_{out} = (P_{LV} - P_B)/R_{av}$ is the flow out of the compartment, P_{LA} is the pressure in the left atrium and P_B is the body pressure. For a model of the right ventricle, MV, AV, P_{LV}, V_{LV}, K_{LV}, $F_{LV}(t)$, P_{LA} and P_B are replaced by TV (tricuspid valve), PV (pulmonary valve), P_{RV} (right ventricular pressure), V_{RV} (right ventricular volume), K_{RV} (a spring attached to the moving plate of the right ventricle), $F_{RV}(t)$ (the force exerted by the muscles on the right ventricle), P_L (lung pressure) and P_{RA} (right atrial pressure), respectively.

The balance of forces across the plate (which we assume is massless), is given by

$$P_{LV}A = K_{LV}(X - X_0) + F_{LV}(t), \tag{2.1}$$

where F_{LV} is a function of time, t, representing the force exerted by the muscles, A is the area of the moving plate, K_{LV} is the spring constant and $(X - X_0)$ is the displacement of the spring from its unstressed state. Defining $E_{LV} = \frac{K_{LV}}{A^2}$ as the elasticity of the left ventricle muscle, $V_{LV} = XA$ as the volume of the left ventricle, $V_{unlv} = X_0A$ as the unstressed volume and $G_{LV}(t) = \frac{F_{LV}(t)}{A}$, we get

$$P_{LV} = E_{LV}(V_{LV} - V_{unlv}) + G_{LV}(t) \tag{2.2}$$

In Eq. (2.2), E_{LV} is constant while G_{LV} is a given function of time. If we eliminate $G_{LV}(t)$ from Eq. (2.2) and consider E_{LV} as a function of time we get

$$P_{LV} = E_{LV}(t)(V_{LV} - V_{unlv}). \tag{2.3}$$

Eq. (2.3) is used routinely in many models of the cardiovascular system when pressure is induced using time-dependent elasticity (see for example, Williams et al. (2013), Olufsen et al. (2004), Heldt et al. (2002)). Eq. (2.2) is a new contribution of this PhD project. We therefore compare the model output using Eq. (2.2) with the model output using Eq. (2.3). As will be shown later in Figure 2.5a and 2.5b, the two representations of the ventricular pressure lead to notable differences in model output. The functions $G_{LV}(t)$ used in Eq. (2.2), and $E_{LV}(t)$ used in Eq. (2.3) are shown in Figure 2.2. Mathematical formulas of these functions are given below.

$$G_{LV}(t) = \begin{cases} 0 & 0 \le t \le d \\ \frac{G_{maxLV}}{2}\left[1 - cos(\frac{\pi(t-d)}{T_S})\right] & d < t \le d + T_S \\ \frac{G_{maxLV}}{2}\left[1 - cos(\frac{\pi(t-(T_S+d))}{T_D})\right] & d + T_S < t \le d + T_S + T_D \\ 0 & d + T_S + T_D < t \le T_L \end{cases} \tag{2.4}$$

$$E_{LV}(t) = \begin{cases} E_{minLV} & 0 \le t \le d \\ E_{minLV} + \frac{E_{maxLV} - E_{minLV}}{2}\left[1 - cos(\frac{\pi(t-d)}{T_S})\right] & d < t \le d + T_S \\ E_{minLV} + \frac{E_{maxLV} - E_{minLV}}{2}\left[1 - cos(\frac{\pi(t-(T_S+d))}{T_D})\right] & d + T_S < t \le d + T_S + T_D \\ E_{minLV} & d + T_S + T_D < t \le T_L \end{cases} \tag{2.5}$$

where T_L is the heart period, T_S is the time from the beginning of contraction to maximum amplitude, T_D is the time from maximum amplitude to end of contraction and d is the delay between the contraction of the atria and the ventricles. For convenience we take $d = 0$ in the isolated model of the ventricle.

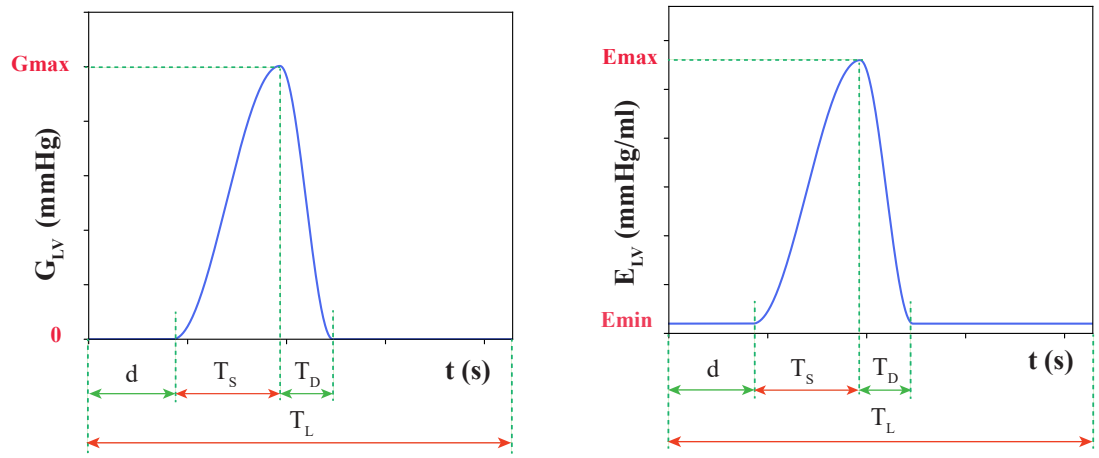

(a) (b)

Fig. 2.2 (a) Pressure exerted by the left ventricular muscles due to external excitation, G_{LV}, as a function of time, t. (b) Elasticity of the left ventricle, E_{LV} as a function of time, t. T_L is the heart period. T_S is the time from the beginning of contraction to maximum amplitude, T_D is the time from maximum amplitude to end of contraction and d is the delay between the contractions of the atria and the ventricles; for the single compartment model, the value of d is equal to zero.

The blood flow, q, in and out of the compartment is taken as

$$q = \frac{P_u - P_d}{R}, \tag{2.6}$$

where P_u and P_d are the upstream and downstream pressures and R is the resistance to the flow. The rate of change of volume within the compartment is given by a differential equation of the form

$$\frac{dV}{dt} = q_{in} - q_{out}, \tag{2.7}$$

where q_{in} and q_{out} are the flows in and out of the compartment. For the left ventricle, Eq. (2.7) takes the following form

$$\frac{dV_{LV}}{dt} = \frac{P_{LA} - P_{LV}}{R_{mv}} - \frac{P_{LV} - P_B}{R_{av}}, \tag{2.8}$$

Where P_{LA}, P_{LV} and P_B are pressures in the left atrium, left ventricle and body, respectively. R_{mv} and R_{av} are resistances of the mitral and the aortic valves and are pressure dependent functions (Williams et al., 2013). The shapes of these functions are shown in Figure 2.3, their mathematical expressions are given in Eqs. (2.9) and (2.10). Hysteresis is added to the

resistance of the aortic valve to mimic the fact that some back flow of blood through this valve occurs before it is closed. Resistance of the valve is given by

$$R_{mv} = R_{cl} - \frac{R_{cl} - R_{opmv}}{1 + e^{-\beta(P_{LA} - P_{LV})}} \tag{2.9}$$

where R_{cl} is the resistance when the mitral valve is closed and R_{opmv} is the resistance when it is open. P_{LA} and P_{LV} are the pressures in the left atrium and left ventricle, respectively. The resistance of the aortic valve is given by

$$R_{av}(t) = \begin{cases} R_{cl} - \frac{R_{cl} - R_{opav}}{1 + e^{-\beta(P_{LV} - P_B)}} & \text{when } (P_{LV} - P_B) \text{ is increasing} \\ R_{cl} - \frac{R_{cl} - R_{opav}}{1 + e^{-\beta(P_{LV} - P_B + Hys)}} & \text{when } (P_{LV} - P_B) \text{ is decreasing} \end{cases} \tag{2.10}$$

where R_{cl}, R_{opav}, β and Hys are constants (see Table 4.4).

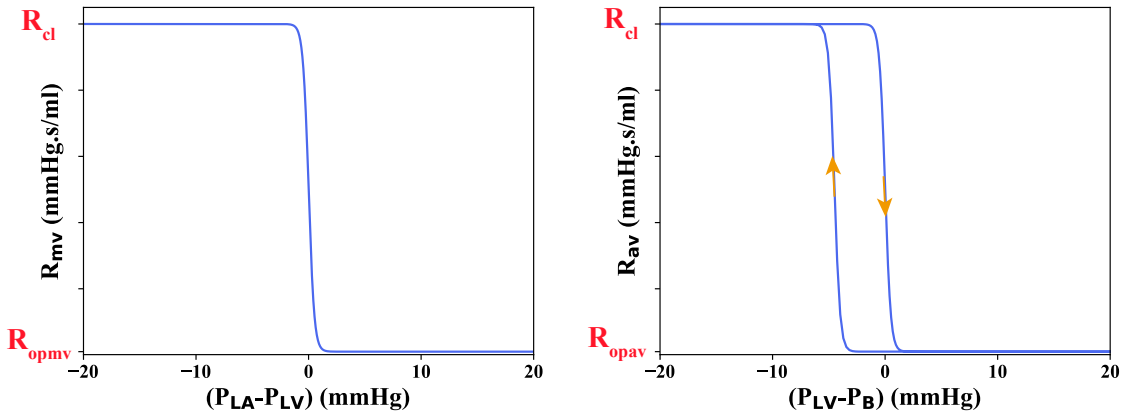

(a) (b)

Fig. 2.3 (a) Resistance of the mitral valve as a function of pressure difference $(P_{LA} - P_{LV})$. R_{opmv} is the resistance constant when the mitral valve is open and R_{cl} is the resistance when the valve is closed. A similar function is used for the tricuspid and pulmonary valves. (b) Resistance of the aortic valve as a function of pressure difference $(P_{LV} - P_B)$. R_{opav} is the resistance when the aortic valve is open. One function is used when the valve is opening and another when the valve is closing (see Eq. (2.9)). This mimics the fact that some back flow of blood through the aortic valve occurs before this valve is closed.

2.1.1 Dependence of contraction timing on heart period

The functions $E_{LV}(t)$ and $G_{LV}(t)$ require time parameters T_L, T_S and T_D as model inputs. An electrocardiogram (ECG), which measures the electrical activity of the heart, can be used to

calculate precise values of T_L (this is usually taken as the RR-interval, as shown on Figure 2.4a). However, the contraction time ($T_S + T_D$) can only be roughly estimated from the ECG measurements as being approximately the RT-interval (see Figure 2.4a) (Hall, 2015). Data presented in Senzaki et al. (1996) suggests that under a wide range of conditions, T_S can be estimated as 2/3rd of the RT-interval. While this ratio seems to be preserved for various heart rates, the contraction time, as a whole, changes when the heart period changes. This crucial relationship between the contraction time and the heart period is unknown. Several functions have been suggested in the past for humans (Funck-Brentano and Jaillon, 1993). For reasons we explain below, we suggest a new formula for the relationship between the contraction time and the heart period,

$$T_S + T_D = \frac{0.65}{(1 + e^{-7.12T_L})} - 0.33. \tag{2.11}$$

Eq. (2.11) was fitted to data of the RT-interval as a function of the RR-interval which we extracted from ECG recordings of 14 sheep (see Figure 2.4b).

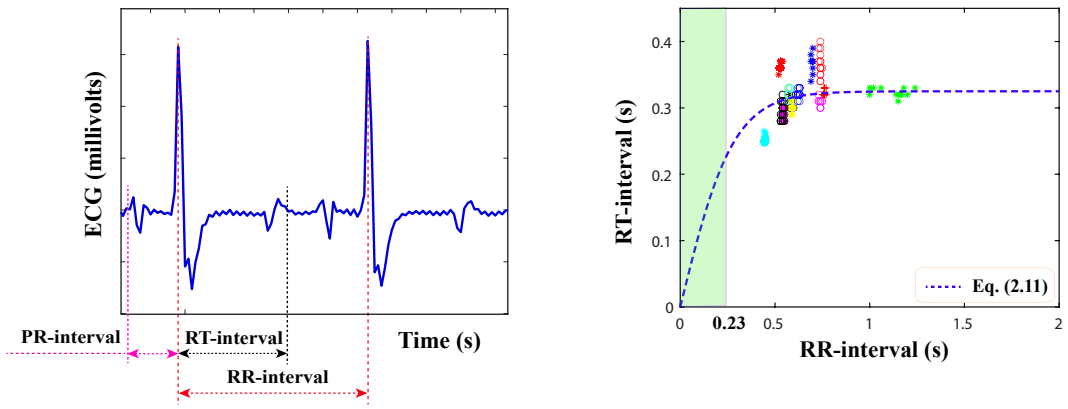

(a) (b)

Fig. 2.4 (a) ECG of a sheep showing two heart periods. The RR-interval is marked between two consecutive peaks of R-waves and the RT-interval starts from the beginning of the R-wave and finishes at the end of the T-wave. The PR-interval starts from the beginning of the P-wave and ends at the R-wave. (b) Contraction time of the ventricle ($T_S + T_D$, estimated by the RT-interval) as a function of the heart period (T_L, calculated from the RR-interval, see Eq. (2.11)), fitted to sheep data. The model is not valid in the shaded region where the contraction time is greater than the heart period.

2.1.2 Model Output

The model of the left ventricle consists of one non-linear differential equation of first order given in Eq. (2.8). We solved this numerically using the subroutine ode45 in Matlab. Figure 2.5a compares the pressure-volume (PV) loops of the new model (the isolated G model), where the ventricular pressure is described by Eq. (2.2), with the standard model (the isolated E model) where the pressure is described by Eq. (2.3). It can be seen that the maximum pressure occurs at lower volumes in the isolated G model compared with the isolated E model which is more realistic (see for example, Maughan et al. (1985)). This illustrates that the new model provides a more realistic shape of the PV loop. Figure 2.5b shows the mean cardiac output as a function of heart rate for the new and standard models. The mean cardiac output was calculated by integrating the aortic blood flow over 100 heart cycles after steady state was reached and dividing the integral by the overall integration time. The integration was done numerically using the trapezoidal rule. We then multiplied the result by $60/1000$ to get the mean cardiac output in units of L/min.

$$meanCO = \left(\frac{60}{1000}\right)\frac{1}{100T_L}\int_0^{100T_L}\frac{(P_{LV}-P_{SA})}{R_{av}}dt. \tag{2.12}$$

An important feature seen in Figure 2.5b is the drop in cardiac output for high heart rates. Such a drop can be seen in experiments (see for example Kumada et al. (1967)) and provides a way to test the relationship between the contraction time and the heart period that we introduced in Eq. (2.11). We found that previously published formulas of this relationship did not lead to a drop in cardiac output at high heart rates when fitted to the sheep data. As can be seen in Figure 2.5b, the new and standard models lead to slightly different curves for the mean cardiac output, with a faster decrease in cardiac output for the standard model (using E).

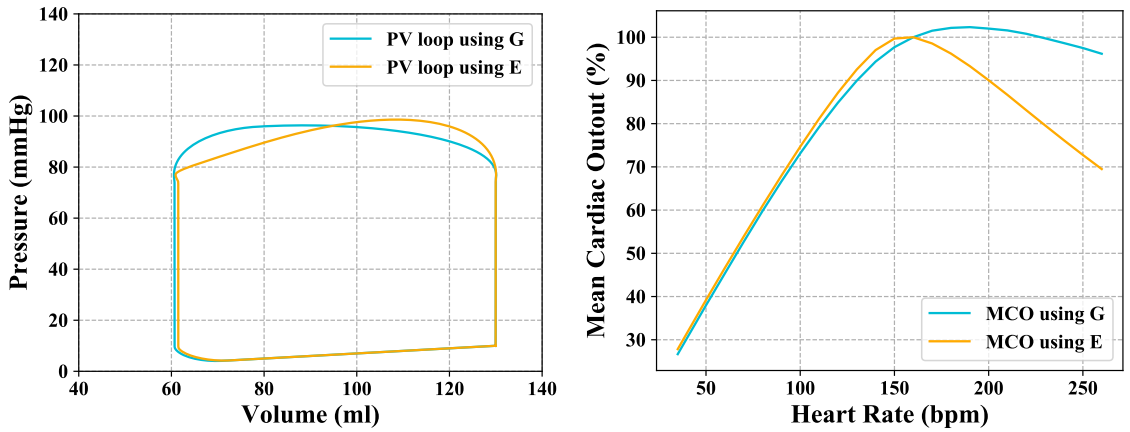

(a) (b)

Fig. 2.5 Output of the isolated model of the left ventricle. (a) Pressure-volume relationship, for the new model (using the isolated G model, Eqs. (2.2) and (2.6)) and for the standard model (using the isolated E model, Eqs. (2.3) and (2.6)). (b) Mean Cardiac Output curve for the new model (using the isolated G model, Eq. (2.2) and (2.6)) and for the standard model (using the isolated E model, Eq. (2.3) and (2.6)). This has been normalized such that the cardiac output at 160 bpm is 100%. The parameter values are given in Table 4.4.

2.2 A model of the atrium and the ventricle

In this section, we present a two compartmental model consisting of either the left atrium and ventricle or the right atrium and ventricle (see Figure 2.6). Similarly to the model presented in the previous section, the two cardiac chambers contain moving massless plates and springs. Fewer studies have put emphasis on atrial P-V loops so less is known on the mathematical modelling of atrial contraction and filling. Here we present a mathematical model containing an additional feature that is required in order to produce a realistic PV-loop for the atrium. We further discuss the delay between the contractions of the atrium and the ventricle in this section.

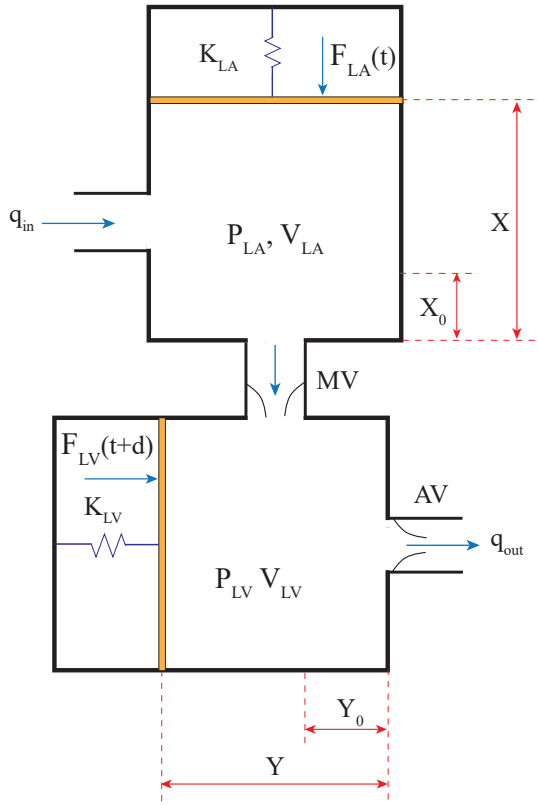

Fig. 2.6 A schematic description of a model for the left atrium and ventricle. The left atrium receives blood from the lungs and transfers it into the left ventricle through the mitral valve (MV). The left ventricle then pumps this blood into the body through the aortic valve (AV). Both compartments contain springs (K_{LA} and K_{LV}). The forces generated by the left atrial and ventricular muscles are denoted by $F_{LA}(t)$ and $F_{LV}(t)$, respectively. V_{LA}, V_{LV}, P_{LA} and P_{LV} are the volumes and pressures inside the left atrium and left ventricle, respectively. q_{in} and q_{out} are the flows into and out of a compartment, X_0 and Y_0 are the positions of the plates when no forces are acting on them. P_L is the lung pressure and P_B is the body pressure. For a model of the right atrium and right ventricle, MV, AV, V_{LA}, V_{LV}, P_{LA}, P_{LV}, K_{LA}, K_{RA}, F_{LA}, F_{LV}, P_L and P_B are replaced by TV, PV, V_{RA}, V_{RV}, P_{RA}, P_{RV}, K_{RA}, K_{RV}, F_{RA}, F_{RV}, P_B and P_L, respectively.

The pressure of the left ventricle is given by Eq. (2.7). We propose a new model for the atrium motivated by our realization that realistic PV loops for the atria cannot be generated when the relationship between the pressure and volume is linear (when $G_{LV}(t) = 0$ in Eq. 2.2 or when $E_{LV}(t) = E_{minLV}$ in Eq. 2.3) as we could assume for the ventricles. The model assumes that the rate of change of the atrial pressure is proportional not only to the rate of change of volume (Eq. (2.2)) but also to the volume itself. These properties depend on whether the atrium is contracting or expanding. For the left atrium the rate of change of

pressure is given by

$$\frac{dP_{LA}}{dt} = \begin{cases} E_{minLA}(\frac{dV_{LA}}{dt}) + \frac{dG_{LA}}{dt} + \alpha_L(V_{LA} - V_{unla}) & \frac{dV_{LA}}{dt} < 0 \\ \beta_L E_{minLA}(\frac{dV_{LA}}{dt}) + \gamma_L \frac{dG_{LA}}{dt} + \omega_L(V_{LA} - V_{unla}) & \frac{dV_{LA}}{dt} \geq 0 \end{cases} \tag{2.13}$$

where $\alpha_L, \beta_L, \gamma_L$ and ω_L are constants representing the fact that elasticity properties are different during contraction and relaxation of the left atrium. E_{minLA} is a constant elasticity of the left atrium, G_{LA} is the pressure exerted by the muscles on the left atrium, V_{LA} is the volume of the left atrium and V_{unla} is an unstressed volume of the left atrium. The rate of change of the left ventricular volume is given by Eq. (2.8). The rate of change of the left atrial volume is given in Eq. (2.14) below (see also Eq. (2.7)).

$$\frac{dV_{LA}}{dt} = \frac{P_L - P_{LA}}{R_L} - \frac{P_{LA} - P_{LV}}{R_{mv}}, \tag{2.14}$$

where P_L and P_{LA} are pressures in the lungs and the left atrium, respectively. R_{mv} is the resistance of the mitral valve (see Eq. 2.9 and Figure 2.3a) and R_L is the resistance of the lungs taken as a constant.

2.2.1 Delay between the atrial and ventricular contractions

The atrioventricular (AV) node, a group of cells located in the junction area of the atria and ventricles, creates a delay between the contraction of the atria and the contraction of the ventricles. This delay ensures that blood is pushed into the ventricles before the valves close and the ventricles contract. This delay is approximated with the the PR-interval using the ECG measurements and this can change with the heart period (see Figure 4.4a). The atrial contraction time continues slightly longer than the delay time and is approximated by a value of 1.5 times the PR-interval. Heldt (2004) scaled the delay time with the square root of the RR-Interval period. In this paper we propose a new formula for the delay, d, based on sheep data (see Eq. (2.15) and Figure 2.7 below). When fitting the data we imposed the condition that $d + T_S + T_D = 0.22$ when $T_L = 0.23$. Similar to the ventricles, the time from the start of the atrial contraction to its maximum amplitude is assumed to be 2/3rd of the contraction time.

$$d = \frac{0.17}{(1 + e^{-18.83(T_L - 0.38)})} - 1.33(10^{-4}). \tag{2.15}$$

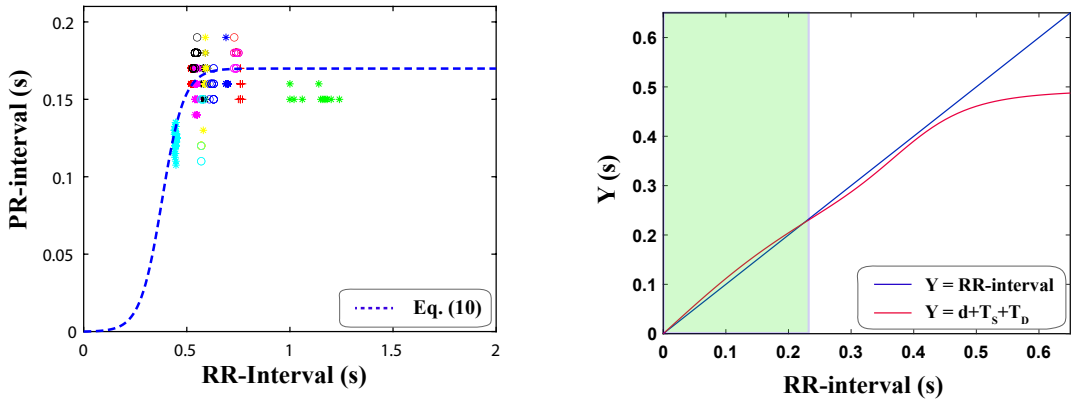

(a) (b)

Fig. 2.7 (a) Delay (d, estimated by the PR-interval) as a function of the heart period (T_L, calculated from the RR-Interval, see Eq. (2.15)), fitted to sheep data. (b) The combined time of ventricular contraction and delay as a function of RR-interval. The model is not valid in the shaded region for values of RR-interval below 0.23.

2.2.2 Model Output

The model consists of 3 first-order nonlinear ordinary differential equations (Eqs. (2.8), (2.13) and (2.14)) and is solved numerically using the subroutine ode45 in Matlab. The P-V loop of the left atrium is shown in Figure 2.8a. As can be seen, it consists of two loops, similar to experimental observations (see for example Zakeri et al. (2016), Pagel et al. (2003), Ferguson et al. (1989)). If we take $\beta_L = \gamma_L = 1$ and $\alpha_L = \omega_L = 0$ in Eq. (2.13) (effectively describing the pressure in the left atrium in the same way as the pressure in the left ventricle) we cannot generate a realistic PV loop (see Figure 2.8b). The P-V loops of the left ventricle are similar to the ones generated for the single compartment model and are not shown here

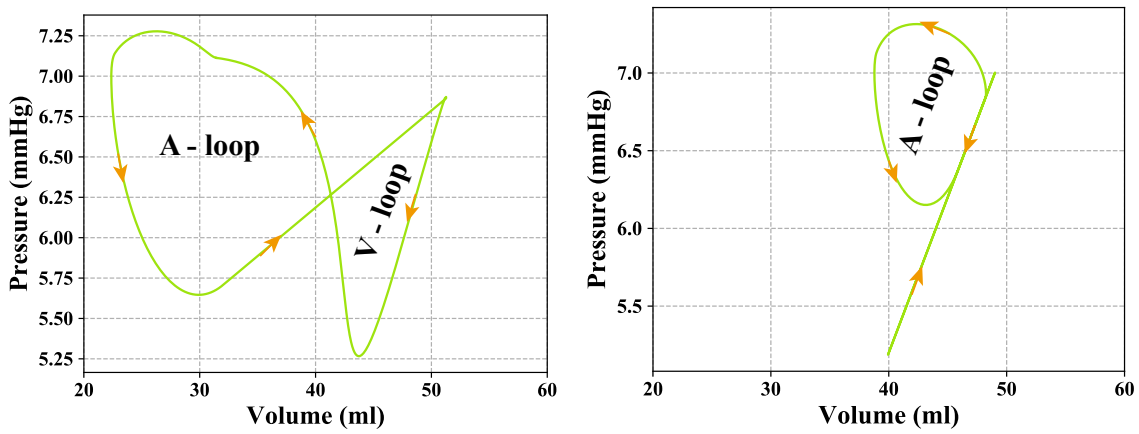

(a) (b)

Fig. 2.8 Model output using Eqs. (2.2), (2.8), (2.13) and (2.14). (a) Pressure-volume relationship of the left atrium using parameters from Table 4.4. (b) Pressure-volume relationship of the left atrium when $\beta_L = \gamma_L = 1$ and $\alpha_L = \omega_L = 0$, effectively describing the pressure in the left atrium in the same way as the pressure in the left ventricle.

2.3 Ventricular Inter-dependence

Because of the close anatomic connection, the pressure and volume of one ventricle can affect the pressure and volume of the other ventricle. This phenomenon is known as ventricular interdependence (Santamore and Burkhoff, 1991). In this section, we develop a mathematical model to include the mechanical interaction between the two ventricles.

A schematic model of ventricular interaction is shown in Figure 2.9a. Both ventricles and their common wall have moving plates with areas A_1, A_2 and A_3 attached to springs K_{RV}, K_{LV} and K_S, respectively. The area of one ventricle is affected by the other as the common wall moves between the two ventricles.

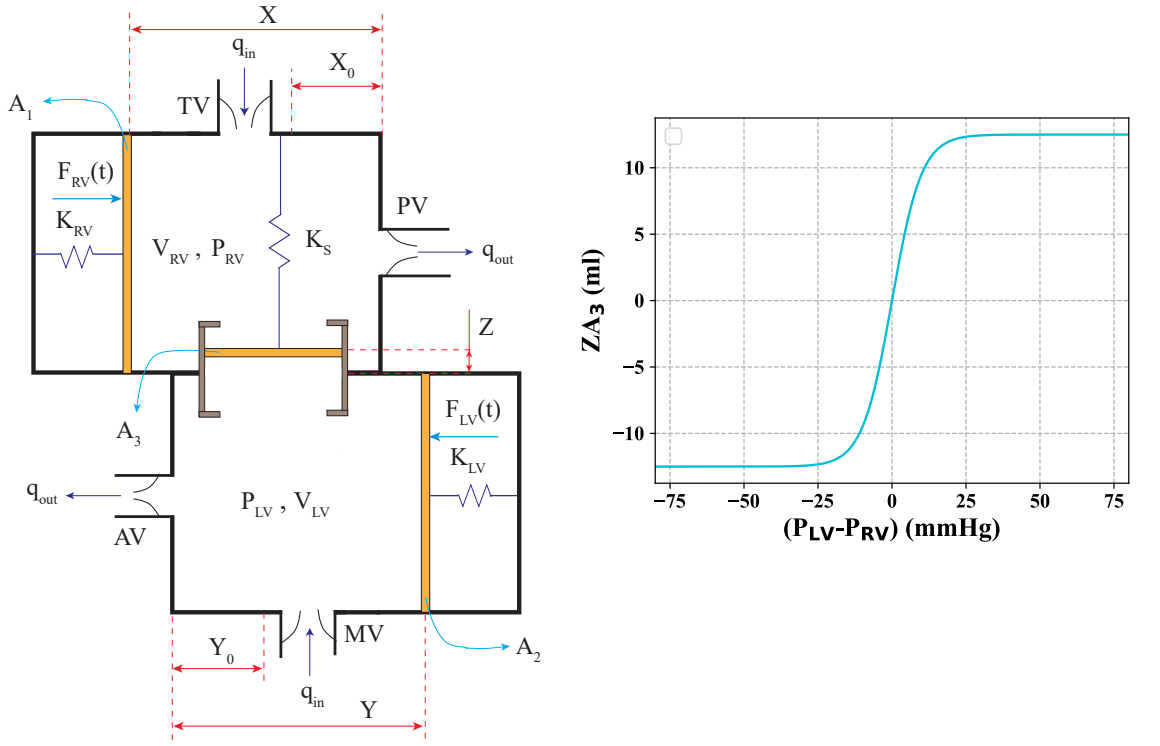

(a) (b)

Fig. 2.9 (a) A schematic model of ventricular interaction. The left and right ventricles have moving plates with areas A_1 and A_2, attached to the springs K_{LV} and K_{RV}, respectively. Both chambers have a shared moving wall, with an area A_3, which is attached to a nonlinear spring K_S. The muscle forces exerted on the left and right ventricles are denoted by $F_{LV}(t)$ and $F_{RV}(t)$, respectively. q_{in} and q_{out} are the flows into and out of a compartment. $P_{LV}, P_{RV}, V_{LV}, V_{RV}$ are the pressures and volumes inside the left and right ventricles, respectively. P_L is the lung pressure and P_B is the body pressure. AV, MV, PV and TV are the aortic, mitral, pulmonary and tricuspid valves respectively. X_0 and Y_0 are the positions of the plates when no forces are acting on them. (b) Change in volume due to movement of the shared wall as a function of pressure difference (see also Eq. (2.19)).

The volumes and forces inside the left and right ventricles are defined as follows

$$V_{RV} = XA_1 - ZA_3 \tag{2.16}$$

$$V_{LV} = YA_2 + ZA_3 \tag{2.17}$$

$$P_{RV}A_1 = K_{RV}(X - X_0) + F_{RV}(t) \tag{2.18}$$

$$P_{LV}A_2 = K_{LV}(Y - Y_0) + F_{LV}(t) \tag{2.19}$$

V_{LV}, V_{RV}, P_{LV}, P_{RV} are volumes and pressures in the left and right ventricles, respectively. X_0 and Y_0 are the lengths of the unstressed springs. $F_{LV}(t)$ and $F_{RV}(t)$ are the muscle forces exerted on the left and right ventricles, respectively. Equations (2.18) and (2.19) are rearranged and can be written in the form given below.

$$X = \frac{P_{RV}A_1}{K_{RV}} + X_0 - \frac{F_{RV}(t)}{K_{RV}} \tag{2.20}$$

$$Y = \frac{P_{LV}A_2}{K_{LV}} + Y_0 - \frac{F_{LV}(t)}{K_{LV}} \tag{2.21}$$

We define Z as a nonlinear function of $P_{LV} - P_{RV}$ such that near $P_{LV} - P_{RV} = 0$ the system behaves as a linear spring but for a larger pressure difference the value of Z reaches a constant (see Figure 2.9b). Z as defined by Eq. (2.22) can take on negative values when the pressure in the right ventricle is greater than the pressure in the left ventricle during the relaxation period. We choose this particular form of Z to reflect the fact that there is a limit to how much the septum wall can stretch.

$$Z = \frac{A_3}{K_S}\left(\frac{4}{a(1+e^{-a(P_{LV}-P_{RV})})} - \frac{2}{a}\right) \tag{2.22}$$

where a is a parameter. Substituting Eqs. (2.20) and (2.21) into Eqs. (2.16) and (2.17) and defining $E_{minRV} = \frac{K_{RV}}{A_1^2}$, $E_{minLV} = \frac{K_{LV}}{A_2^2}$, $E_S = \frac{K_S}{A_3^2}$, $V_{unrv} = X_0A_1$, $V_{unlv} = Y_0A_2$, $G_{LV}(t) = \frac{F_{RV}(t)}{A_1}$, $G_{RV}(t) = \frac{F_{LV}(t)}{A_2}$, we obtain

$$(V_{RV} - V_{unrv}) = \frac{P_{RV}}{E_{minRV}} - \frac{G_{RV}(t)}{E_{minRV}} - ZA_3 \tag{2.23}$$

$$(V_{LV} - V_{unlv}) = \frac{P_{LV}}{E_{minLV}} - \frac{G_{LV}(t)}{E_{minLV}} + ZA_3 \tag{2.24}$$

Differentiating Eqs. (2.23) and (2.24) with respect to t, we get

$$\frac{dV_{RV}}{dt} = \frac{1}{E_{minRV}}\left(\frac{dP_{RV}}{dt} - \frac{dG_{RV}}{dt}\right) - \frac{dZA_3}{dt} \tag{2.25}$$

$$\frac{dV_{LV}}{dt} = \frac{1}{E_{minLV}}\left(\frac{dP_{LV}}{dt} - \frac{dG_{LV}}{dt}\right) + \frac{dZA_3}{dt} \tag{2.26}$$

where

$$\begin{aligned}\frac{dZA_3}{dt} &= \frac{\partial ZA_3}{\partial P_{RV}}\frac{dP_{RV}}{dt} + \frac{\partial ZA_3}{\partial P_{LV}}\frac{dP_{LV}}{dt} \\ &= S\left(\frac{dP_{LV}}{dt} - \frac{dP_{RV}}{dt}\right)\end{aligned} \tag{2.27}$$

and

$$S = \frac{4e^{-a(P_{LV}-P_{RV})}}{E_S(1+e^{-a(P_{LV}-P_{RV})})^2} \tag{2.28}$$

Solving Eqs. (2.25) and (2.26) simultaneously for $\frac{dP_{LV}}{dt}$ and $\frac{dP_{RV}}{dt}$, we obtain

$$\begin{aligned}\frac{dP_{RV}}{dt} = &\frac{1}{\frac{1}{S}(S+\frac{1}{E_{minRV}})(S+\frac{1}{E_{minLV}})-S}\left[\frac{dV_{LV}}{dt}+\right.\\ &\left.+\left(1+\frac{1}{SE_{minLV}}\right)\left(\frac{1}{E_{minRV}}\frac{dG_{RV}}{dt}+\frac{dV_{RV}}{dt}\right)+\frac{1}{E_{minLV}}\frac{dG_{LV}}{dt}\right]\end{aligned} \tag{2.29}$$

$$\begin{aligned}\frac{dP_{LV}}{dt} = &\frac{1}{\frac{1}{S}(S+\frac{1}{E_{minRV}})(S+\frac{1}{E_{minLV}})-S}\left[\frac{dV_{RV}}{dt}+\right.\\ &\left.+\left(1+\frac{1}{SE_{minRV}}\right)\left(\frac{1}{E_{minLV}}\frac{dG_{LV}}{dt}+\frac{dV_{LV}}{dt}\right)+\frac{1}{E_{minRV}}\frac{dG_{RV}}{dt}\right]\end{aligned} \tag{2.30}$$

The isolated ventricular interaction model consists of four differential equations: Eq. (2.8) for the left ventricle and a similar equation for the right ventricle with the rate of change of pressures described by Eqs. (2.29) and (2.30). We do not show the model output for the isolated model. Instead, we show the effects of the ventricular interaction when the model is integrated with other compartments in the next chapter.

Chapter Summary

In this chapter, we have developed isolated models of the cardiovascular system to capture important features of heart mechanics. We have started with the isolated model of the ventricle where we used two representations of the pressure: the standard E model in which we take elasticity as a function of time and the newly introduced G model in which we considered elasticity as a constant. The two models produced different P-V loops and mean cardiac output curves (Figures 2.4a and 2.4b). Then, we have developed an isolated model of the atrium and ventricle that generates a realistic P-V loop for the atrium, see Figure 2.8a. We have also modelled the ventricular inter-dependence. This model will be investigated further in the next chapter when coupled with a closed loop model of the circulation.

Chapter 3

An eight-compartment model of the cardiovascular system

In this chapter, we present an eight compartment model of the cardiovascular system that contains all the features of the models discussed in the previous chapter. First, we perform simulations at constant heart rate to validate the model by comparing it with some literature values. We then investigate the effects of different aspects of our modelling on model outputs when the heart rate varies.

3.1 An eight-compartment model of the cardiovascular system

A schematic model of the cardiovascular system, combining all the features discussed in the previous sections is shown in Figure 3.1. It consists of two compartments representing the systemic arteries and the systemic veins, four compartments representing the cardiac chambers, and two compartments depicting the pulmonary arteries and veins. The entire model (which we call the "full G model") is described mathematically by a set of nine first-order nonlinear differential equations which have been solved using the subroutine ode45 in Matlab. The model equations are given in Eqs. (3.1-3.16).

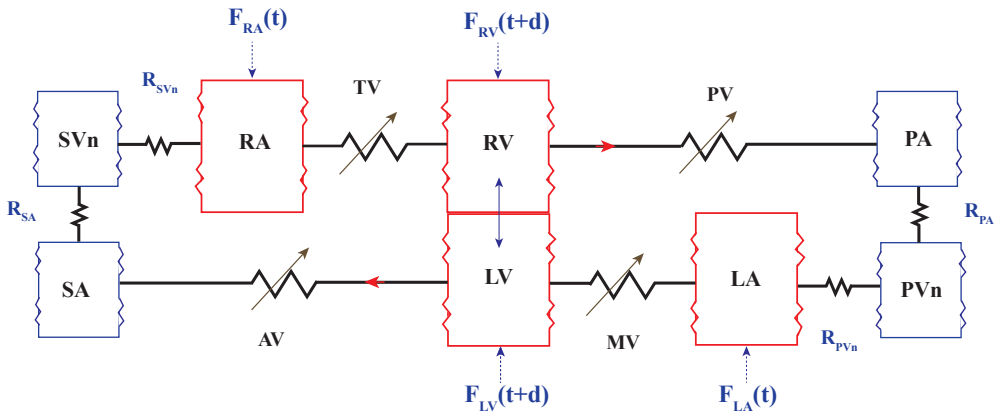

Fig. 3.1 A schematic representation of the eight-compartment model. RA: right atrium, RV: right ventricle, LA: left atrium, LV: left ventricle, SA: systemic arteries, SVn: systemic veins, PA: pulmonary arteries and PVn: pulmonary veins. The muscles forces acting on the left and right heart are denoted by $F_{LA}(t)$, $F_{LV}(t+d)$, $F_{RA}(t)$ and $F_{RV}(t+d)$ respectively, where d is the delay in contraction between the atrium and the ventricle. The aortic valve (AV), the pulmonary valve (PV), the tricuspid valve (TV) and the mitral valve (MV) are represented by pressure-dependent resistances. R_{PA}, R_{PVn}, R_{SA} and R_{SVn} are resistances to blood flow. The red arrows indicate the direction of blood flow.

The full G model

The full G model includes all the modelling features discussed in Chapter 2. The model consists of 9 ordinary differential equations, describing the rate of change of the volumes in the left atrium, systemic arteries, right atrium, pulmonary arteries and pulmonary veins, as well as the rate of change of pressures in the left atrium, left ventricle, right atrium and right ventricle.

$$\frac{dV_{LA}}{dt} = \frac{P_{PVn} - P_{LA}}{R_{PVn}} - \frac{P_{LA} - P_{LV}}{R_{mv}} \tag{3.1}$$

$$\frac{dV_{SA}}{dt} = \frac{P_{LV} - P_{SA}}{R_{av}} - \frac{P_{SA} - P_{SVn}}{R_{SA}} \tag{3.2}$$

$$\frac{dV_{RA}}{dt} = \frac{P_{SVn} - P_{RA}}{R_{SVn}} - \frac{P_{RA} - P_{RV}}{R_{tv}} \tag{3.3}$$

$$\frac{dV_{PA}}{dt} = \frac{P_{RV} - P_{PA}}{R_{pv}} - \frac{P_{PA} - P_{PVn}}{R_{PA}} \tag{3.4}$$

$$\frac{dV_{PVn}}{dt} = \frac{P_{PA} - P_{PVn}}{R_{PA}} - \frac{P_{PVn} - P_{LA}}{R_{PVn}} \tag{3.5}$$

$$\frac{dP_{LA}}{dt} = \begin{cases} E_{minLA}(\frac{dV_{LA}}{dt}) + \frac{dG_{LA}(t)}{dt} + \alpha_L(V_{LA} - V_{unla}) & \frac{dV_{LA}}{dt} < 0 \\ \beta_L E_{minLA}(\frac{dV_{LA}}{dt}) + \gamma_L \frac{dG_{LA}(t)}{dt} + \omega_L(V_{LA} - V_{una}) & \frac{dV_{LA}}{dt} \geq 0 \end{cases} \tag{3.6}$$

$$\frac{dP_{RA}}{dt} = \begin{cases} E_{minRA}(\frac{dV_{RA}}{dt}) + \frac{dG_{RA}(t)}{dt} + \alpha_R(V_{RA} - V_{unra}) & \frac{dV_{RA}}{dt} < 0 \\ \beta_R E_{minRA}(\frac{dV_{RA}}{dt}) + \gamma_R \frac{dG_{RA}(t)}{dt} + \omega_R(V_{RA} - V_{unra}) & \frac{dV_{RA}}{dt} \geq 0 \end{cases} \tag{3.7}$$

$$\frac{dP_{LV}}{dt} = \frac{1}{\frac{1}{S}(S + \frac{1}{E_{minRV}})(S + \frac{1}{E_{minLV}}) - S} \left[\frac{P_{RA} - P_{RV}}{R_{tv}} - \frac{P_{RV} - P_{PA}}{R_{pv}} + \left(1 + \frac{1}{SE_{minRV}}\right) \left(\frac{1}{E_{minLV}} \frac{dG_{LV}}{dt} + \frac{P_{LA} - P_{LV}}{R_{mv}} - \frac{P_{LV} - P_{SA}}{R_{av}} \right) + \frac{1}{E_{minRV}} \frac{dG_{RV}}{dt} \right] \tag{3.8}$$

$$\frac{dP_{RV}}{dt} = \frac{1}{\frac{1}{S}(S + \frac{1}{E_{minRV}})(S + \frac{1}{E_{minLV}}) - S} \left[\frac{P_{LA} - P_{LV}}{R_{mv}} - \frac{P_{LV} - P_{SA}}{R_{av}} + \left(1 + \frac{1}{SE_{minLV}}\right) \left(\frac{1}{E_{minRV}} \frac{dG_{RV}}{dt} + \frac{P_{RA} - P_{RV}}{R_{tv}} - \frac{P_{RV} - P_{PA}}{R_{pv}} \right) + \frac{1}{E_{minLV}} \frac{dG_{LV}}{dt} \right] \tag{3.9}$$

Where R_{PVn}, R_{SA}, R_{SVn}, R_{PA}, R_{PVn}, α_L, α_R, β_L, β_R, ω_L, ω_R, λ_L and λ_R are constants (see Table 4.5). S is a function of pressure difference $P_{LV} - P_{RV}$ (see Eq. 2.28). R_{mv}, R_{av}, R_{tv} and R_{pv} are functions of the pressures (see equations 2.9 and 2.10). The volume in the left and right ventricles is given by

$$V_{LV}(t) = \frac{1}{E_{minLV}}(P_{Lv} - G_L V(t)) + V_{unlv} + \frac{1}{E_S} Z \tag{3.10}$$

$$V_{RV}(t) = \frac{1}{E_{minRV}}(P_{Rv} - G_R V(t)) + V_{unrv} - \frac{1}{E_S} Z \tag{3.11}$$

The volume in the systemic veins can be calculated by assuming conservation of mass.

$$V_{SVn} = V_{total} - (V_{LA} + V_{LV} + V_{SA} + V_{RA} + V_{RV} + V_{PA} + V_{PVn}). \tag{3.12}$$

The pressures for the other compartments are given by

$$P_{SA} = \frac{(V_{SA} - V_{unsa})}{C_{SA}} \tag{3.13}$$

$$P_{SVn} = \frac{(V_{SV} - V_{unsv})}{C_{SVn}} \tag{3.14}$$

$$P_{PA} = \frac{(V_{PA} - V_{unpa})}{C_{PA}} \tag{3.15}$$

$$P_{PV} = \frac{(V_{PV} - V_{unpv})}{C_{PVn}}. \tag{3.16}$$

Th derivative of the function $G_X(t)$, used in Eqs. (3.8) and (3.9) is given by

$$\frac{dG_X(t)}{dt} = \begin{cases} \frac{\pi G_{max_X}}{2T_S}\left[sin(\frac{\pi t}{T_S})\right] & 0 < t \leq T_S \\ \frac{\pi G_{max_X}}{2T_D}\left[sin(\frac{\pi (t-T_S)}{T_D})\right] & T_S < t \leq T_S + T_D \\ 0 & T_S + T_D < t \leq T_L \end{cases} \tag{3.17}$$

Resistance of the valve is given by

$$R_Y = R_{cl} - \frac{R_{cl} - R_{opY}}{1 + e^{-\beta(P_{in} - P_{out})}} \tag{3.18}$$

where Y represents mv, tv or pv. Resistance of the aortic valve is given by Eq. (2.10) in Chapter 2.

3.2 Model outputs at constant heart rate

Table 3.1 compares the numerical simulations with the normal range of physiological values. It shows that all the variables of the model output lie within or very close to the normal range. The pressures on the left and right sides of the heart are plotted in Figure 3.2 and the blood flows through the four heart valves, systemic veins and pulmonary veins are plotted in Figure 3.3. The PV loops of the atria and the ventricles are shown in Figure 3.4.

Table 3.1 Comparison of the model simulations in steady state with literature values of sheep. Stars (*) indicate literature values for humans where sheep data was unavailable. The results are generated using the full G model (Eqs. (3.1-3.16)) with a heart rate of 70 bpm (Matlab program of the full G model is given in the Appendix A.2).

Variables	Simulations	Physiological Range
Blood pressure min/max	56/96 (mmHg)	(55 - 100) / (100 - 150) (mmHg)
Left ventricular pressure maximum	101 (mmHg)	100 - 140 (mmHg)
Left ventricular pressure minimum	3.6 (mmHg)	3 - 12 (mmHg) *

Left atrial pressure (mean)	10.8 (mmHg)	Less than 12 (mmHg) *
Pulmonary arteries pressure min/max	11/17 (mmHg)	(4 - 12) / (15 - 30) (mmHg)
Righ ventricular pressure maximum	22 (mmHg)	18 - 30 (mmHg)
Right ventricular pressure minimum	1 (mmHg)	1 - 4.5 (mmHg) *
Right atrial pressure (mean)	5.8 (mmHg)	Less than 5 (mmHg) *
Stroke volume (ml/beat)	68 (ml / beat)	60 - 100 (ml / beat)
Cardiac output (l/min)	4.5 (L/min)	4 - 8 (l/min)
Ejection fraction (%)	53 %	50 - 70 %
Blood volume in the heart	5.3%	8-11 % *
Blood volume in the systemic arteries	17.3%	12-14 % *
Blood volume in the systemic veins	60.4%	62-72 % *
Blood volume in the pulmonary arteries	4%	4-5 % *
Blood volume in the pulmonary veins	13%	7-8 % *

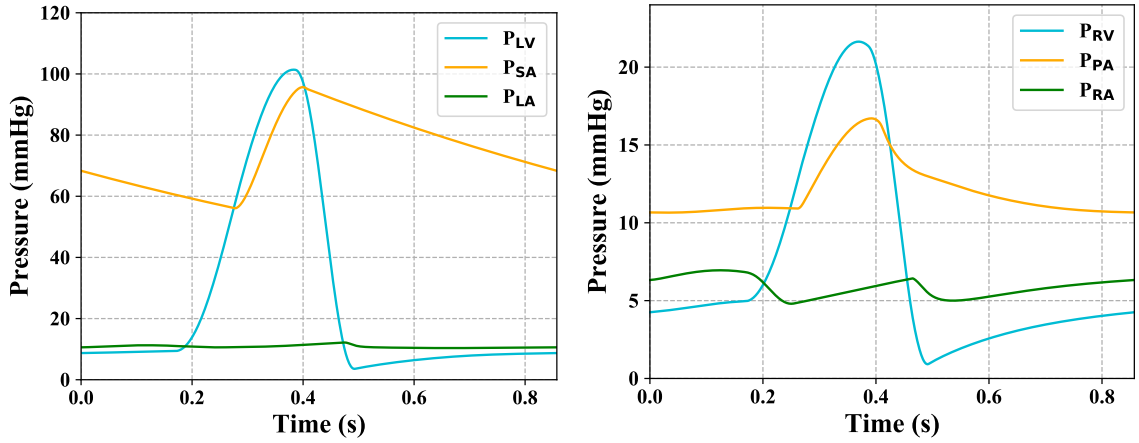

(a) (b)

Fig. 3.2 Model output using the full G model (Eqs. (3.1-3.16) with parameters from Table 4.5). (a) Pressures on the left side of the heart. P_{LV}: left ventricle pressure, P_{LA}: left atrium pressure and P_{SA}: pressure in the systemic arteries. (b) Pressures on the right side of the heart. P_{RV}: right ventricle pressure, P_{RA}: right atrium pressure and P_{PA}: pressure in the pulmonary arteries.

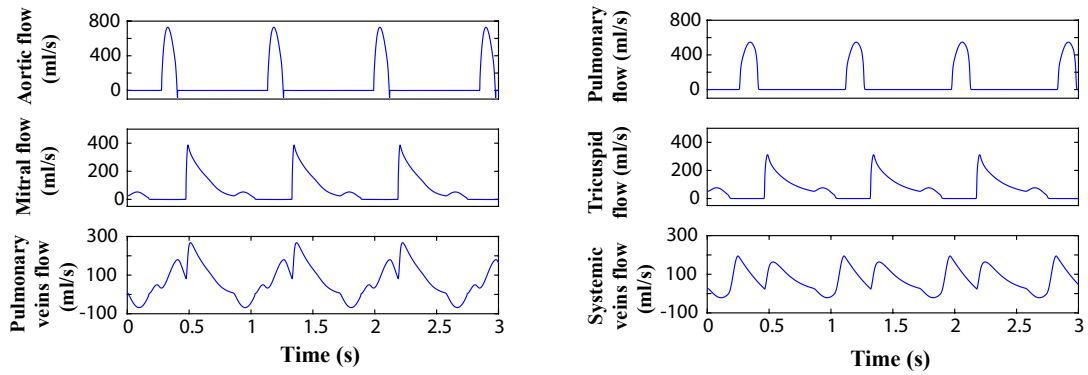

(a) (b)

Fig. 3.3 Model output using the full G model (Eqs. (3.1-3.16) with parameters from Table 4.5). (a) Blood flows on the left side of the heart, panels from top to bottom show the aortic valve, mitral valve and pulmonary veins blood flows. (b) Blood flows on the right side of the heart, panels from top to bottom show the pulmonary valve, tricuspid valve and systemic veins blood flow.

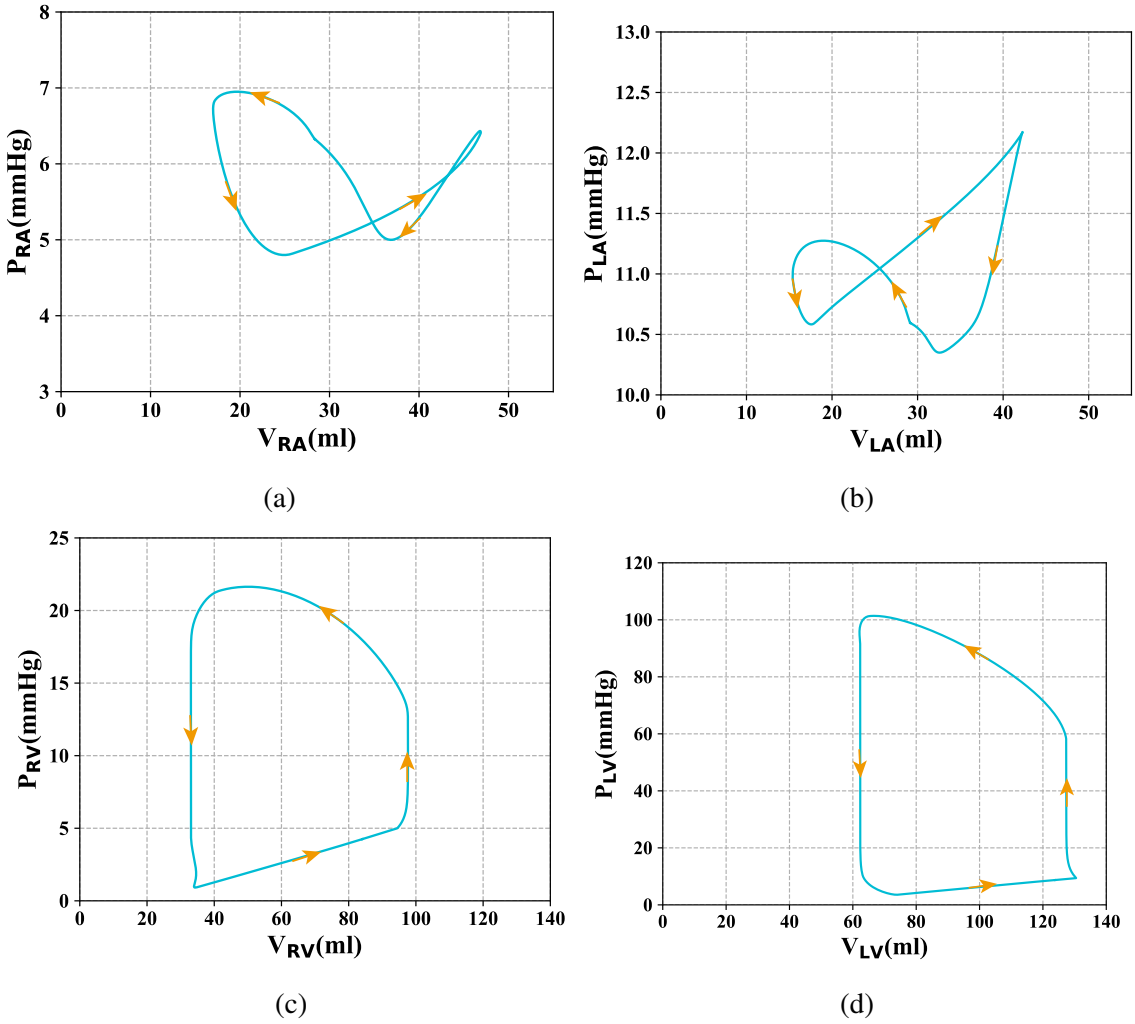

Fig. 3.4 Model output using the full G model (Eqs. (3.1-3.16) with parameters from Table 4.5). (a) PV loop of the right atrium. (b) PV loop of the left atrium. (c) PV loop of the right ventricle. (d) PV loop of the left ventricle The arrows show the direction of time.

3.3 Model outputs at variable heart rates

The main aim of this study is to develop a model of the cardiovascular system that can be used to study conditions in which the heart rate changes significantly. In this section, we study the effects of different heart rates on the output of several models, all derived from the full G model: the GNH model which only takes into account the new hypothesis we introduced in section 2.2, the GVI model which only takes into account the ventricular interactions, the G model which does not include the new hypothesis and ventricular interactions, and the E model in which the contraction of the cardiac chambers is achieved with time dependent

elasticity. The description of all these models is given below. By studying these different models we can examine how the different features we have introduced into the full G model affect the model output.

The G model with the new hypothesis (GNH)

The GNH model is the same as the full G model but without the ventricular interactions, that is, it includes only the new hypothesis in relation to the contraction of the atria. The GNH model consists of Eqs. (3.1-3.7). The pressures in the systemic arteries, systemic veins, pulmonary arteries and pulmonary veins are computed using Eqs. (3.13-3.16). While the rate of change of volume, and pressures in the left and right ventricles are described according to

$$\frac{dV_{LV}}{dt} = \frac{P_{LA} - P_{LV}}{R_{mv}} - \frac{P_{LV} - P_{SA}}{R_{av}} \tag{3.19}$$

$$\frac{dV_{RV}}{dt} = \frac{P_{RA} - P_{RV}}{R_{tv}} - \frac{P_{RV} - P_{PA}}{R_{pv}} \tag{3.20}$$

$$P_{LV} = (V_{LV} - V_{unv})E_{minLV} + G_{LV}(t) \tag{3.21}$$

$$P_{RV} = (V_{RV} - V_{unv})E_{minRV} + G_{RV}(t) \tag{3.22}$$

The G model with ventricular interactions (GVI)

The GVI model is the same as the full G model but without the new hypothesis, that is, it includes only the ventricular interactions. The GVI model consists of Eqs. (3.1-3.5). The pressures in the left and right ventricles are calculated using Eqs. (3.8) and (3.9), while the left and right atrial pressures are expressed by

$$P_{LA} = (V_{LV} - V_{unv})E_{minLA} + G_{LA}(t) \tag{3.23}$$

$$P_{RA} = (V_{RA} - V_{unv})E_{minRA} + G_{RA}(t) \tag{3.24}$$

The pressures in the other four compartments are given by Eqs. (3.13-3.16).

The G model

The G model does not include the new hypothesis and the ventricular interactions. The only difference between this model and the E model (described below) is the way the external excitation of the heart muscle is taken into account. The G model includes a time-dependent external force with a constant elasticity. The rate of change of volumes in the G model are

described by Eqs. (3.1-3.5), Eqs. (3.19) and (3.20). The left and right atrial pressures are described by Eqs. (3.23) and (3.24). The left and right ventricular pressures are given by Eqs. (3.21) and (3.22). The pressures in the four other compartments are given by Eqs. (3.13-3.16).

The E model

The E model includes time-dependent elasticity and does not include the new hypothesis and ventricular interactions. It consists of 7 ordinary differential equations comprising Eqs. (3.1-3.5), (3.19) and (3.20). The pressures in each compartment are given by Eqs. (3.13-3.16) and the following equations:

$$P_{LV} = E_{LV}(t)(V_{LV} - V_{unv}) \tag{3.25}$$

$$P_{RV} = E_{RV}(t)(V_{RV} - V_{unv}) \tag{3.26}$$

$$P_{LA} = E_{LA}(t)(V_{LA} - V_{una}) \tag{3.27}$$

$$P_{RA} = E_{RA}(t)(V_{RA} - V_{una}) \tag{3.28}$$

The constant V_{unv} and V_{una} are the same as in the full G, GNH, GVI and the G model. The elasticity functions are given by

$$E_X(t) = \begin{cases} E_{min_X} & 0 \le t \le d \\ E_{min_X} + \frac{E_{max_X} - E_{min_X}}{2}\left[1 - cos(\frac{\pi(t-d)}{T_S})\right] & d < t \le d + T_S \\ E_{min_X} + \frac{E_{max_X} - E_{min_X}}{2}\left[1 - cos(\frac{\pi(t-(T_S+d))}{T_D})\right] & d + T_S < t \le d + T_S + T_D \\ E_{min_X} & d + T_S + T_D < t \le T_L \end{cases} \tag{3.29}$$

Where X can be replaced by LV, RV, LA and RA. In the case of LA and RA the value of d = 0.

Figure 3.5 shows the mean cardiac output, the stroke volume the ejection time, and the ejection fraction as a function of heart rate using the G, GNH, GVI and E models, marked with solid yellow, dashed black, dashed green and solid blue lines, respectively, along with experimental values (Kumada et al., 1967) marked with red circles. The mean cardiac output was calculated using Eq. (2.12) in chapter 2, the stroke volume was obtained using the

following expression:

$$SV = max(V_{LV}) - min(V_{LV}),$$

the ejection time was the time between the opening and closing of the aortic valve and we calculated the ejection fraction using the formula:

$$EF = \frac{SV}{max(V_{LV})} \times 100.$$

Both the simulations and literature values in Figures 3.5a, 3.5b and 3.5c are normalized such that the values of the mean cardiac output, stroke volume and ejection time are 100% at 160bpm. Figure 3.5a shows that there is not a significant difference between the G, GNH and GVI models. The E model has a narrow peak and is closest to the experimental data over the range 100 - 120 bpm and 220 - 260 bpm. The other models are closer to the experimental data in the lower and middle HR. The stroke volume as a function of HR is best captured by the GNH and G models (Figure 3.5b). The GVI model has higher values at low heart rates but still it approximates the stroke volume data better than the E model. All models oscillate in a similar fashion around the experimental data in Figure 3.5c that shows the ejection time as a function of HR. In Figure 3.5d the E model gives lower values of the ejection fraction (EF) at low and high heart rates in comparison to the G, GNH and GVI models.

The PV loops for different heart rates using the GNH, GVI, G and E models are shown in Figures 3.6a, 3.6b, 3.6c and 3.6d respectively. The PV loops of the left ventricle in Figures 3.6a, 3.6b, 3.6c and 3.6d (lower right panel) shift towards the right as HR increases up to 120 bpm but these return towards the left with a further increase of HR. Also, the pressure in the left ventricle increases when the heart rate increases up to 120 bpm but then it decreases with further increase of HR. This trend has been observed with all models, although the increase in pressure is more prominent when we use the E model (see Figure 3.6d lower right panel) and the shift of the PV loops is more obvious with the GNH, GVI and G models. The pressure in the right ventricle decreases with high HR and this behaviour is consistent in all models (see Figures 3.6a, 3.6b, 3.6c and 3.6d lower left panel). The pressure in the left atrium (top right panel in Figures 3.6a, 3.6b, 3.6c and 3.6d) increases with high HR, while the opposite effect can be seen in the right atrial pressure (top left panel in Figures 3.6a, 3.6b, 3.6c and 3.6d) as it decreases as HR increases. Overall the PV loops of the left and right ventricles are similar in the G, GNH and GVI models and are markedly different than the E model. While the PV loops of the left and right atria are markedly different (resembling reality) in the GNH model.

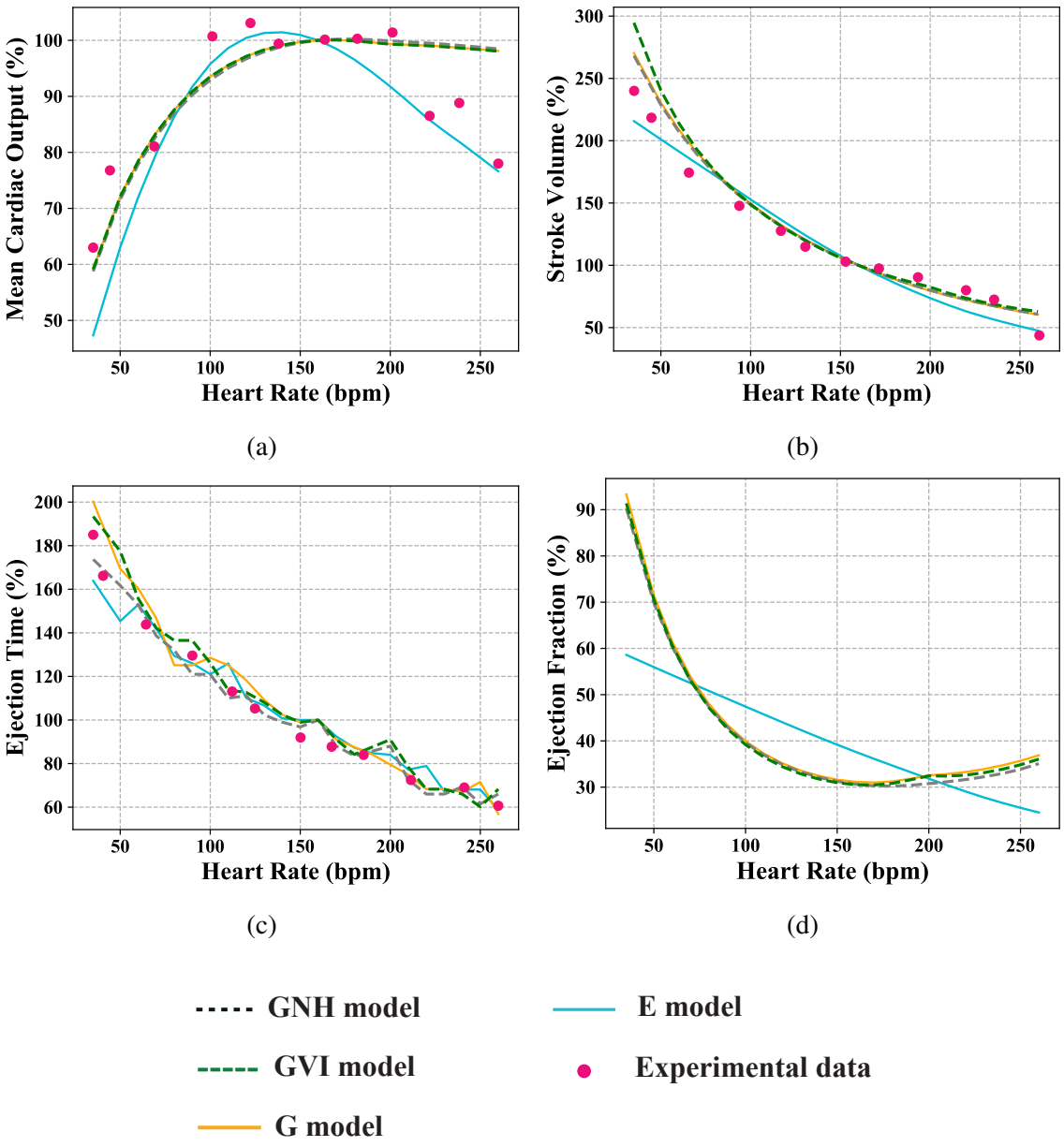

Fig. 3.5 (a) Mean cardiac output as a function of heart rate. (b) Stroke volume as a function of heart rate. (c) Ejection time as a function of heart rate. (d) Ejection fraction as a function of heart rate. Red solid circles: data taken from Fig. 2 in (Kumada et al., 1967). Experiments were done on dogs. All values in Figures 3.5a, 3.5b and 3.5c have been normalized such that the mean cardiac output, stroke volume and ejection time are 100% at 160 bpm.

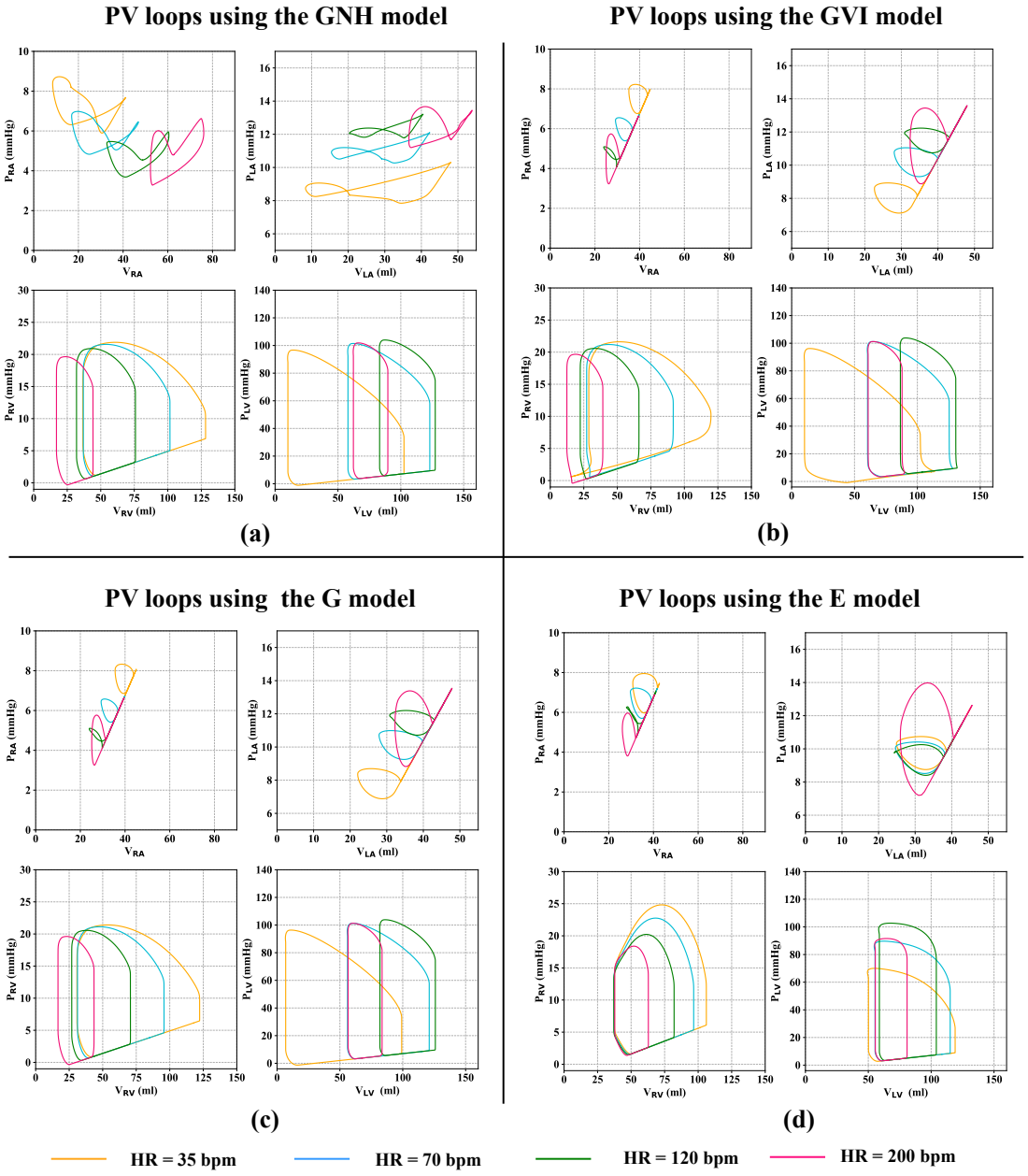

Fig. 3.6 The PV loops of the four compartments of the heart using (a) the GNH model; (b) the GVI model; (c) the G model and (d) the E model. P_{RA}, P_{LA}, P_{RV} and P_{LV} are pressures in the right atrium, left atrium, right ventricle and left ventricle respectively and V_{RA}, V_{LA}, V_{RV} and V_{LV} are volumes in the right atrium, left atrium, right ventricle and left ventricle respectively.

Chapter Summary

In this chapter we developed and validated a mathematical model of the cardiovascular system that can be simulated over a wide range of heart rates. We first simulated a model that contains all the modelling features we introduced in this thesis (called the "full G model") at a constant heart rate of 70 bpm. The model outputs agreed well with physiological values. Then we introduced four sub-models of the full G model, the GNH, the GVI, the G and the E models, to explore the effects of the different modelling features we introduced under variable heart rates. The GNH model was the only model that generated realistic PV loops of the atria but other than this there was little difference between the GNH, GVI and G models. There was a marked difference between the G-based models (GNH, GVI and G) and the E model when the ejection fraction and cardiac output were plotted as a function of heart rate. The G-based models fitted experimental data of mean cardiac output reasonably well up to 200 bpm while at higher heart rates the E model agreed well with the experimental data. The ejection fraction graph was nonlinear with a clear minimum around 170 bpm when generated with the G-based models while the E model generated a nearly linear graph. PV loops using these models had similar trend at different heart rates.

Chapter 4

Parameter Settings

Finding appropriate values for the parameters is an essential part of mathematical modelling but it is often difficult because many of the parameters cannot be directly measured. In this chapter we discuss in detail how we assign values to model parameters.

4.1 Model parameters from the literature

Some of the parameters in our model have already been estimated from the literature. The data we provide below is based on extensive search of the literature.

4.1.1 Values of E_{min} and E_{max}

The time-dependent elasticity function described in chapter 2 requires E_{max} and E_{min} as input values. To find these values for each chamber, simultaneous measurements of pressure and volume are needed. Most of the currently-used methods that measure the heart volume rely on assumptions of the geometric shape of the heart chambers and only give approximate values (Nguyen and Leger, 2002). Magnetic resonance imaging (MRI) and more recently four-dimensional phase-array ultrasound imaging do not rely on geometrical assumptions. However, MRI requires long acquisition times (approximately 10 minutes for one cardiac cycle) and four-D ultrasound imaging is a new technology that is still in its validation phase.

E_{max} and E_{min} in the left ventricle

The left ventricle has been studied widely because of its physiological importance. Rodriguez et al. (2015) used MRI and optical pressure sensors within the left ventricle to generate the pressure volume loop. Two female sheep were used in their study and they reported: $E_{maxLV} =$

1.62 ± 0.19 (mmHg/ml). Bauer et al. (2002) calculated $E_{maxLV} = 2.71 \pm 0.35$ (mmHg/ml) from the pressure-volume loop of four healthy sheep. Ratcliffe et al. (2000) generated the pressure volume graph by using the conductance catheter method in an experiment, in which they used six sheep and calculated the value of maximum elasticity $E_{maxLV} = 2.52 \pm 0.27$ (mmHg/ml). Pilla et al. (2003) used ten sheep in their study and analysed the pressure-volume relationship with MRI. They calculated a slightly higher value of $E_{maxLV} = 3.4$ (mmHg/ml). Segers et al. (2001) calculated an average value of $E_{maxLV} = 1.34$ (mmHg/ml) in sheep by using a model-generated data set. We chose a value of $E_{maxLV} = 2.8$ (mmHg/ml) for the closed-loop models we constructed in Chapter 3, while for the isolated models we chose a value of $E_{maxLV} = 2.5$ (mmHg/ml), both these values are closer to (Bauer et al., 2002).

Values of E_{minLV} can also be evaluated from the pressure-volume relationship by calculating end-diastolic volume (EDV) and end-diastolic pressure (EDP). If we use information provided by Rodriguez et al. (2015), $V_{unv} = 35.13$ (ml), EDV=99.04 (ml) and EDP=10.01 (mmHg), E_{min} is calculated as 0.15 (mmHg/ml). We chose a value of $E_{minLV} = 0.1$ (mmHg/ml), a little lower value than Rodriguez et al. (2015) for both the isolated and closed-loop models. This choice of parameter gave a maximum pressure of P_{LV} = 101 (mmHg) and a maximum volume of V_{LV} = 130 (ml) which are within the physiological range.

E_{max} and E_{min} in the right ventricle

The right ventricle has been studied less than the left ventricle. The pressure volume relationship can also be applied to the right ventricle to calculate the values of E_{maxRV} and E_{minRV}. Yerebakan et al. (2009) used the cardiac catheterization method for the direct beat-to-beat functional analysis of the heart in eighteen sheep. He reported $E_{maxRV} = (0.5 \pm 0.2)$ (mmHg/ml) and $E_{minRV} = (0.3 \pm 0.1)$ (mmHg/ml). For our closed-loop models we chose a higher value of $E_{maxRV} = 1.4$ (mmHg/ml) and $E_{minRV} = 0.07$ (mmHg/ml). We chose these values to get an appropriate ventricular pressure within the physiological range.

E_{max} and E_{min} in the left atrium

The atria have not been studied as much as the ventricles. Therefore less information is available on the atria and all the data we have is from humans. For the left atrium, Dernellis et al. (1998) calculated the value of $E_{maxLA} = (0.61 \pm 0.07)$ (mmHg/ml) which Heldt (2004) also used in his model. To calculate the minimum elastance of the left atrium, Dernellis et al. (1998) performed the echocardiographic method on the human left atrium. He reported the value of $E_{minLA} = (0.5 \pm 0.10)$ (mmHg/ml). We chose the value $E_{minLA} = 0.4$ (mmHg/ml) which is within the range reported by Dernellis et al. (1998) and the value $E_{maxLA} = 0.96$

(mmHg/ml) such that the mitral flow lies within physiological range. We used these values for the closed-loop models we developed in Chapter 3.

E_{max} and E_{min} in the right atrium

Heldt (2004) used the data reported by Lau et al. (1979) and calculated the value of maximum elastance of the right atrium for humans as $E_{maxRA} = 0.74 \pm 0.1$ (mmHg/ml) and $E_{minRA} = 0.3 \pm 0.05$ (mmHg/ml). We use $E_{maxRA} = 0.74$ (mmHg/ml) the same as Lau et al. (1979) and $E_{minRA} = 0.26$ (mmHg/ml) which is within the range reported by Lau et al. (1979).

4.1.2 Total Blood Volume

The total circulating blood volume in a healthy adult sheep is approximately 58-64 ml/kg (Wolfensohn and Lloyd, 2003). The average weight lies within a range of values (45-160) (Fox, 2015). In our model we choose the total blood volume to be 4500 (ml) based on estimates provided to us by our Physiology colleagues at Auckland University.

4.1.3 Unstressed Volume

Unstressed volume is a volume of blood in a vessel at zero transmural pressure (difference in pressure between two sides of a separator) while stressed volume is a volume of blood in a blood vessel when the transmural pressure is above zero. The sum of the stressed and unstressed volume in the circulatory system is equal to the total blood volume (Gelman, 2008).

The unstressed volume of the ventricles

For the E model the ventricular unstressed volume can be estimated from the pressure-volume relationship, it is the volume intercept in the pressure volume graph. We are assuming here that the unstressed volume remains constant throughout the cardiac cycle. Rodriguez et al. (2015) used optical sensors and MRI to obtain the left ventricular measures in sheep and they suggested the value $V_{unv} = (38.49 \pm 3.36)$ (ml). Heldt (2004) suggested $V_{unv} = (46 \pm 21)$ (ml) for the human cardiovascular model. We assume here that the unstressed volume for the left and right ventricle is the same. Our assumption is based on the fact that unstressed volumes are not the influential parameters (see Section 4.4) and to reduce the number of parameters we can merge unstressed volumes of the ventricles. We chose the value $V_{unv} = 30$ (ml) in all our models which seems reasonable for the size of the sheep at Auckland University (70-77Kg) compared with the sheep Rodriguez had (56-60 Kg).

The unstressed volume of the atria

Less information is given in the literature about unstressed volumes of the atria. Alexander et al. (1987) determined the pressure-volume relationship of the left atrium in 10 dogs. He reported the value $V_{una} = 5.84 \pm 2.6$ (ml). Heldt (2004) used in his model the values $V_{una} = 24$ (ml) and $V_{una} = 14 \pm 1$ (ml) for the left and right atrium respectively. Here we assume that the unstressed volumes in the left and right atria are the same and choose the value $V_{una} = 14$ (ml) for all the models. This value reflects the size of a sheep compared to dogs and humans.

4.2 Model parameters from experimental data

In this section, we estimate parameters from experiments in sheep and humans, provided to us by our physiology colleagues at the University of Auckland and the University of Oslo, respectively.

4.2.1 Determining the timings of heart contraction using ECG of humans and sheep

The formulas of the contraction and delay timings have been used in Chapter 2. Here we describe in detail how we extracted key time intervals from the ECG measurements and how they were used to estimate the contraction timings of the heart. We only used extracted values of the RT-interval and PR-interval in our models, but we also extracted the length of the P-wave and QRS-complex to make comparisons between the sheep and human ECG.

Figure 4.1 shows ECG of a sheep where we placed markers at the start and end of important waves. A matlab program has been developed that can automatically detect the timings of the P-wave, QRS-complex, PR-interval, RT-interval and RR-interval (see Appendix A.1). A sample ECG of a sheep is plotted in Figure 4.1 showing the markers placed by the program. Note that the shape of the ECG is different from the one shown in Figure 2.4a due to the position of the measuring electrodes.

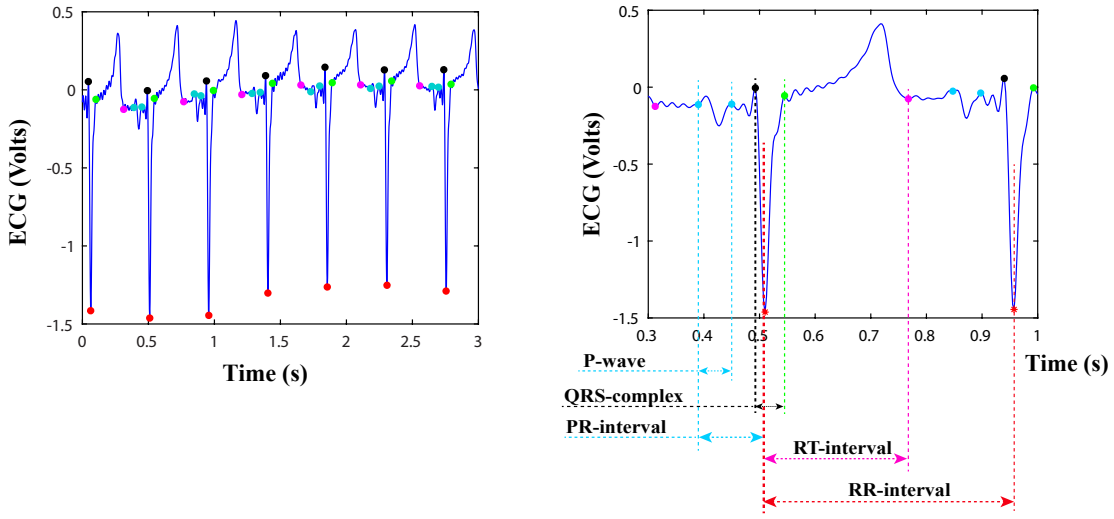

(a) (b)

Fig. 4.1 (a) ECG of a sheep showing six heart periods where the markers are placed at the start and end of important waves. (b) A zoom-in view of (a) showing one heart period and the timing intervals extracted. The shape of the ECG is different from the one shown in Figure 2.4a due to the positions of the measuring electrodes.

The combined data of 14 sheep is plotted in Figure 4.2 and the combined data of 8 humans is shown in Figure 4.3. The lengths of the P-wave (Figures 4.2a and 4.3a) and QRS-complex (Figures 4.2b and 4.3b) do not change much with respect to the RR-interval in both sheep and humans. Therefore, an average value for the P-wave and the QRS-complex can be used. However, the RT-interval (Figures 4.2c and 4.3c) and the delay time (Figures 4.2d and 4.3d) change with the RR-interval, and need to be fitted with some curves.

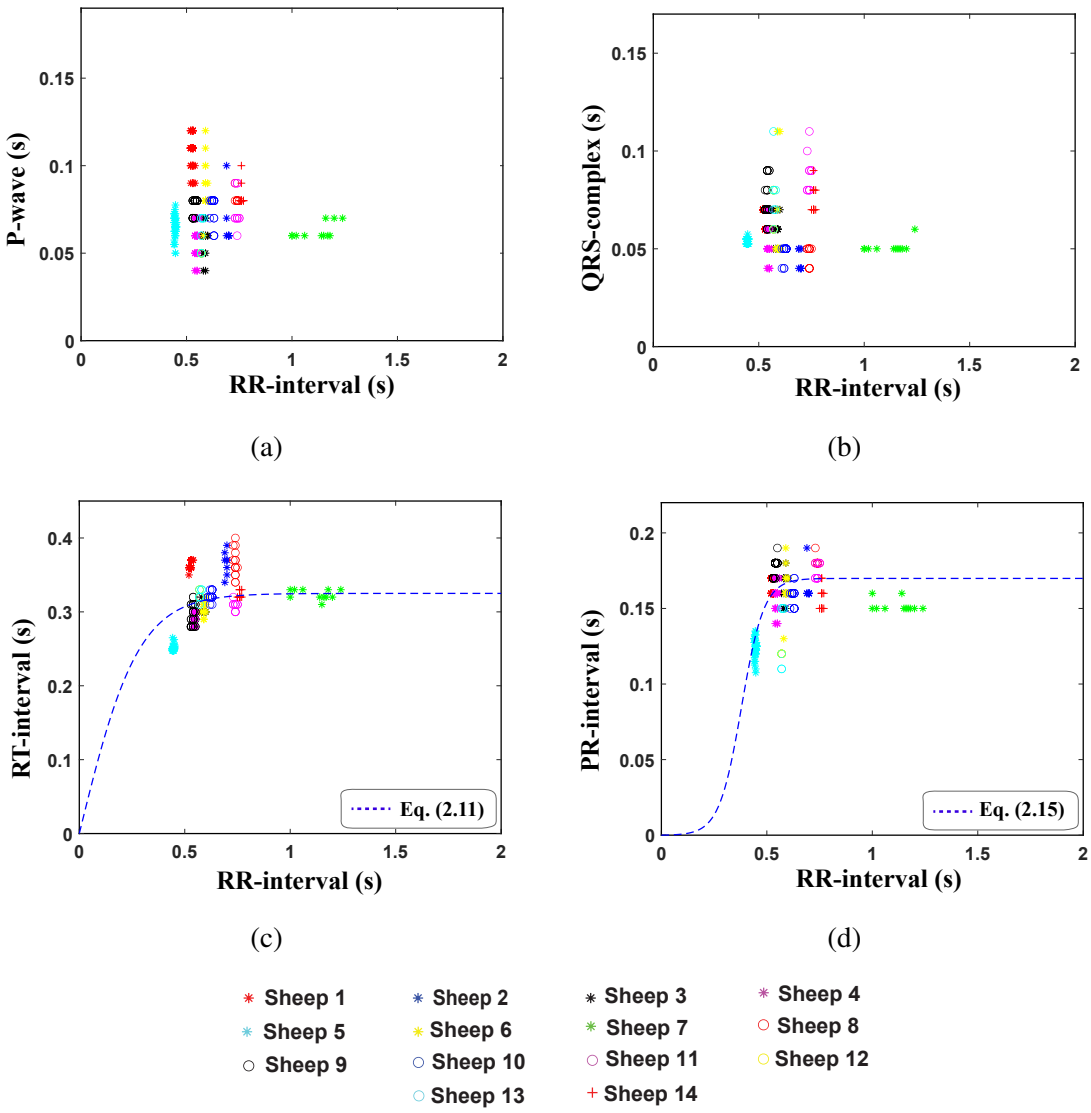

Fig. 4.2 ECG data of 14 sheep: (a) Length of the P-wave as a function of the RR-interval. (b) Length of the QRS-complex as a function of the RR-interval. (c) Length of the RT-interval as a function of the RR-interval. The dashed line is a curve fitting the data (see Eq. (2.11), the contraction time of the ventricle $T_S + T_D$ is estimated by the RT-interval and the heart period T_L is calculated from the RR-interval). (d) Delay (estimated by the PR-interval) as a function of the heart period, calculated from the RR-Interval (see Eq. (2.15)). The dashed line is a curve fitting the data. Figures (c) and (d) are the same as Figures 2.4b and 2.7a and are presented here again for convenience.

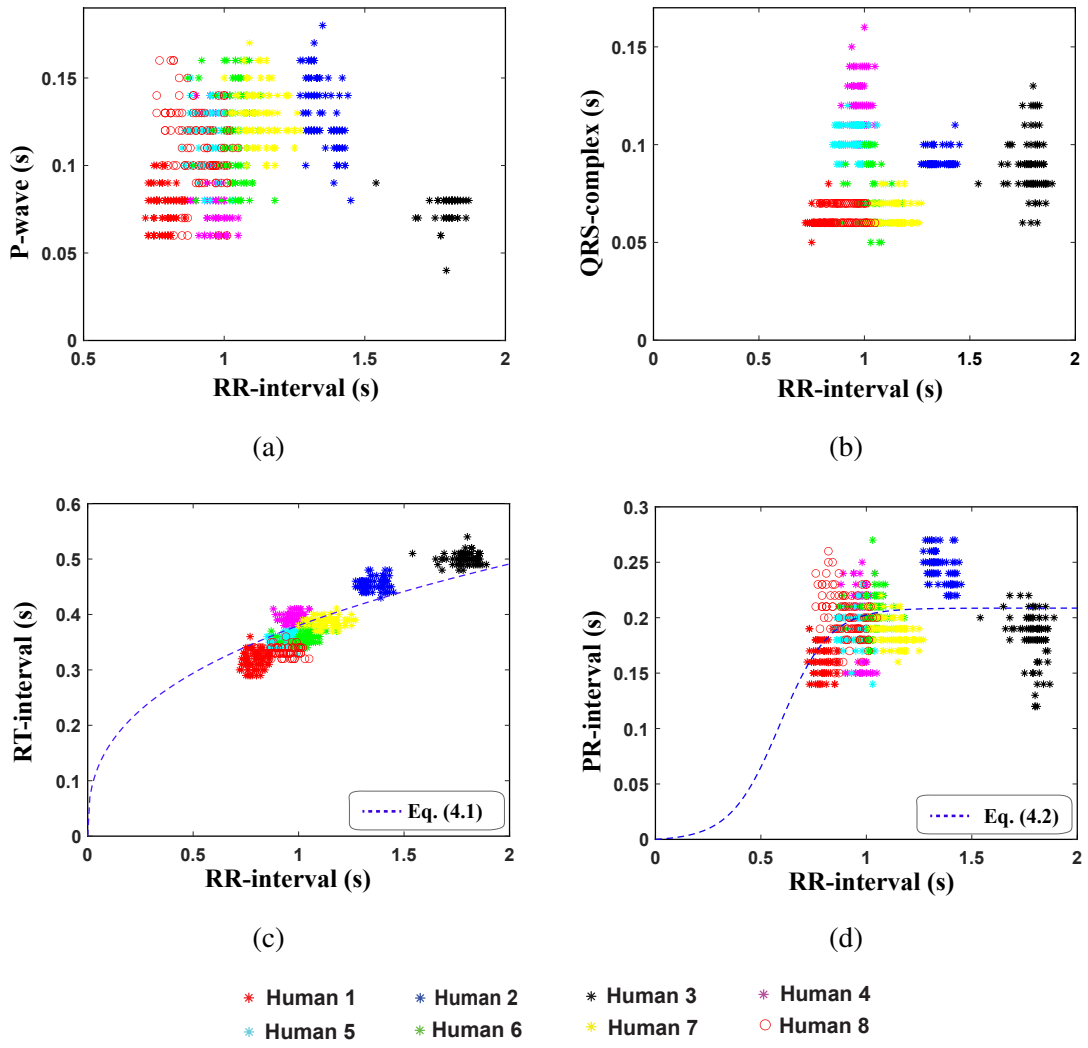

Fig. 4.3 ECG data of 8 humans: (a) Length of the P-wave as a function of the RR-interval. (b) Length of the QRS-complex as a function of the RR-interval. (c) Length of the RT-interval as a function of the RR-interval. The dashed line is a curve fitting the data (see Eq. (4.1), the contraction time of the ventricle, $T_S + T_D$, is estimated by the RT-interval and the heart period T_L is calculated from the RR-interval). (d) Delay (estimated by the PR-interval) as a function of the heart period, calculated from the RR-Interval (see Eq. (4.2)). The dashed line is a curve fitting the data.

Recall that in Chapter 2 we fitted data of the RT-interval and the PR-interval extracted from ECG recordings of 14 sheep by Eqs. (2.11) and (2.15) (see also Figures 4.2c and 4.2d). Here we fit the data of the RT-interval and the PR-interval to the human data (see also Figures

4.3c and 4.3d, $T_S + T_D$ and d are given in seconds).

$$T_S + T_D = 0.38(T_L)^{0.37} \tag{4.1}$$

$$d = \frac{0.21}{(1 + e^{-8.53(T_L - 0.59)})} - 0.0014 \tag{4.2}$$

We also compare important wave lengths detected from the ECG of both humans and sheep. The lengths of the P-wave and QRS-complex in sheep are shorter than in humans as sheep have a slightly faster heart rate than humans. The RT-intervals are fitted by different curves for sheep and humans while for the PR-interval we used the same formula for sheep and humans with different parameters. This comparison is given in Table 4.1.

To compare the heart rate variability of sheep and humans, the RR-interval is plotted as a function of time in Figures 4.4a and 4.4b respectively. On the basis of these measurements we can say that for humans there is more fluctuation in heart rate than sheep but it could be the result of the measurement conditions. For example, perhaps humans were asked to breath deep and slow - conditions that are known to increase RSA. Also, for sheep most of the data is for RR-interval ≤ 0.75 (sec) while for humans the data is for RR-interval ≥ 0.75 (sec).

Table 4.1 Comparison of human and sheep ECG

ECG measurements	Sheep	Humans
P-wave (sec)	0.07	0.11
QRS-complex (sec)	0.06	0.08
RT-interval (sec)	$\frac{0.65}{(1+e^{-7.12T_L})} - 0.33$	$0.38(T_L)^{0.37}$
PR-interval (sec)	$\frac{0.17}{1+e^{-18.83(T_L-0.38)}} - 0.00013$	$\frac{0.21}{1+e^{-8.53(T_L-0.59)}} - 0.0014$

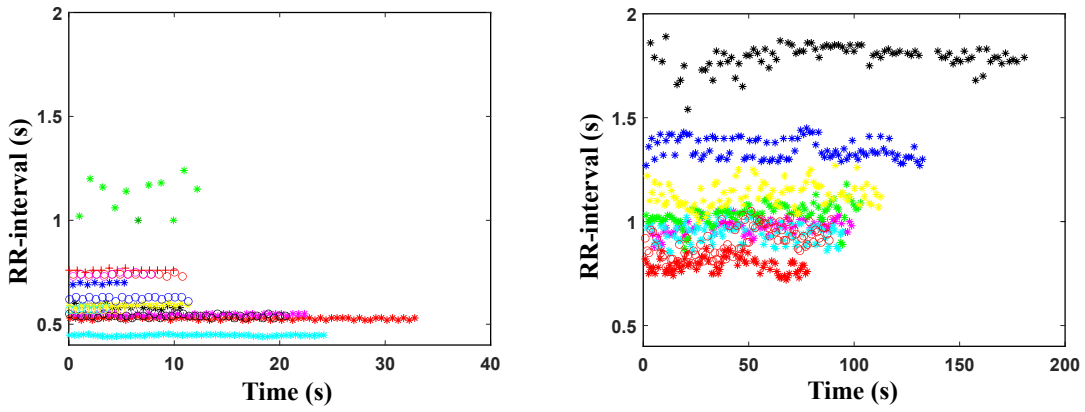

(a) (b)

Fig. 4.4 (a) Heart period as a function of time using ECG measurements of 14 sheep. (b) Heart period as a function of time using ECG measurements of 8 humans.

4.2.2 Comparison of formulae of contraction timing and delay between the atrial and ventricular contractions as functions of the heart period.

In this section, we compare the formulae we proposed in Section 4.2.1 with some other formulae that have been suggested in the literature. The formulae presented in Tables 4.2 and 4.3 were fitted to sheep data and are based on formulae suggested by Bezzet (Eqs. 4.3 and 4.6), Fredricia (Eqs. 4.4 and 4.7) and Framingham (Eqs. 4.5 and 4.8) (Funck-Brentano and Jaillon, 1993). For convenience, we write again the formulae we suggested in Eqs. (2.11) and (2.15). Table 4.2 shows that Eq. (2.11) gives the best fit in terms of the least square error and is also valid for lower T_L (see Figure 4.5a). On the other hand, Eq. (2.15) doesn't give the best fit in terms of the error (see Table 4.3), but it resembles the shape of the data better (Figure 4.5b). Furthermore, when the delay time is added to the contraction time, the formulas we choose to use in this paper are valid for $T_L > 0.23\ (sec)$ while other formulae are valid for $T_L > 0.38\ (sec)$ or $T_L > 0.42(sec)$ (see Figure 4.5c).

Table 4.2 Formulae of the contraction time (estimated by the RT-interval, given in seconds) as a function of heart period, fitted to sheep ECG data.

Eq. No	$RT =$	Error
(4.3)	$0.41\sqrt{T_L}$	0.5124
(4.4)	$0.37(T_L)^{1/3}$	0.4211
(4.5)	$0.38-0.154(1-T_L)$	0.4448
(2.11)	$\frac{0.65}{(1+e^{-7.12T_L})}-0.33$	0.4075

Table 4.3 Formulae of the delay, d, (estimated by the PR-interval, given in seconds) as a function of heart period, fitted to sheep ECG data.

Eq. No	$d =$	Error
(4.6)	$0.21\sqrt{T_L}$	0.0688
(4.7)	$0.19(T_L)^{1/3}$	0.0556
(4.8)	$0.22-0.154(1-T_L)$	0.1057
(2.15)	$\frac{0.17}{(1+e^{-18.83(T_L-0.38)})}-1.33(10^{-4})$	0.0660

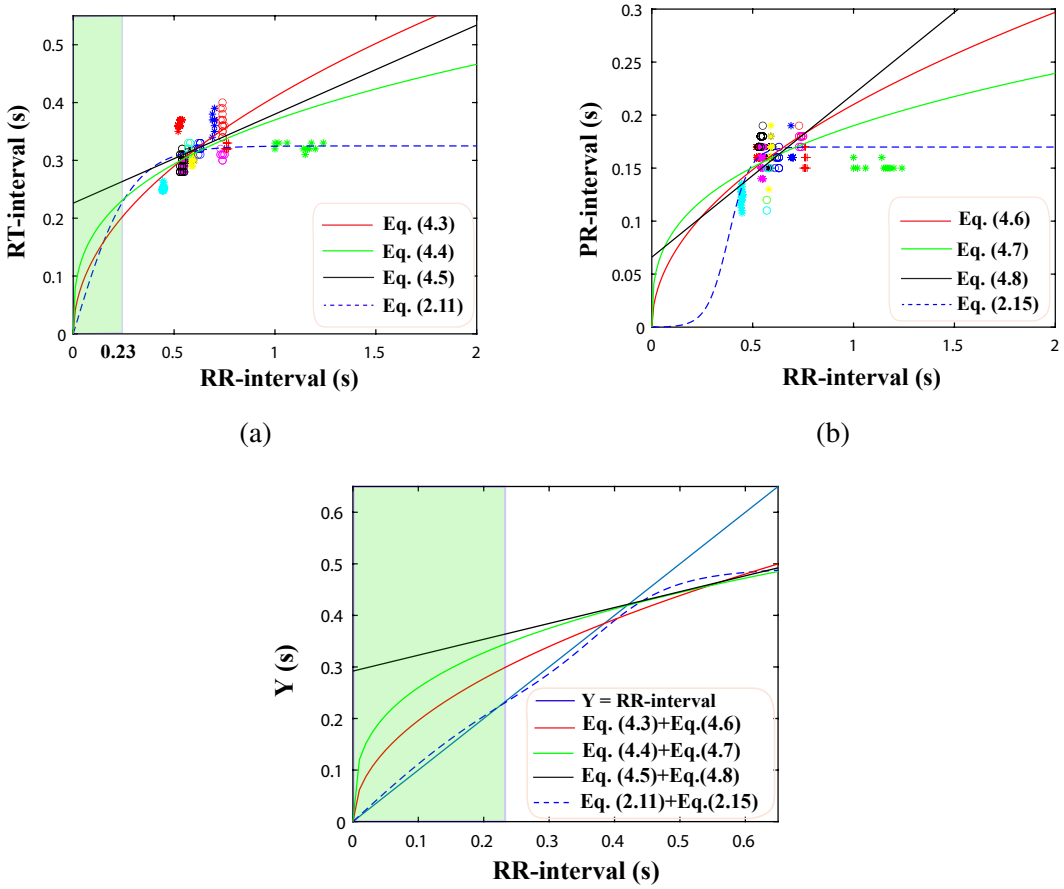

Fig. 4.5 Comparison of formulae. (a) Ventricular contraction (estimated by the RT-interval) as a function of the heart period (T_L, calculated by the RR-interval). (b) Delay time as a function of the RR-interval. (c) The sum of the ventricular contraction and delay timings as a function of the RR-interval. The shaded area shows the region in which the model used in this paper is not valid - this is where the sum of the contraction time (Eq. 2.11) and the delay (Eq. 2.15) are greater than the heart period.

4.2.3 Calculation of Resistance Parameters

To find the value of the resistance when the aortic valve is open, we used systemic arteries pressure, left ventricular pressure and cardiac output data of two sheep. Using Eq. (2.6), we get

$$q = \frac{P_{LV} - P_{SA}}{R_{av}} \Rightarrow R_{av} = \frac{P_{LV} - P_{SA}}{q} \tag{4.9}$$

We first calculated all the resistance values of the aortic valve. In Figure 4.6a, we plotted the data of the cardiac output, left ventricle pressure, systemic arteries pressure and resistance.

We then selected the small values of the resistance where the valve is open, that is where the left ventricular pressure is greater than the systemic arteries pressure and the blood flow is positive. A closer look at Figure 4.6a is shown in Figure 4.6b. The average of all the values of the resistance when the aortic valve is open for sheep 1 and sheep 2 gives a value of 0.02 (mmHg s(ml)$^{-1}$). We use this value for the mitral valve as well. The resistances during the opening of the tricuspid and pulmonary valves have been reported in the literature as (0.005±0.001) and (0.01±0.001), respectively (Heldt, 2004). We assign the same value as reported by Heldt (2004) for the pulmonary valve (0.01 mmHg s (ml)$^{-1}$). While for the tricuspid valve we choose a value of 0.015 (mmHg s (ml)$^{-1}$). This is a lower value than the one we calculated for the aortic valve and was selected such that the right ventricular pressure lies within the physiological range.

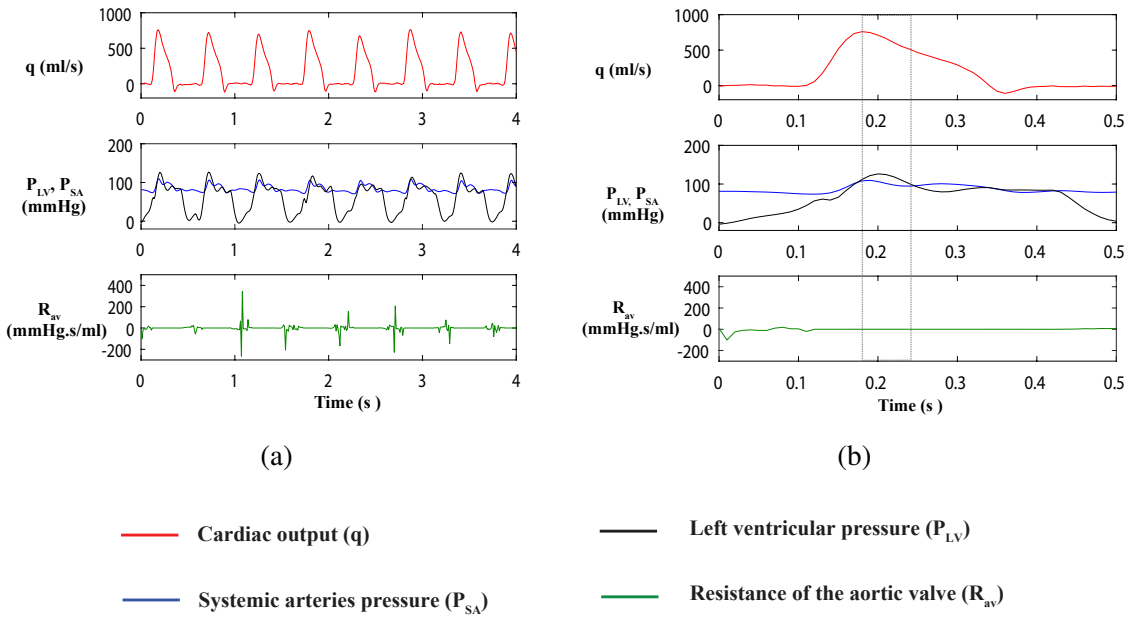

Fig. 4.6 (a) Cardiac output (q), left ventricular pressure (P_{LV}), systemic arteries pressure (P_{SA}) and resistance of the aortic valve (R_{av}) detected from the experimental data (see also Eq. 4.9). (b) A closer look of (a), where the vertical rectangle represents the area where R_{av} is small and blood flow is positive.

4.3 List of Model Parameters

There are some parameters that could not be found in the literature nor calculated from the experimental data. We adjusted the values of these parameters such that the model output

would lie within the physiological range. All the model parameters are listed in Tables 4.4 and 4.5.

Table 4.4 List of parameters representing the heart of a sheep for the isolated models in Chapter 2.

Notation	Description	Value (Units)	Reference
α_L	Parameter in Eq. (2.13)	0.7 (mmHg (ml s)$^{-1}$)	Estimated value
β	Rate constant to switch between opening and closing of the valve	4 (mmHg^{-1})	(Heldt, 2004)
β_L	Parameter in Eq. (2.13)	0.3	Estimated value
E_{maxLA}	Maximum elasticity of the left atrium	0.3 (mmHg (ml)$^{-1}$)	Estimated value to get right shape of the atrial PV loop
E_{minLA}	Minimum elasticity of the left atrium	0.2 (mmHg (ml)$^{-1}$)	Estimated value to get right shape of the atrial PV loop
E_{maxLV}	Maximum elasticity of the left ventricle	2.5 (mmHg (ml)$^{-1}$)	See Section 4.1.1
E_{minLV}	Minimum elasticity of the left ventricle	0.1 (mmHg (ml)$^{-1}$)	See Section 4.1.1
γ_L	Parameter in Eq. (2.13)	1	Estimated value
G_{maxLA}	Maximum pressure of the left atrium applied by $F_{LA}(t)$	2 (mmHg)	Estimated value
G_{maxLV}	Maximum pressure of the left ventricle applied by $F_{LV}(t+d)$	91 (mmHg)	Estimated value such that P_{LV} lies within normal range
mHR	Mean heart rate	70 (bpm)	Experimental data
ω_L	Parameter in Eq. (2.13)	0.1 (mmHg (ml s)$^{-1}$)	Estimated value
P_B	Pressure in the body	77 (mmHg)	Estimated value
P_L	Pressure in the lungs	7 (mmHg)	Estimated value

Continued on next page

Table 4.4 – continued from previous page

Notation	Description	Value (Units)	Reference
P_{LA}	Pressure in the left atrium	11 (mmHg)	Estimated value
R_L	Resistance of the lungs	0.006 (mmHg s $(\text{ml})^{-1}$)	Estimated value
R_{cl}	Resistance when the valve is closed	100 (mmHg s $(\text{ml})^{-1}$)	(Heldt, 2004)
R_{opav}	Resistance when the aortic valve is open	0.02 (mmHg s $(\text{ml})^{-1}$)	See Section 4.2.3
R_{opmv}	Resistance when the mitral valve is open	0.01 (mmHg s $(\text{ml})^{-1}$)	See Section 4.2.3
V_{una}	unstressed volume of the left atrium	14 (ml)	See Section 4.1.3
V_{unv}	Unstressed volume of the left ventricle	30 (ml)	See Section 4.1.3

Table 4.5 List of parameters representing the heart of a sheep for the full G, GNH, GVI, G and the E models in Chapter 3.

Notation	Description	Value (Units)	Reference
α_L	Parameter in Eq. (3.6)	0.5 (mmHg (ml s)$^{-1}$)	Estimated value
α_R	Parameter in Eq. (3.7)	0.6 (mmHg (ml s)$^{-1}$)	Estimated value
β	Rate constant to switch between opening and closing of valve	4 (mmHg^{-1})	(Heldt, 2004)
β_L	Parameter in Eq. (3.6)	0.1	Estimated value
β_R	Parameter in Eq. (3.7)	0.1	Estimated value
C_{PA}	Compliance of pulmonary arteries	3.4 (ml $(\text{mmHg})^{-1}$)	Estimated value such that P_{PA} lies within normal range

Continued on next page

Table 4.5 – continued from previous page

Notation	Description	Value (Units)	Reference
C_{PVn}	Compliance of pulmonary veins	18 (ml (mmHg)$^{-1}$)	Estimated value such that P_{RA} lie within normal range
C_{SA}	Compliance of systemic arteries	1.4 (ml (mmHg)$^{-1}$)	Estimated value such that P_{SA} lies within normal range
C_{SV}	Compliance of systemic veins	60 (ml (mmHg)$^{-1}$)	Estimated value such that P_{LA} lies within normal range
E_{maxLA}	Maximum elasticity of the left atrium	0.96(mmHg (ml)$^{-1}$)	See Section 4.1.1
E_{maxLV}	Maximum elasticity of the left ventricle	2.8 (mmHg (ml)$^{-1}$)	See Section 4.1.1
E_{maxRA}	Maximum elasticity of the right atrium	0.74 (mmHg (ml)$^{-1}$)	See Section 4.1.1
E_{maxRV}	maximum elasticity of the right ventricle	1.4 (mmHg (ml)$^{-1}$)	See Section 4.1.1
E_{minLA}	Minimum elasticity of the left atrium	0.4 (mmHg (ml)$^{-1}$)	See Section 4.1.1
E_{minLV}	Minimum elasticity of the left ventricle	0.1 (mmHg (ml)$^{-1}$)	See Section 4.1.1
E_{minRA}	Minimum elasticity of the right atrium	0.26 (mmHg (ml)$^{-1}$)	See Section 4.1.1
E_{minRV}	Minimum elasticity of the right ventricle	0.07 (mmHg (ml)$^{-1}$)	See Section 4.1.1
γ_L	Parameter in Eq. (3.6)	0.1	Estimated value
γ_R	Parameter in Eq. (3.7)	0.92	Estimated value
G_{maxLA}	Maximum pressure of the left atrium applied by $F_{LA}(t)$	5.2 (mmHg)	Estimated value such that P_{LA} lies within normal range

Continued on next page

Table 4.5 – continued from previous page

Notation	Description	Value (Units)	Reference
G_{maxLV}	Maximum pressure of the left ventricle applied by $F_{LV}(t+d)$	98.3 (mmHg)	Estimated value such that P_{LV} lies within normal range
G_{maxRA}	Maximum pressure of the right atrium applied by $F_{RA}(t)$	2.5 (mmHg)	Estimated value such that P_{RA} lies within normal range
G_{maxRV}	Maximum pressure of the right ventricle applied by $F_{RV}(t+d)$	20.2 (mmHg)	Estimated value such that P_{RV} lies within normal range
Hys	Parameter in Eq. (2.10)	4.5 (mmHg)	Estimated value
mHR	Mean heart rate	70 (bpm)	Experimental data
ω_L	Parameter in Eq. (3.6)	0.2 (mmHg (ml s)$^{-1}$)	Estimated value
ω_R	Parameter in Eq. (3.7)	0.2 (mmHg (ml s)$^{-1}$)	Estimated value
R_{cl}	Resistance when valve is closed	100 (mmHg s (ml)$^{-1}$)	(Heldt, 2004)
R_{opav}	Resistance when the aortic valve is open	0.02 (mmHg s (ml)$^{-1}$)	See Section 4.2.3
R_{opmv}	Resistance when the mitral valve is open	0.02 (mmHg s (ml)$^{-1}$)	See Section 4.2.3
R_{oppv}	Resistance when the pulmonary valve is open	0.01 (mmHg s (ml)$^{-1}$)	See Section 4.2.3
R_{optv}	Resistance when the tricuspid valve is open	0.015 (mmHg s (ml)$^{-1}$)	See Section 4.2.3
R_{PA}	Resistance of the pulmonary arteries	0.01 (mmHg s (ml)$^{-1}$)	Estimated value such that P_{PA} lies within normal range

Continued on next page

Table 4.5 – continued from previous page

Notation	Description	Value (Units)	Reference
R_{PVn}	Resistance of the pulmonary veins	0.006 (mmHg s $(ml)^{-1}$)	Estimated value such that CO lies within normal range
R_{SA}	Resistance of the Systemic arteries	0.9 (mmHg s $(ml)^{-1}$)	Estimated value such that P_{SA}, CO lie within normal range
R_{SVn}	Resistance of the systemic veins	0.01 (mmHg s $(ml)^{-1}$)	Estimated value such that CO lies within normal range
V_{total}	Total volume of blood	4500 (ml)	See Section 4.1.2
V_{una}	Unstressed volume of atria	14 (ml)	See Section 4.1.3
V_{unv}	Unstressed volume of ventricles	30 (ml)	See Section 4.1.3
V_{unpa}	Unstressed volume of pulmonary arteries	139 (ml)	Estimated value
V_{unpv}	Unstressed volume of pulmonary veins	374 (ml)	Estimated value
V_{unsa}	Unstressed volume of systemic arteries	675 (ml)	Estimated value
V_{unsv}	Unstressed volume of systemic veins	2327 (ml)	Estimated value

4.4 Sensitivity analysis

The sensitivity of the full G model is studied by varying one parameter at a time, solving the differential equations and measuring how the pressures and volumes change with such a deviation. Let x_0 be the parameter being perturbed, q the perturbation and y the model output (pressure or volume). We use the L_1 norm to measure the difference between two perturbed signals:

$$L_1(y) = \int_0^{20T_L} \mid y((1+q)x_0) - y((1-q)x_0) \mid dt, \tag{4.10}$$

where T_L is the heart period. We chose to integrate over $20T_L$, a period of time that seemed long enough to average numerical errors, and performed the calculation after steady state has been achieved. The L_1 norm of the deviation is normalized by the L_1 norm of the unperturbed signal:

$$m(y) = \int_0^{20T_L} \mid y(x_0) \mid dt. \tag{4.11}$$

We divide $L_1(y)$ by 2 to get the perturbation in one direction and multiply by 100 to get the sensitivity as a percentage:

$$s(y) = (100)\frac{1}{2}\left(\frac{L_1(y)}{m(y)}\right) \tag{4.12}$$

Our analysis when we perturbed each parameter by $\pm 10\%$ is presented in Tables 4.6 and 4.7. It shows that V_{total} and V_{unsv} are the most sensitive parameters. A change of 10% in V_{total} changes the pressure in the right atrium by 71% and the volume of the right ventricle by 84%. A change of 10% in V_{unsv} changes the pressure in the right atrium by 36% and the volume of the right ventricle by 43%. The model outputs are also sensitive to change in the parameters V_{unsa}, G_{maxRV}, G_{maxLV}, C_{SV}, V_{unpv} and V_{unpa}, changing the output by up to $\pm 11\%$ in some cases. Changing other parameters by $\pm 10\%$ does not have significant effect on the model output and the atrial PV loops still preserve their shapes. Figure 4.7 shows shifts in the PV loops of the four heart chambers when we perturbed the most sensitive parameters by $\pm 5\%$, however, the shapes of the PV loops remain the same.

Table 4.6 Perturbation as a percentage of model outputs when parameters were changed by $\pm 10\%$. $s(y)$ was calculated when $q = 0.1$ and $T_L = 60/70$ (see Eq. 4.12), y is one of the pressures in the full G model (see Figure 3.1 chapter 3) and x_0 is the parameter perturbed.

x_0	$s(P_{LV})$	$s(P_{LA})$	$s(P_{RV})$	$s(P_{RA})$	$s(P_{SA})$	$s(P_{SVn})$	$s(P_{PA})$	$s(P_{PVn})$
E_{minLA}	0.11	0.24	0.16	0.19	0.05	0.17	0.12	0.14
E_{minLV}	0.73	0.95	1.17	1.31	0.34	1.11	0.81	0.89
E_{minRA}	0.09	0.22	0.30	0.58	0.02	0.08	0.20	0.21
E_{minRV}	0.26	0.61	1.97	1.85	0.04	1.61	0.60	0.59
G_{maxLA}	0.08	0.16	0.03	0.05	0.04	0.04	0.08	0.10
G_{maxLV}	8.20	6.49	1.62	2.47	8.23	3.18	4.97	5.88
G_{maxRA}	0.07	0.17	0.19	0.85	0.01	0.55	0.16	0.16
G_{maxRV}	3.88	9.32	7.98	7.59	0.88	6.55	8.55	9.01
C_{SA}	0.96	2.08	1.35	1.24	1.69	0.93	1.71	1.93
C_{SV}	1.46	3.45	5.21	6.36	0.50	5.64	3.10	3.31
C_{PA}	0.15	0.31	0.94	1.10	0.03	0.96	0.55	0.31
C_{PV}	0.58	1.52	2.67	3.25	0.21	2.87	1.37	1.46
R_{SA}	2.31	3.82	1.66	3.30	3.13	3.64	2.81	3.41
R_{SV}	0.05	0.12	0.50	0.85	0.01	0.38	0.11	0.12
R_{PA}	0.58	1.41	0.96	1.16	0.13	1.00	0.99	1.37
R_{PV}	0.07	0.34	0.08	0.10	0.01	0.09	0.13	0.14
R_{opmv}	0.27	0.28	0.04	0.02	0.02	0.01	0.24	0.26
R_{opav}	0.32	0.51	0.13	0.21	0.65	0.26	0.39	0.46
R_{optv}	0.05	0.13	0.54	0.34	0.01	0.23	0.12	0.13
R_{pv}	0.73	1.77	1.33	1.45	0.17	1.25	1.62	1.71
V_{total}	16.38	38.77	58.85	71.42	5.65	63.33	34.90	37.22
V_{una}	0.11	0.25	0.37	0.45	0.04	0.40	0.22	0.24
V_{unv}	0.11	0.26	0.39	0.48	0.04	0.42	0.24	0.25
V_{unsa}	2.46	5.82	8.83	10.71	0.85	9.50	5.24	5.59
V_{unsv}	8.46	20.03	30.41	36.90	2.92	32.72	18.03	19.23
V_{unpa}	0.51	1.20	1.82	2.21	0.18	1.96	1.08	1.15
V_{unpv}	1.37	3.23	4.91	5.95	0.47	5.28	2.91	3.11
α_L	0.06	0.11	0.09	0.11	0.02	0.10	0.07	0.08
β_L	0.03	0.11	0.09	0.11	0.01	0.09	0.10	0.11
γ_L	0.02	0.07	0.10	0.12	0.00	0.10	0.04	0.04
ω_L	0.02	0.06	0.05	0.06	0.00	0.05	0.06	0.06
α_R	0.04	0.11	0.22	0.32	0.01	0.10	0.10	0.10
β_R	0.00	0.01	0.02	0.19	0.00	0.14	0.01	0.01
γ_R	0.00	0.02	0.07	0.69	0.01	0.48	0.02	0.02
ω_R	0.00	0.01	0.03	0.20	0.00	0.15	0.01	0.01

Table 4.7 Perturbation as a percentage of model outputs when parameters were changed by $\pm 10\%$. $s(y)$ was calculated when $q = 0.1$ and $T_L = 60/70$ (see Eq. 4.12), y is one of the volumes in the full G model (see Figure 3.1 Chapter 3) and x_0 is the parameter perturbed.

x_0	$s(V_{LV})$	$s(V_{LA})$	$s(V_{RV})$	$s(V_{RA})$	$s(V_{SA})$	$s(V_{SVn})$	$s(V_{PA})$	$s(V_{PVn})$
E_{minLA}	0.25	4.18	0.23	0.01	0.01	0.03	0.03	0.05
E_{minLV}	6.67	0.69	1.65	0.05	0.05	0.16	0.19	0.32
E_{minRA}	0.21	0.02	0.43	2.90	0.01	0.01	0.05	0.08
E_{minRV}	0.55	0.21	5.78	0.94	0.01	0.24	0.14	0.21
G_{maxLA}	0.19	1.48	0.05	0.01	0.01	0.01	0.02	0.04
G_{maxLV}	8.27	5.96	2.26	0.78	1.10	0.47	1.13	2.07
G_{maxRA}	0.15	0.04	0.28	4.55	0.00	0.08	0.04	0.06
G_{maxRV}	8.52	0.71	8.52	0.30	0.12	0.96	1.95	3.17
C_{SA}	2.20	1.02	2.05	0.18	1.51	0.14	0.39	0.68
C_{SV}	3.47	0.00	7.45	0.19	0.07	0.64	0.71	1.17
C_{PA}	0.32	1.62	1.28	0.01	0.01	0.14	2.34	0.11
C_{PV}	1.40	3.40	3.79	0.01	0.03	0.42	0.31	3.01
R_{SA}	5.18	4.10	2.12	0.52	0.42	0.53	0.64	1.20
R_{SV}	0.12	0.03	0.69	1.89	0.00	0.06	0.03	0.04
R_{PA}	1.27	1.12	1.22	0.02	0.02	0.15	0.23	0.48
R_{PV}	0.15	2.09	0.09	0.01	0.00	0.02	0.03	0.05
R_{opmv}	0.60	0.31	0.10	0.02	0.00	0.00	0.06	0.09
R_{opav}	0.72	0.45	0.18	0.07	0.09	0.04	0.09	0.16
R_{optv}	0.14	0.02	0.74	0.34	0.00	0.04	0.03	0.05
R_{pv}	1.61	0.46	1.70	0.03	0.02	0.18	0.37	0.60
V_{total}	39.07	0.02	84.18	0.00	0.76	9.26	7.94	13.10
V_{una}	0.25	5.00	0.53	4.43	0.01	0.06	0.05	0.08
V_{unv}	2.53	0.00	0.56	0.00	0.01	0.06	0.06	0.09
V_{unsa}	5.87	0.00	12.63	0.00	8.55	1.39	1.19	1.97
V_{unsv}	20.19	0.01	43.49	0.00	0.39	3.75	4.10	6.77
V_{unpa}	1.21	0.00	2.60	0.00	0.03	0.29	7.48	0.41
V_{unpv}	3.26	0.00	7.02	0.00	0.07	0.77	0.66	5.41
α_L	0.13	2.95	0.13	0.00	0.00	0.01	0.02	0.03
β_L	0.06	2.87	0.13	0.00	0.00	0.01	0.02	0.04
γ_L	0.04	1.70	0.13	0.00	0.00	0.02	0.01	0.02
ω_L	0.04	1.54	0.07	0.00	0.00	0.01	0.01	0.02
α_R	0.11	0.00	0.31	3.11	0.00	0.01	0.02	0.04
β_R	0.00	0.01	0.03	1.63	0.00	0.02	0.00	0.00
γ_R	0.01	0.02	0.09	5.71	0.00	0.07	0.00	0.01
ω_R	0.00	0.01	0.04	1.84	0.00	0.02	0.00	0.00

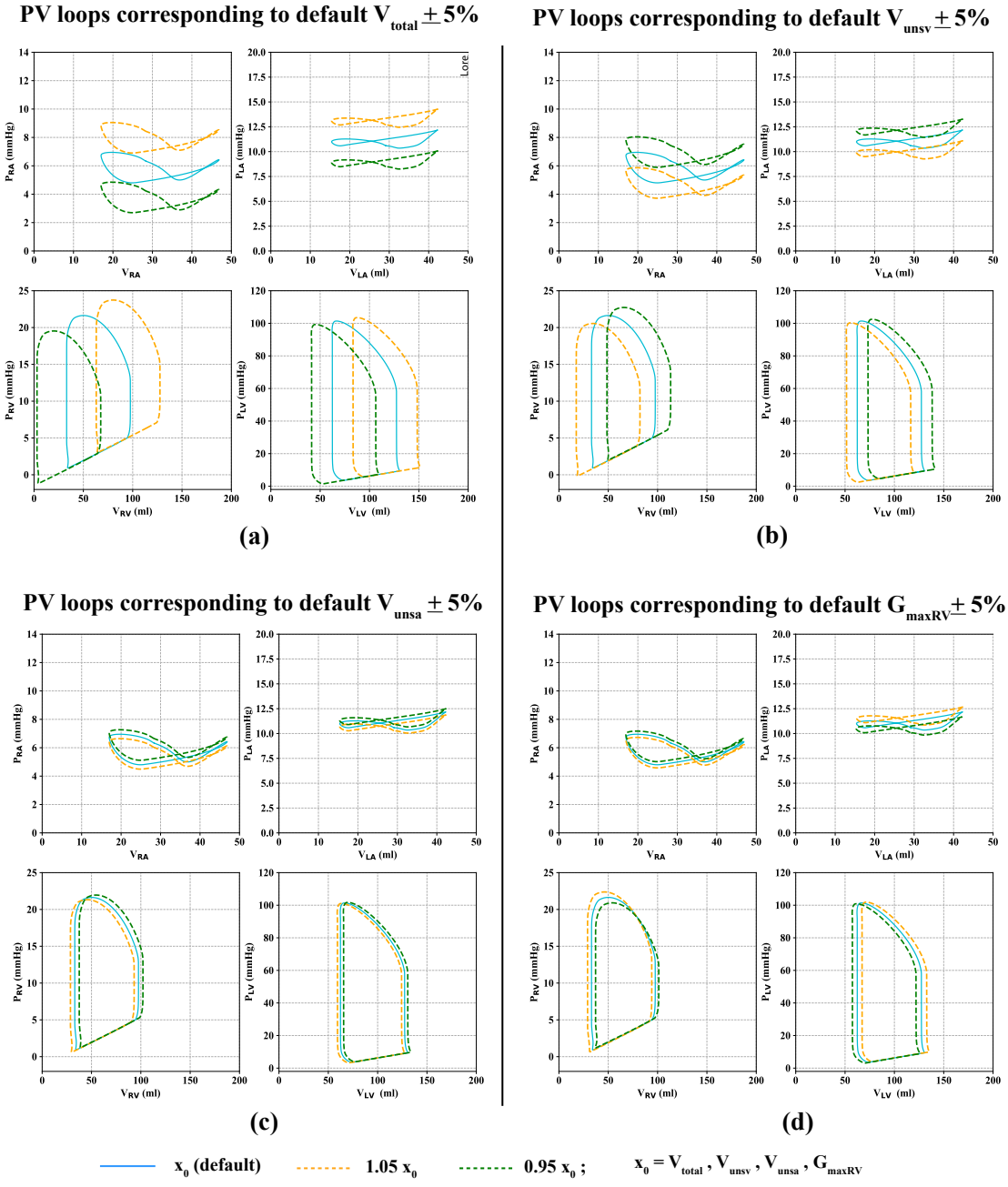

Fig. 4.7 The PV loops of the four compartments of the heart using the full G model corresponding to ±5% perturbation of parameters: (a) V_{total} (b) V_{unsv} (c) V_{unsa} and (d) G_{maxRV}.

Chapter Summary

In this chapter, we discussed in detail how we found parameter values for the cardiovascular models. Some of the parameters were taken from the literature and some were calculated from ECG, pressures and blood flow measurements. The remaining parameters were estimated in this thesis such that the model outputs were within the physiological range. We presented two tables that list all the parameter values along with a reference to how they were obtained. We compared the ECG data of sheep and humans by detecting timings of key intervals and suggested new relations for the contraction timing of sheep and delay timing for both sheep and humans. Furthermore, we compared the newly introduced formulas of sheep with already existed formulas in the literature. We also studied the sensitivity of the full G model to changes in parameters by varying one parameter at a time and measuring the resulting changes in the pressure and volumes. Our analyses have shown that V_{total} and V_{unsv} are the most sensitive parameters. These two parameters had the largest effect on the PV loops of the four cardiac chambers in response to $\pm 5\%$ perturbation.

Chapter 5

Effects of respiratory sinus arrhythmia

Respiratory sinus arrhythmia (RSA) is a fluctuation of heart rate with breathing and serves as an index of a healthy heart. A number of physiological benefits of RSA have been suggested. For example, it has been proposed that RSA increases pulmonary gas exchange, minimizes the work done by the heart while maintaining physiological levels of arterial CO_2 or stabilizes the arterial blood pressure and the systemic blood flow. In this chapter, we use our models to simulate the effects of RSA on the mean cardiac output, blood pressure and blood flow. We further modify our models to incorporate two potential sources of RSA. We introduce a periodic heart rate to mimic central control of heart rate in the brainstem as well as a periodic systemic vein resistance to mimic one possible effect of the pleural pressure (the pressure that drives breathing).

5.1 Model modifications

In this section, we introduce periodic functions for the heart rate and the systemic vein resistance. We also include the ventricular interactions in the E model and call it the "EVI" model.

5.1.1 Periodic heart rate

On a beat-by-beat basis, the heart rate is not constant, but rather it has periodic fluctuations. The basic heart rate is determined by the sinoatrial (SA) node - the pacemaker of the heart, but the pacemaker is under autonomic control from the brainstem. The brainstem regulates HR by either speeding it up or slowing it down. We include this fact in our model by changing

the heart period, T_L with time. For this we introduce a periodic heart rate function.

$$HRf(t) = meanHR - \frac{amp}{2}\cos\left(\frac{2\pi}{60}BFt\right) \tag{5.1}$$

where *meanHR* is the mean heart rate in beats per minute (bpm), *amp* is the *RSA* amplitude (bpm) measured as the difference between the maximum HR and the minimum HR and *BF* is the breathing frequency (breaths per minute). We then calculate the function $T_L = 60/HRf$ which is needed as an input to the heart model. At time $t = 0$, $T_L = T_{L1}$, at $t = T_{L1}$, $T_L = T_{L2}$ and so on. If we take the values: meanHR=72 (bpm), RSA amplitude=30 (bpm) and BF = 12 breaths/min, we get the following graphs.

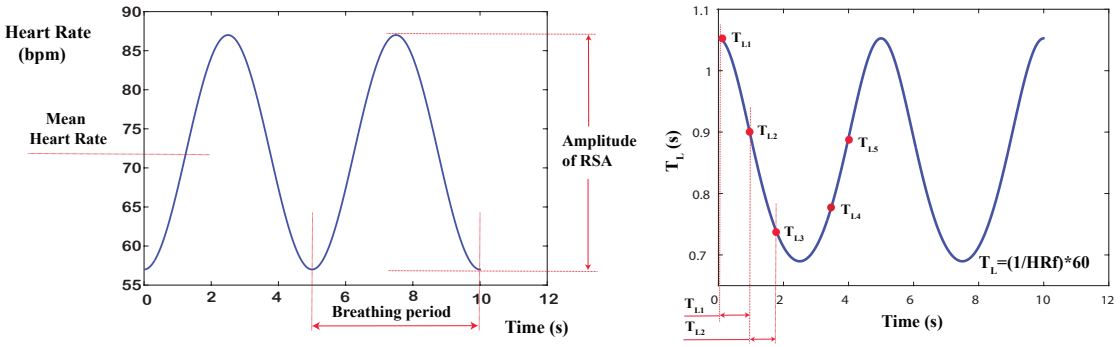

(a) (b)

Fig. 5.1 (a) Heart rate function. (b) Heart rate period, T_L (RR-interval). At time t=0, $T_L = T_{L1}$ is provided as an input to the heart model, at time $t = T_{L1}$, $T_L = T_{L2}$ is provided as an input to the heart model and so on.

5.2 Periodic systemic vein resistance

The lung is surrounded by the pleural space and inspiration is driven in part by a change in the pleural pressure. At normal breathing, the pleural pressure is negative, that is, it is below the atmospheric pressure. During inspiration, the pleural pressure becomes more negative which causes the expansion of the lungs, right atrium, right ventricle, thoracic superior and inferior vena cava. We model this effect by changing the resistance of the systemic veins (R_{SV}) with breathing according to the function below

$$R_{SV}(t) = R_{SV0} + \frac{ampR_{SV}}{2}\cos\left(\frac{2\pi}{60}BFt\right) \tag{5.2}$$

R_{SV0} is the mean value of the resistance, amp_{SV} is the amplitude of $R_{SV}(t)$ measured between the maximum and the minimum value of $R_{SV}(t)$ and BF is the breathing frequency (breaths per minute). The periodic function of R_{SV} is shown in Figure 4.2. During inspiration the resistance in the systemic veins falls down and an opposite effect occurs in case of expiration. Therefore, the HR function is also plotted along with the systemic veins resistance to show that difference in phase.

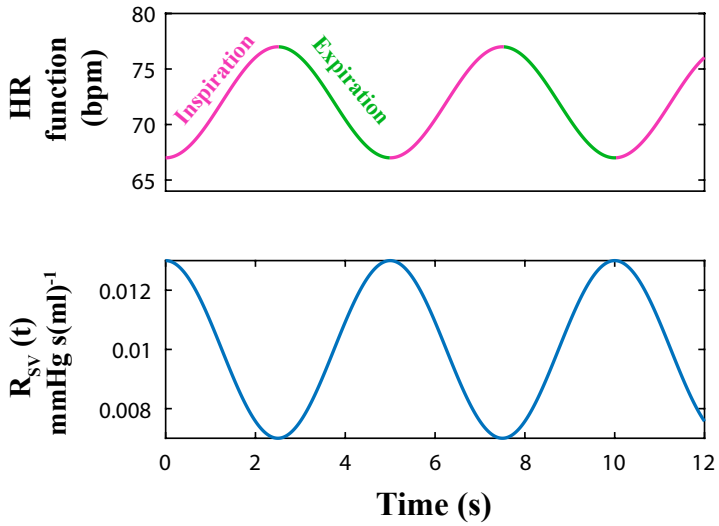

Fig. 5.2 Changes in heart rate and the systemic veins resistance with breathing. The heart rate (top panel) increases during inspiration while the systemic resistance decreases during this time. The top graph was generated by Eq. (5.1) with parameters meanHR = 72 bpm, amp = 10 bpm and BF = 12 breath/pm, and the bottom graph was generated with Eq. (5.2) and parameters R_{SV0} = 0.01, $ampR_{SV}$ = 0.006 and Bf = 12 breaths/m.

5.3 The EVI model

Recall that in Section 3.3, we described the E model and its governing equations. We did not include the new hypothesis (i.e., the new equations we introduced in Section 2.2 that generate a realistic PV loop for the atrium) and the inter-ventricular interactions in the E model. Here we write the equations of the E model with ventricular interactions and call it the "EVI" model. We add the EVI model to check if the use of this model could change our conclusions regarding the effects of respiratory sinus arrhythmia.

The EVI model is the same as the E model but with the ventricular inter-dependence. The EVI model consists of Eqs. (3.1-3.5), (3.19) and (3.20). The left and right atrial pressures

are given by Eqs. (3.28) and (3.29), while the pressure in the left and right ventricles are expressed by

$$\frac{dP_{LV}}{dt} = \frac{1}{\frac{1}{S}(S+\frac{1}{E_{RV}(t)})(S+\frac{1}{E_{LV}(t)})-S}\left[\frac{P_{RA}-P_{RV}}{R_{tv}} - \frac{P_{RV}-P_{PA}}{R_{pv}} + \left(1+\frac{1}{SE_{RV}(t)}\right)\left(\frac{P_{LV}}{E_{LV}^2(t)}\frac{dE_{LV}(t)}{dt} + \frac{P_{LA}-P_{LV}}{R_{mv}} - \frac{P_{LV}-P_{SA}}{R_{av}}\right) + \frac{P_{RV}}{E_{RV}^2(t)}\frac{dE_{RV}(t)}{dt}\right] \tag{5.3}$$

$$\frac{dP_{RV}}{dt} = \frac{1}{\frac{1}{S}(S+\frac{1}{E_{RV}(t)})(S+\frac{1}{E_{LV}(t)})-S}\left[\frac{P_{LA}-P_{LV}}{R_{mv}} - \frac{P_{LV}-P_{SA}}{R_{av}} + \left(1+\frac{1}{SE_{LV}(t)}\right)\left(\frac{P_{RV}}{E_{RV}^2(t)}\frac{dE_{RV}(t)}{dt} + \frac{P_{RA}-P_{RV}}{R_{tv}} - \frac{P_{RV}-P_{PA}}{R_{pv}}\right) + \frac{P_{LV}}{E_{LV}^2(t)}\frac{dE_{LV}(t)}{dt}\right] \tag{5.4}$$

where S is a function of the pressure difference $P_{LV}-P_{RV}$ (see Eq. 2.28). R_{mv}, R_{av}, R_{tv} and R_{pv} are functions of the pressures (see equations 4.9 and 2.10). E_LV and E_{RV} are given by Eq. (3.29). The derivative of the function $E_X(t)$, used in Eqs. (5.3) and (5.4) is described by

$$\frac{dE_X(t)}{dt} = \begin{cases} 0 & 0 < t \leq d \\ \frac{\pi(E_{max_X}-E_{min_X})}{2T_S}\left[\sin(\frac{\pi t}{T_S})\right] & d < t \leq d+T_S \\ \frac{\pi(E_{max_X}-E_{min_X})}{2T_D}\left[\sin(\frac{\pi(t-T_S)}{T_D})\right] & d+T_S < t \leq d+T_S+T_D \\ 0 & d+T_S+T_D < t \leq T_L \end{cases} \tag{5.5}$$

where X can be replaced by LV and RV. The pressures in other compartments are given by Eqs. (3.13-3.16). The volume in the left and right ventricles is given by

$$V_{LV} = \frac{P_{LV}}{E_{LV}} + V_{unlv} + \frac{1}{E_S}Z \tag{5.6}$$

$$V_{RV} = \frac{P_{RV}}{E_{RV}} + V_{unrv} - \frac{1}{E_S}Z \tag{5.7}$$

where Z is a nonlinear function of the pressure difference and its expression is given by Eq. (2.22).

5.4 Studying the effects of RSA on mean cardiac output

In this section, we investigate the effects of RSA on mean cardiac output (CO) using the E, EVI, GNH and full G models. Figures 5.3a and 5.3c show the effects of RSA when it

is mimicked by periodic HR. First we show the cardiac output against different values of *amp* in Eq. (5.1) for three distinct mean heart rates when the breathing frequency is constant. Then we keep the value of *amp* constant and vary the breathing frequency. In Figures 5.3b and 5.3d we report the impacts of RSA when it is mimicked by periodic R_{SV} on mean cardiac output. We first show the mean cardiac output for different values of $ampR_{SV}$ in Eq. (5.2) while keeping the breathing frequency fixed. Then we vary the breathing frequency while keeping $ampR_{SV}$ constant. In Figure 5.4 we show the mean cardiac output when the periodic HR and R_{SV} are combined. Figures 5.5a and 5.5b compare the stroke volume of the left ventricle in the presence of periodic HR and periodic R_{SV} using the E and GNH models respectively.

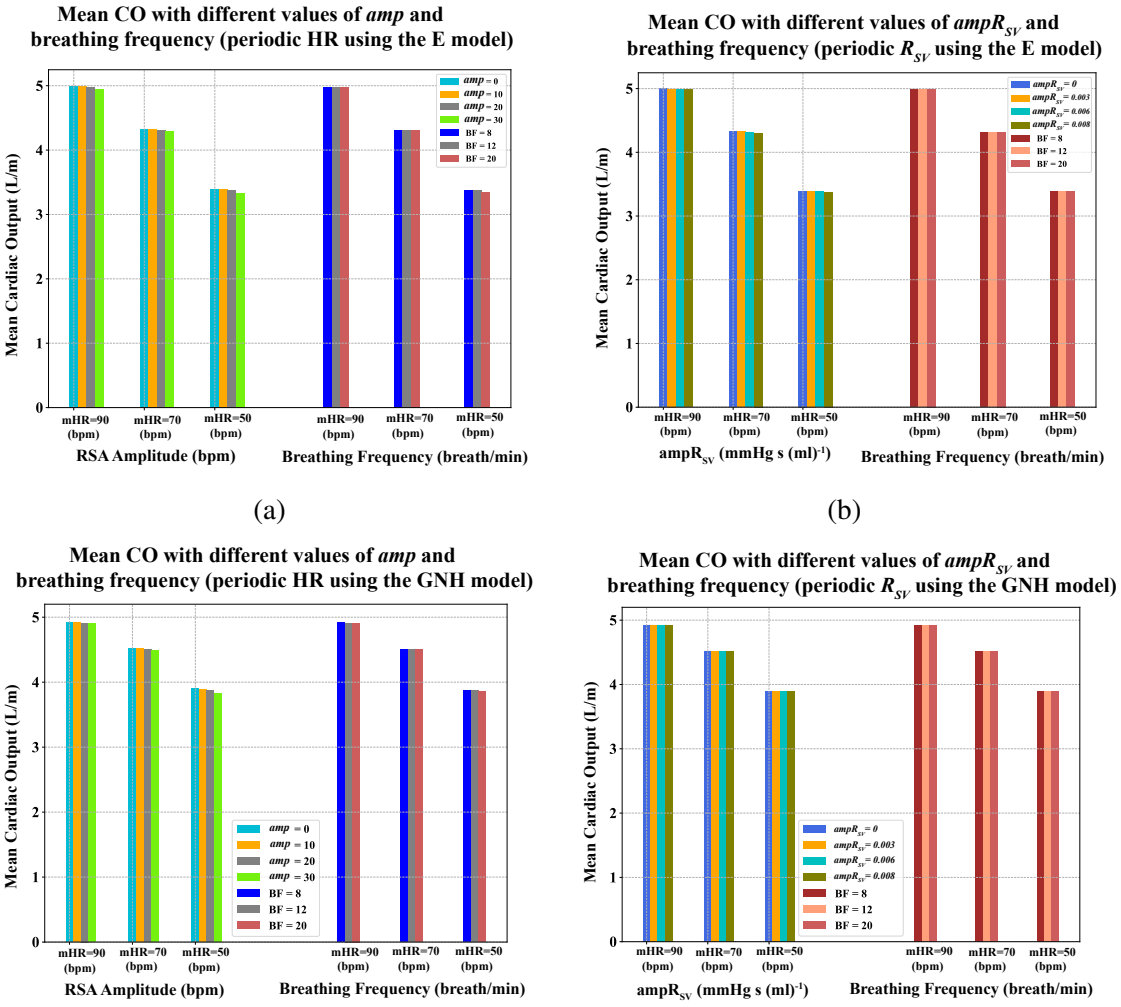

Fig. 5.3 The mean cardiac output calculated with periodic HR (panels a and c) or with periodic R_{SV} (panels b and d). When the value of *amp* is changed, the breathing frequency is kept constant at 12 breaths/m and when the breathing frequency is changed, the value of *amp* is kept constant at 20 bpm. When the value of $ampR_{SV}$ is changed the breathing frequency is kept at constant at 12 breaths/m and when the breathing frequency is changed, the value of $ampR_{SV}$ is kept at constant at 0.006 mmHg s $(\text{ml})^{-1}$. The results are generated using the E model (panel a and b) or the GNH model (panel c and d).

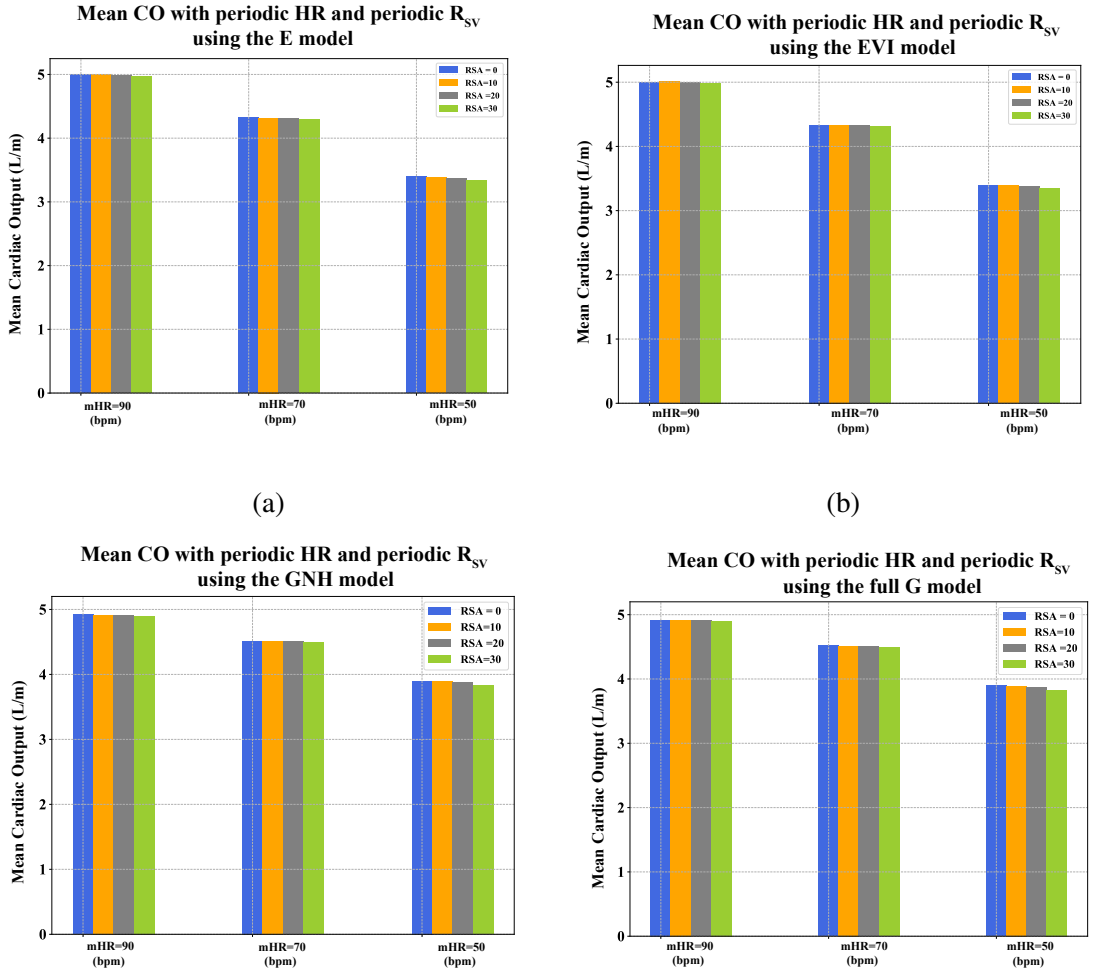

Fig. 5.4 The mean cardiac output calculated using both periodic heart rate and periodic R_{SV}. The values of breathing frequency and amplitude of the resistance oscillation are kept constant at 12 breaths/m and 0.006 mmHg s $(\text{ml})^{-1}$ respectively and the RSA amplitude is changed. The results are generated using: (a) the E model; (b) the EVI model; (c) the GNH model; (d) the full G model.

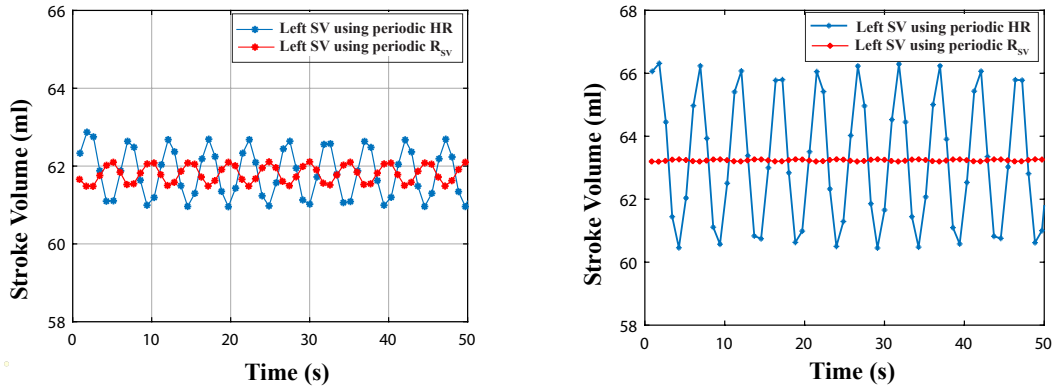

(a) (b)

Fig. 5.5 The effects of periodic HR and periodic R_{SV} on the left stroke volume when HR = 70 bpm, RSA amp = 10 bpm, $ampR_{SV}$ = 0.006 mmHg s m(ml)$^{-1}$ using: (a) the E model; and (b) the GNH model.

From Figures 5.3a and 5.3c it is observed that mean CO is decreased by 2% at HR = 50 bpm when *amp* = 30 bpm, using both the E and GNH models, if we include periodicity of HR only. On the other hand, when we include the periodicity of the R_{SV} alone there is no notable difference in the mean CO at various heart rates. When we plot the effects of RSA using both periodicity of HR and R_{SV} we find the same outcome, i.e. 2% decrements in mean CO at HR = 50 bpm when RSA amp = 30 bpm, using both the E-type and G-type models (see Figure 5.4). Figure 5.4b indicates that the ventricular inter-dependence (the EVI model) causes a slight increase in the mean CO at HR = 90 bpm (about 0.5%) relative to the E model, however, this effect is not seen in the full G model. There are no other marked differences in mean CO at other heart rates using all types of models. In Figure 5.5 the amplitude of the left stroke volume (SV) is larger under periodic HR and smaller under periodic R_{SV} using both the E and GNH models. But the amplitude of the SV using the GNH model under periodic HR has strong fluctuations relative to the amplitude of SV of the E model. An opposite effect is seen in the amplitude of SV of the GNH and E models with periodic R_{SV}.

5.5 Studying the effects of RSA on stroke volume, blood pressure and blood flows

It has been reported in (Toska and Eriksen, 1993, Elstad et al., 2001) that the left and right cardiac stroke volumes are generally in opposite phases throughout the respiration period. Elstad (2012) suggested that RSA along with the respiratory oscillations has the

same phase as the right cardiac stroke volume and consequently produce large fluctuations in the pulmonary blood flow (Elstad, 2012). Motivated by these findings, in this section, we explore the impacts of RSA on stroke volumes, blood pressure and blood flow by combining periodic HR and periodic R_{SV}. Figures 5.6 and 5.7 show the blood pressure in the systemic arteries as well as the stroke volumes and cardiac outputs of the left and right ventricles for three different heart rates using the EVI and full G models respectively. The blood flows on the left and right sides of the heart using the EVI and full G models are shown in Figure 5.8.

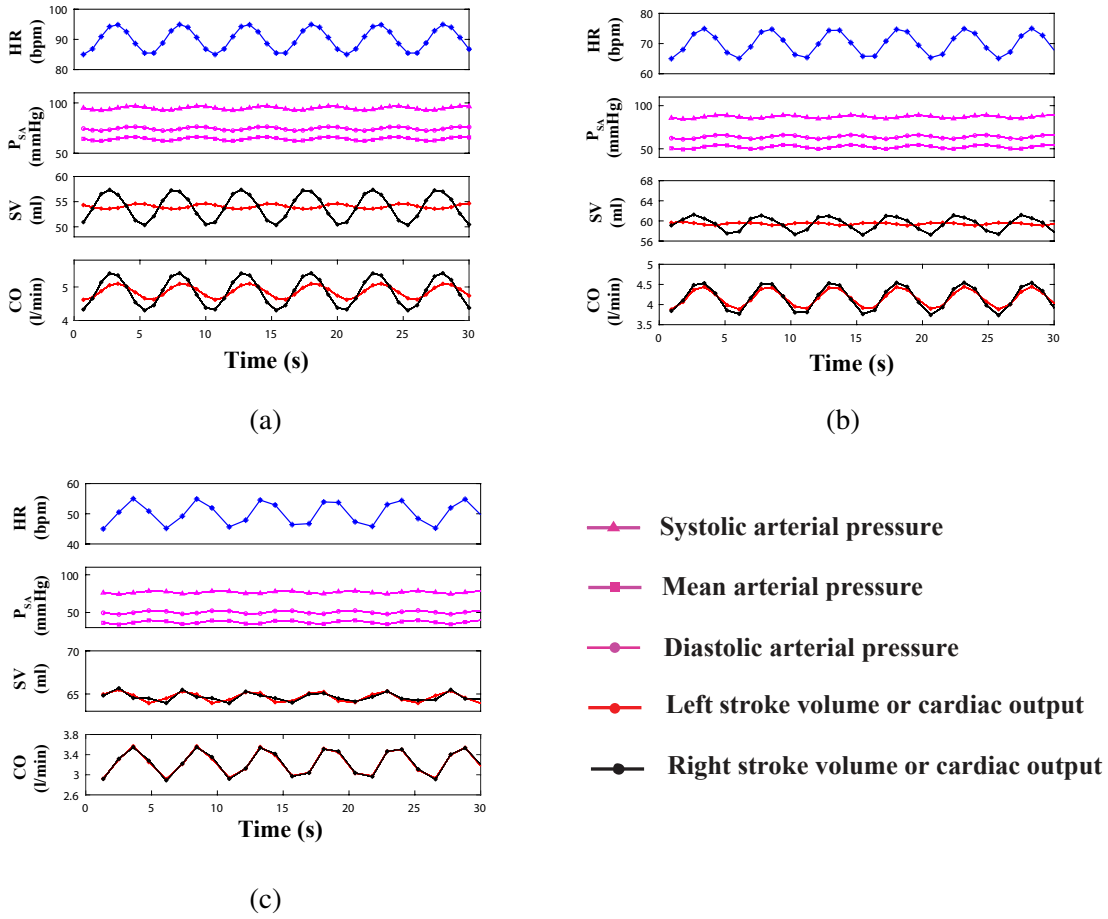

Fig. 5.6 The graphs show from top to bottom, heart rate, blood pressure, stroke volume and cardiac output as a function of time using the EVI model with values of RSA amp = 10 bpm, $ampR_{SV} = 0.006$ mmHg s $(\text{ml})^{-1}$. (a) mean HR = 90 bpm. (b) mean HR = 70 bpm. (c) mean HR = 50 bpm.

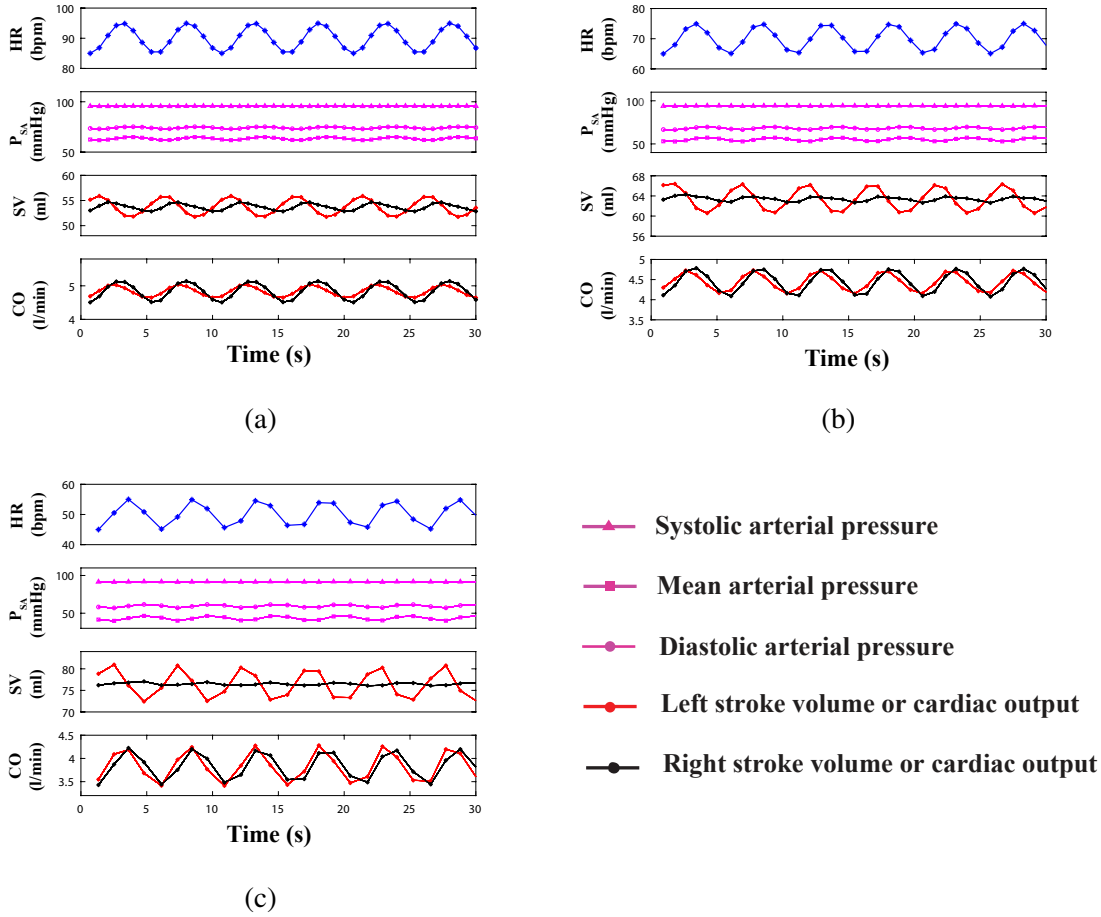

Fig. 5.7 The graphs show from top to bottom, heart rate, systemic arteries pressure, stroke volume and cardiac output as a function of time using the full G model with values of RSA amp = 10 bpm, $ampR_{SV} = 0.006$ mmHg s $(\text{ml})^{-1}$. (a) mean HR = 90 bpm. (b) mean HR = 70 bpm. (c) mean HR = 50 bpm.

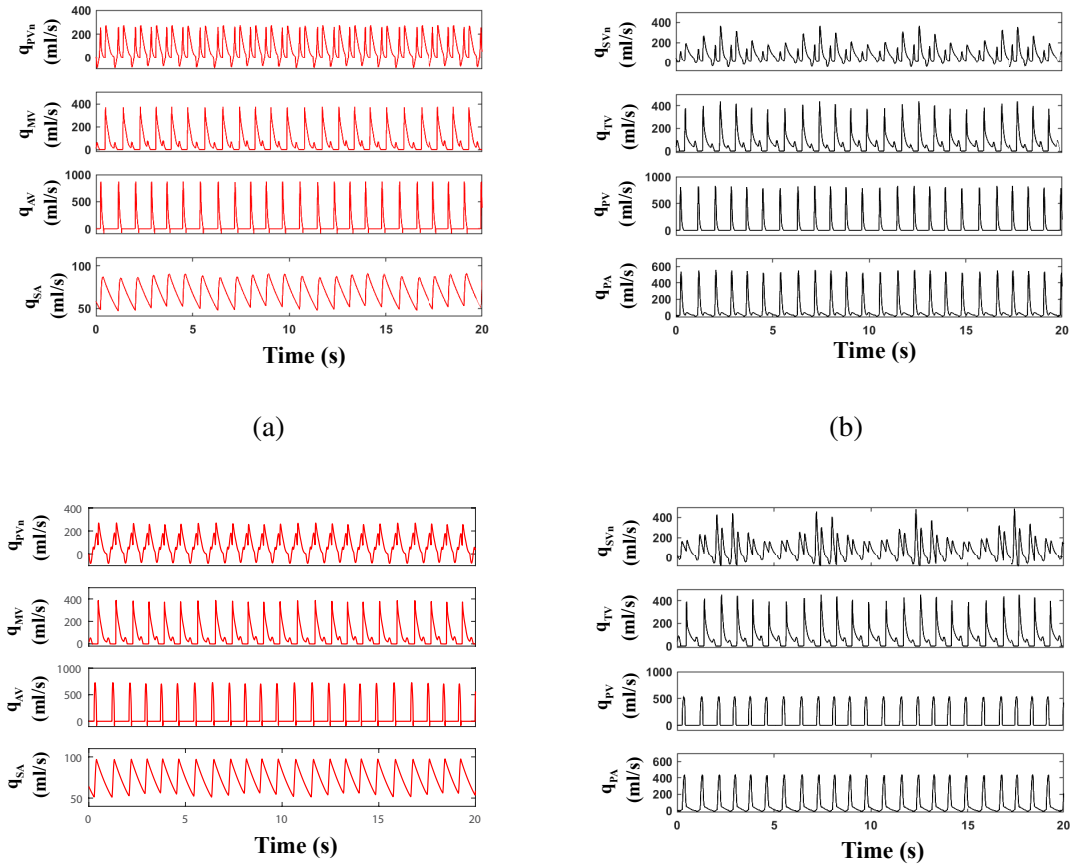

Fig. 5.8 Blood flows in the circulatory system with periodic HR and values of mean HR = 70 bpm, $ampR_{SV} = 0.006$ mmHg s $(\text{ml})^{-1}$. (a) and (c) From top to bottom, pulmonary veins flow (q_{PVn}), mitral valve flow (q_{MV}), aortic valve flow (q_{AV}) and systemic arteries flow (q_{SA}). (b) and (d) From top to bottom, systemic veins flow (q_{SVn}), tricuspid valve flow (q_{TV}), pulmonary valve flow (q_{PV}) and pulmonary arteries blood flow (q_{PA}). Flows are calculated using the EVI model (panels a and b) or the full G model (panels c and d).

Our results using the EVI model show that the left and right stroke volumes are in opposite phase at high heart rate but their phase is matching gradually as the heart rate decreases (see Figure 5.6). While using the full G model the left and right stroke volumes are in opposite phase at low heart rate and move towards having the same phase (but not completely) as heart rate increases (see Figure 5.7). Hence our simulation results do not support the findings of Elstad et al. (2001) that the left and right stroke volumes stay in opposite phase of each other throughout the respiration period. Moreover, there is a difference in amplitudes of the left and right stroke volumes using both models. With the EVI model, the amplitude of the

right SV is higher than the left SV at HR = 90 bpm (by 6 ml) and 70 bmp (by 2 ml) . In contrast, with the full G model the amplitude of the left SV is larger than the right SV for all types of heart rates, prominent difference occurs at HR = 50 bpm (by 8 ml).

In relation to the systemic arteries pressure, the systolic pressure shows strong fluctuations using the EVI model while it stays almost constant if we use the full G model. The mean arterial pressure and the diastolic pressure exhibit oscillations over a range of heart rates and the results are consistent with both the EVI and the full G models. The left and right cardiac outputs oscillate with the same phase at all heart rates in both types of models. Also, the amplitudes of the left and right cardiac outputs are almost the same in both types of models, except at HR = 50 bpm (using the EVI model) when the amplitude of the right CO is larger than the amplitude of the left CO.

In Figure 5.8 the systemic veins and tricuspid blood flows exhibit more fluctuations in comparison of others blood flows using the EVI and full G models.

Chapter Summary

In this chapter, we used the E, EVI, GNH and full G models to study the effects of respiratory sinus arrhythmia. The EVI model is an extension of the E model that includes the ventricular inter-dependence and was introduced in this chapter. To take into account different possible sources of RSA we included in the models periodicity of the HR and systemic vein resistance. The models results demonstrated that mean cardiac output didn't change significantly by RSA. However, interesting differences exist, between the outputs of the EVI and full G models in relation to the left and right stroke volumes. In both types of models the left and right stroke volumes were in opposite phase but this happened at high heart rate in the E-type models and at low heart rate in the G-type models. The blood flows through the systemic veins and tricuspid valve exhibited more oscillations than the other flows using both the EVI and full G models.

Chapter 6

Mathematical modelling of heart failure

Over the past two decades mathematical and computational modelling of the cardiovascular system has attracted both the mathematics and the bio-engineering communities because of the increased impact of cardiovascular diseases in our lives. According to Mozaffarian et al. (2015) cardiovascular diseases are the leading cause of death worldwide. Every year 17.3 million people die due to cardiac diseases, a number that is expected to grow to more than 23.6 million by 2030. In New Zealand , 33% of deaths annually are caused by cardiac diseases.

In this chapter, we provide physiological background of heart failure and review the current literature of its mathematical modelling. We then use our mathematical models to simulate two types of heart failure: diastolic and systolic heart failure.

6.1 Physiological Background

Heart failure is a clinical pathological condition in which the heart is unable to generate enough cardiac output to meet the body's metabolic demands. The rate of heart failure is increasing rapidly throughout the word, including developing countries. Despite of advances in its treatment, heart failure still has a poor prognosis (Katz and Konstam, 2012). Heart failure can occur on either side of the heart or both sides of the heart at the same time. It can occur over a short time or be an ongoing condition. Left-sided heart failure occurs when the left ventricle cannot pump blood properly and the body cannot get enough oxygenated blood. Right-sided heart failure occurs when the right ventricle cannot do its job efficiently. It is usually stimulated by left-sided heart failure. There are other diseases as well that can cause right-sided heart failure such as lung disease, swelling in the legs, feet and abdomen. Left-sided heart failure can further be classified as: diastolic heart failure and systolic heart failure.

Diastolic heart failure

Diastolic heart failure also called heart failure with preserved ejection fraction, occurs when the heart muscle becomes stiffer and the left ventricle loses its ability to relax normally. The stiffness of the heart muscle, which is usually due to some disease, does not allow proper filling of the heart with blood during its relaxation period of each beat.

The mitral flow plays an important role in assessing diastolic heart failure. The mitral flow is the pressure difference between the left atrium and the left ventricle and consists of two waves, the E-wave and the A-wave. The E-wave represents the passive filling of the ventricle and the A-wave corresponds to the atrial contraction. If the filling pressure in the left ventricle is not normal it can effect the shape and velocity of the mitral flow. We can estimate diastolic function with the following parameters: the ratio of the E and the A wave i.e. E/A, the E-wave deceleration time DT which reflects how rapidly the flow velocity decreases during filling of the ventricle and the length of the isovolumic relaxation time which is the time that starts with the closure of the aortic valve and ends with the opening of the mitral valve.

In healthy hearts, the E-wave is taller than the A-wave and the ratio E/A lies between 1 and 1.5. A ratio E/A greater than 2 is also acceptable (Kossaify and Nasr, 2019). The normal range for the values of the DT is $140 - 240$ ms. A simulated mitral blood flow using the E model with default parameters (Table 4.5) is shown in Figure 6.1. Here E/A = 6.33 and DT = 220 ms.

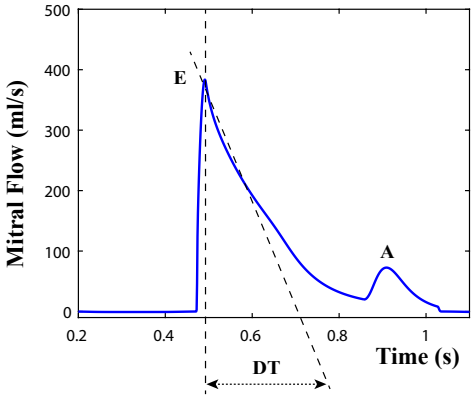

Fig. 6.1 Simulated mitral flow of a normal heart using the E model with HR = 70 bpm. All other parameters are as given in Table 4.5.

There are four grades of diastolic heart failure: Grade I or impaired relaxation (IR); Grade II pseudonormal; Grade III restrictive filling pattern (RFP) and Grade IV fixed restrictive. In this thesis we will be modelling the Grade III diastolic heart failure which is characterized

by high left atrial pressure, less compliant left ventricle, an increased E/A ratio and reduced deceleration time i.e. it becomes less than 160 ms.

Systolic heart failure

Systolic heart failure is also termed as heart failure with reduced ejection fraction. In this type of heart failure the left ventricle loses its ability to contract normally, it becomes weak. As a result, the heart can not pump with enough force to push blood throughout the body organs in an efficient way. The most common causes of systolic heart failure are high blood pressure, coronary artery disease, heart muscle disease and heart valve diseases. In systolic heart failure the E/A ratio and the DT stay normal and the ejection fraction is calculated. Systolic heart failure is characterized by having ejection fraction below 40% (Maeder and Kaye, 2009).

6.2 Literature Review of models of heart failure

The time-varying elastance models of the cardiovascular system have been widely used to model cardiac function. These have also been used for different clinical purposes such as evaluating heart failure, left ventricular assist device support or simulating the interaction between the cardiovascular and respiratory systems (Bozkurt, 2019). Previous studies of heart failure include Tsuruta et al. (1994), Kotani et al. (2005), Karaaslan et al. (2005), Luo et al. (2011), Warriner et al. (2014). Some of these focus only on specific aspects of heart failure. For example, Tsuruta et al. (1994) studied heart failure conditions by reducing the maximum elasticity of the heart muscle and presented a quantitative diagnosis and evaluation of drug effects. Their model results agreed well with the clinical and experimental data. Kotani et al. (2005) presented a dynamical model of cardiovascular autonomic regulation to model normal and disease conditions. Their simulations captured the general statistical and transient characteristics of nerve blockades in chronic heart failure without applying their results to clinical medicine. In Karaaslan et al. (2005) a physiological model of the cardiovascular system was developed to study long term interactions between the renal sympathetic nerve activity (RSNA) and arterial pressure, as high RSNA is known to contribute the high blood pressure and heart failure.

Most studies are concerned with left-sided heart failure. Luo et al. (2011) modelled several cases of left ventricular diastolic dysfunction: impaired relaxation; restrictive filling pattern; the combination of both or pseudo-normal by changing some of the model parameters. Their simulation results show that an increase in contractility can compensate for reduction in

the left ventricle ejection fraction, but would not reduce pulmonary pressures or blood volume so pulmonary congestion would continue in the case of diastolic heart failure. Mohammed et al. (2018) studied and modelled a disease of the heart muscle in which the left ventricle stretches and becomes thin, one of the causes of systolic heart failure. They decreased the ventricular elastance parameter to represent poor ability of ventricular muscle contraction. Their simulations found that a decrease in the maximum left ventricular elastance leads to a decline in stroke volume, ejection fraction and left ventricular systolic pressure while the heart rate and left ventricular diastolic pressure increase.

For this study, we can get insight into the conditions of heart failure by simulating the cardiovascular system by varying certain parameter values using the E and full G models. Although this approach has been used before in many studies (see for example, Luo et al. (2011), Mohammed et al. (2018)), here we use the full G model to simulate systolic and diastolic heart failure which has not been done earlier. Similar to the previous studies, we compare the model outputs of normal and diseased hearts, specifically, we show the PV loops in the four cardiac chambers for normal and heart failure conditions as well as the volume distribution in the body and lung compartments. We also show the mean cardiac output over a range of heart rates for normal and heart failure conditions which has not been presented before. A comparison between the outputs of the E and full G models in the case of heart failure is presented in their relative sections.

6.3 Mathematical modelling of diastolic heart failure

Diastolic heart failure or heart failure with preserved ejection fraction is modelled using the E model by increasing the value of the parameter E_{minLV}, making the left ventricle stiffer. When using the full G model, this condition is simulated by increasing the value of E_{minLV} and decreasing the value of G_{maxLV}.

Tables 6.1 and 6.2 show the cardiac output (CO), stroke volume (SV), ejection fraction (EF), mean left atrial pressure (meanP_{LA}) and the minimum left ventricular pressure (minP_{LV}) in normal and stiffer hearts when the mean HR is kept at 70 bpm. As we increase the value of E_{minLV} the mean left atrial and the minimum left ventricular pressure elevate, while the mean cardiac output and the stroke volume decrease. These results are true for both the E and full G models. There is a small drop in the ejection fraction, using the E model but when the ventricle becomes 150% stiffer, the ejection fraction still lies within the normal physiological range. When we use the full G model the value of ejection fraction almost remains the same. These facts agree well with the results of Luo et al. (2011) and physiological findings (Litwin and Grossman, 1993). To compare between the models, in Figure 6.2 we show the

SV, EF, mean P_{LA} and min P_{LV} as functions of mean CO for normal and diastolic heart failure conditions.

Table 6.1 Simulating diastolic heart failure using the E model at a HR of 70 bpm.

E_{minLV}	CO (l/m)	SV (ml)	EF (%)	MeanP_{LA} (mmHg)	MinP_{LV} (mmHg)
0.1(Normal value)	4.33	63.04	53.13	10.53	3.23
0.15	3.77	55.06	51.23	12.81	4.57
0.20	3.34	48.88	49.46	14.60	5.82
0.25	2.99	43.95	47.82	16.04	7.00
0.30	2.71	39.95	46.28	17.23	8.12

Table 6.2 Simulating diastolic heart failure using the full G model at a HR of 70 bpm.

G_{max}/E_{minLV}	CO (l/m)	SV (ml)	EF (%)	MeanP_{LA} (mmHg)	MinP_{LV} (mmHg)
98.3/0.1(Normal values)	4.52	68.39	52.51	10.84	3.55
83.5/0.15	3.83	57.06	51.74	12.36	4.19
73.7/0.2	3.36	49.82	51.11	13.43	4.70
66.5/0.25	3.02	44.57	50.34	14.23	5.16
61.5/0.3	2.77	40.81	49.91	14.81	5.53

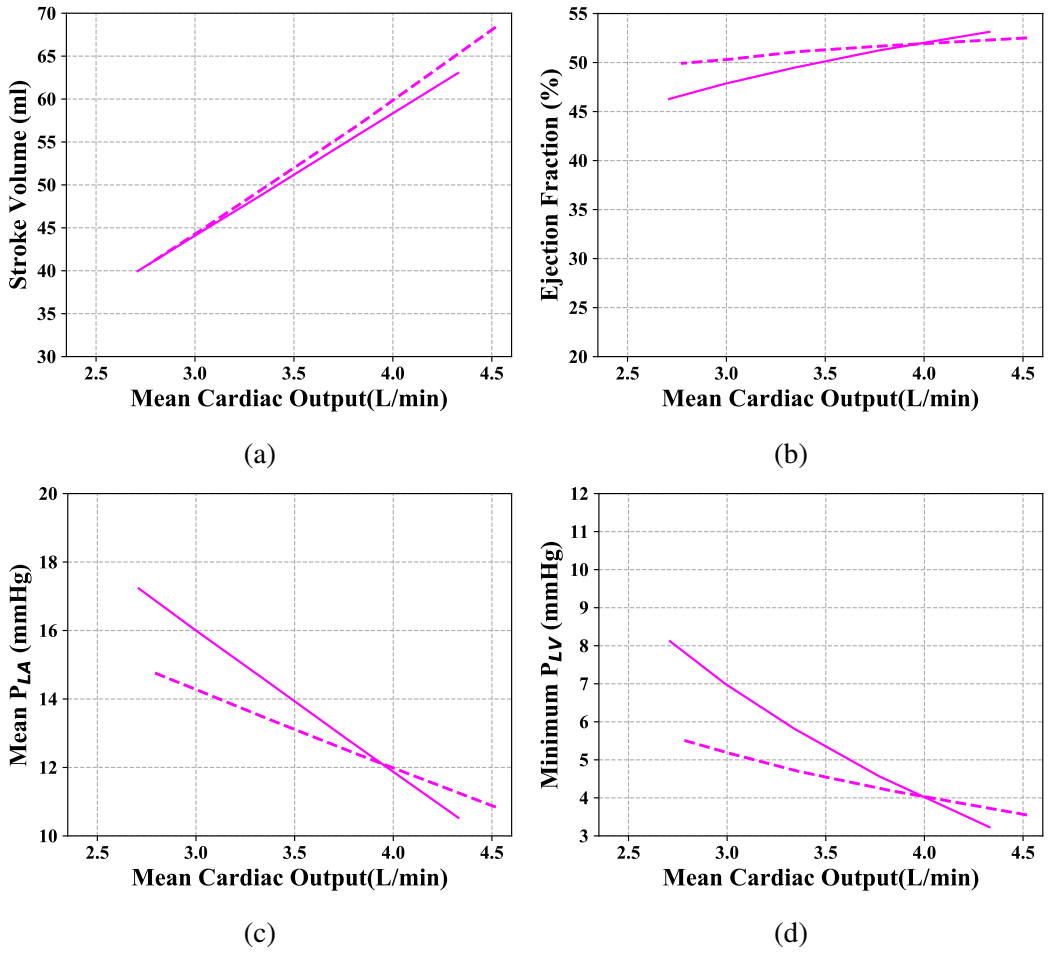

Fig. 6.2 Model outputs as functions of mean CO in the case of diastolic heart failure using the E and full G models. (a) Stroke volume (b) ejection fraction (c) mean left atrial pressure (d) minimum left ventricular pressure. Solid line - the E mode, Dashed line - the full G model (see also Tables 6.1 and 6.2).

Figure 6.3 shows the PV loops of the four chambers of the heart under normal and diastolic heart failure conditions when the E and full G models are used. In both models, under diastolic heart failure conditions, there is a decrease in the left and right ventricular stroke volumes. Under diastolic heart failure conditions, the maximum left ventricular pressure is declined relative to normal conditions and the minimum (filling) pressure is elevated. In the case of diastolic heart failure, the right ventricle also experiences a rise in the maximum and filling pressures relative to normal conditions using both types of models. Also the left ventricular end-diastolic volume EDV (the volume of the ventricle at the end of contraction) decreases under diastolic heart failure conditions using the E and full G models. In contrast, the EDV of the right ventricle increases in diastolic heart failure conditions using both models, but this increase is prominent when we use the full G model. The PV loops of

the atria are shown in Figures 6.3c and 6.3d. Under diastolic heart failure conditions, the pressure in the left atrium increases using both models. There is a prominent increase in the left atrial volume using the E model but it decreases slightly when we use the full G model. In relation to the right atrium, under diastolic heart failure both the pressure and the volume are lower than normal conditions using both models. Our results related to the PV loops of the ventricles matches with the findings of Luo et al. (2011).

To see the distribution of blood when the left ventricle can not fill properly, the blood volumes in the pulmonary and systemic compartments are shown in Figures 6.4a and 6.4b. The blood volumes in the pulmonary arteries and pulmonary veins are rising under diastolic heart failure using both models. In contrast, the blood volume reduces in the systemic arteries and systemic veins using both models. Hence our model results agree well with the biological findings that due to improper filling of the left ventricle the blood can not reach the body organs properly and accumulates in the lung compartment.

In Figure 6.4c, the mitral blood flow of normal and diastolic heart failure conditions is shown for the E and full G models. The ratio of the E and A wave is greater than 2 and DT shortens in the mitral flow waveform that reflects difficulty in the ventricular filling. Both models show similar results. We have also generated the mean cardiac output curves of normal and diastolic heart failure conditions using the E and full G models (Figure 6.4d). The mean CO curve under diastolic heart failure conditions is lower and flatter than normal conditions using both models. Also the maximum of the mean CO shifts towards a higher heart rate under diastolic heart failure conditions when we generate this curve with both models.

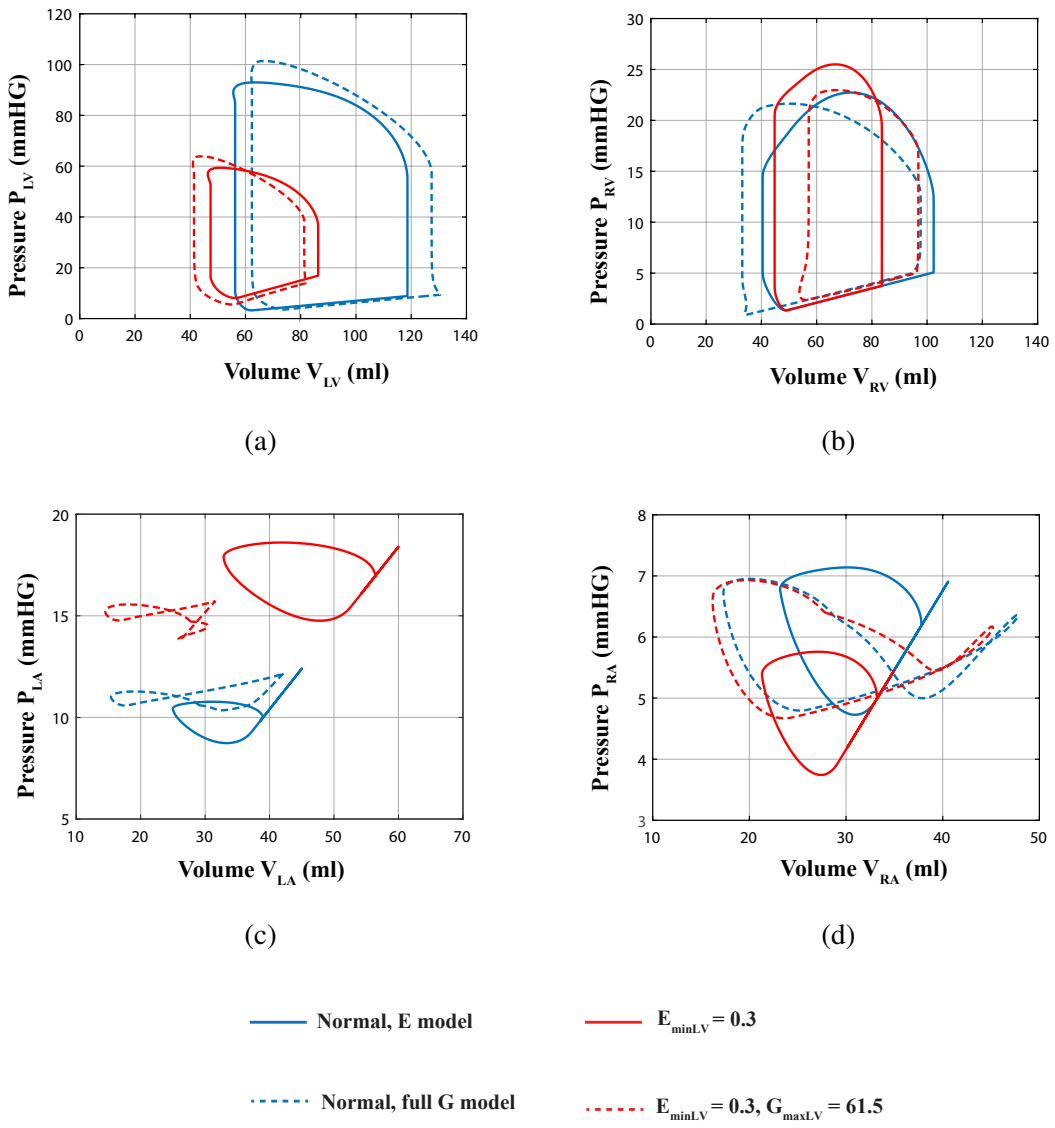

Fig. 6.3 Comparison of PV loops in a normal and a diastolic heart failure at HR = 70 bpm (a) left ventricle (b) right ventricle (c) left atrium (d) right atrium. Solid line - the E model, Dashed line - the full G model.

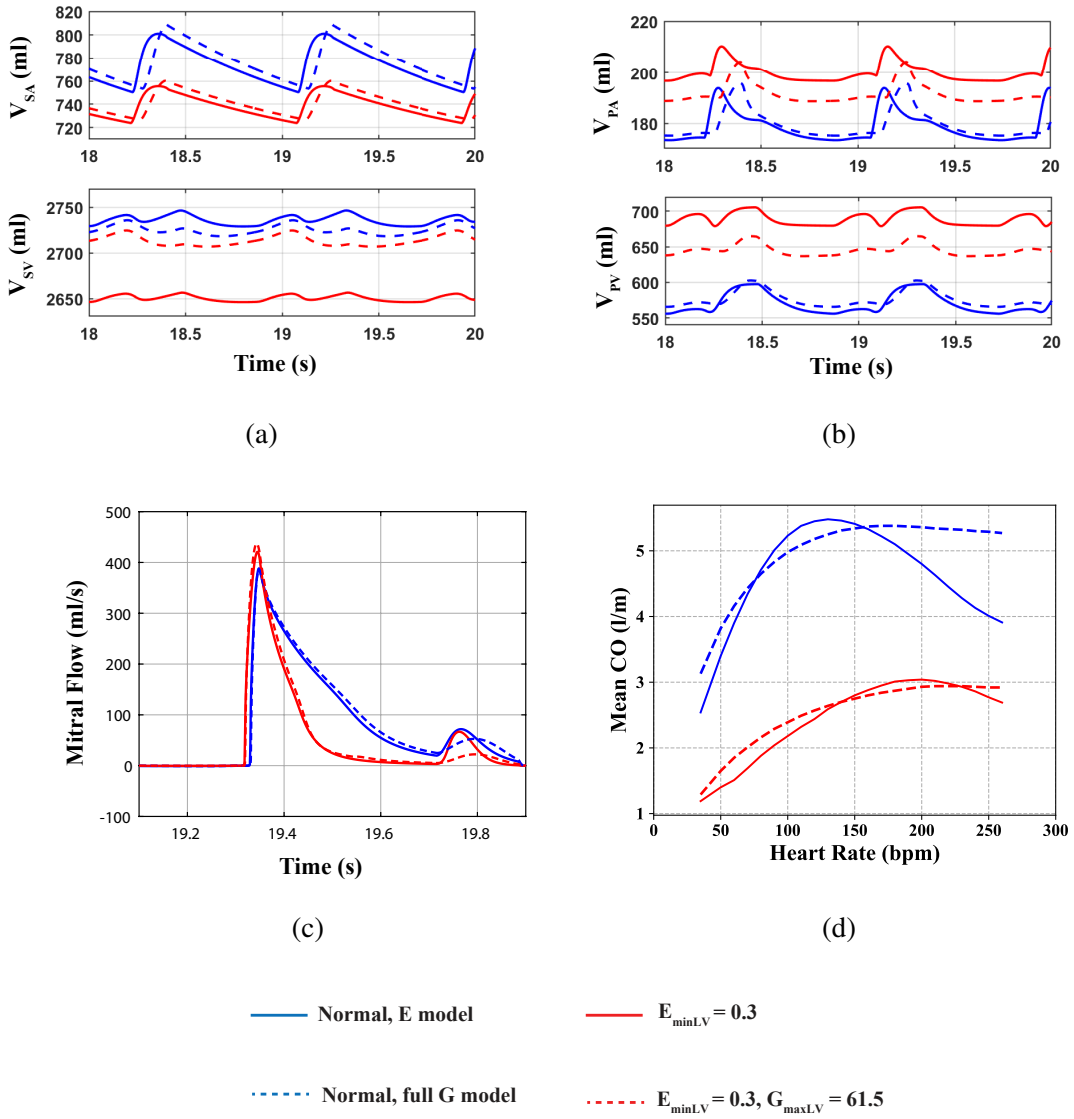

Fig. 6.4 (a) Comparison of normal and diastolic heart failure at HR = 70 bpm: (a) blood volume in the systemic arteries (V_{SA}) and systemic veins (V_{SV}) (b) blood volume in the pulmonary arteries (V_{PA}) and pulmonary veins (V_{PV}) (c) mitral blood flow (d) mean cardiac output (CO) over a range of heart rates. Solid line - the E model, Dashed line - the full G model.

6.4 Mathematical modelling of systolic heart failure

The systolic heart failure is simulated by reducing the value of the parameter E_{maxLV} in the E model and this condition is simulated by decreasing the value of G_{maxLV} in the full G model.

Tables 6.3 and 6.4 show the mean CO, SV, EF, mean left atrial pressure and the minimum left ventricular pressure in normal and systolic heart failure conditions using the E and full G models. Under systolic heart failure conditions, the mean cardiac output and stroke volume decrease using both types of models. The ejection fraction also decreases rapidly under systolic heart failure conditions using the E and full G models. The pressure in the left atrium is elevated and the filling pressure in the left ventricle rises when we use both types of models. To compare results of both models in the case of systolic heart failure, we show the SV, EF, mean P_{LA} and minimum P_{LV} as functions of the mean CO (see Figure 6.5).

Table 6.3 Simulating systolic heart failure using the E model at a HR of 70 bpm.

E_{maxLV}	CO (l/m)	SV (ml)	EF (%)	MeanP_{LA} (mmHg)	MinP_{LV} (mmHg)
2.8 (Normal value)	4.33	63.04	53.13	10.53	3.23
1.85	4.06	59.08	46.93	11.17	4.31
1.4	3.83	55.78	42.23	11.72	5.23
0.81	3.26	47.50	32.12	13.12	7.55
0.40	2.40	35.15	20.43	15.27	11.08

Table 6.4 Simulating systolic heart failure using the full G model at a HR of 70 bpm.

G_{maxLV} (mmHg)	CO (l/m)	SV (ml)	EF (%)	MeanP_{LA} (mmHg)	MinP_{LV} (mmHg)
98.3(Normal value)	4.52	68.39	52.51	10.84	3.55
86	4.02	60.22	43.26	11.73	5.10
81	3.83	57.01	39.90	12.10	5.75
67	3.26	48.31	31.44	13.18	7.57
45.2	2.40	35.37	20.63	14.94	10.52

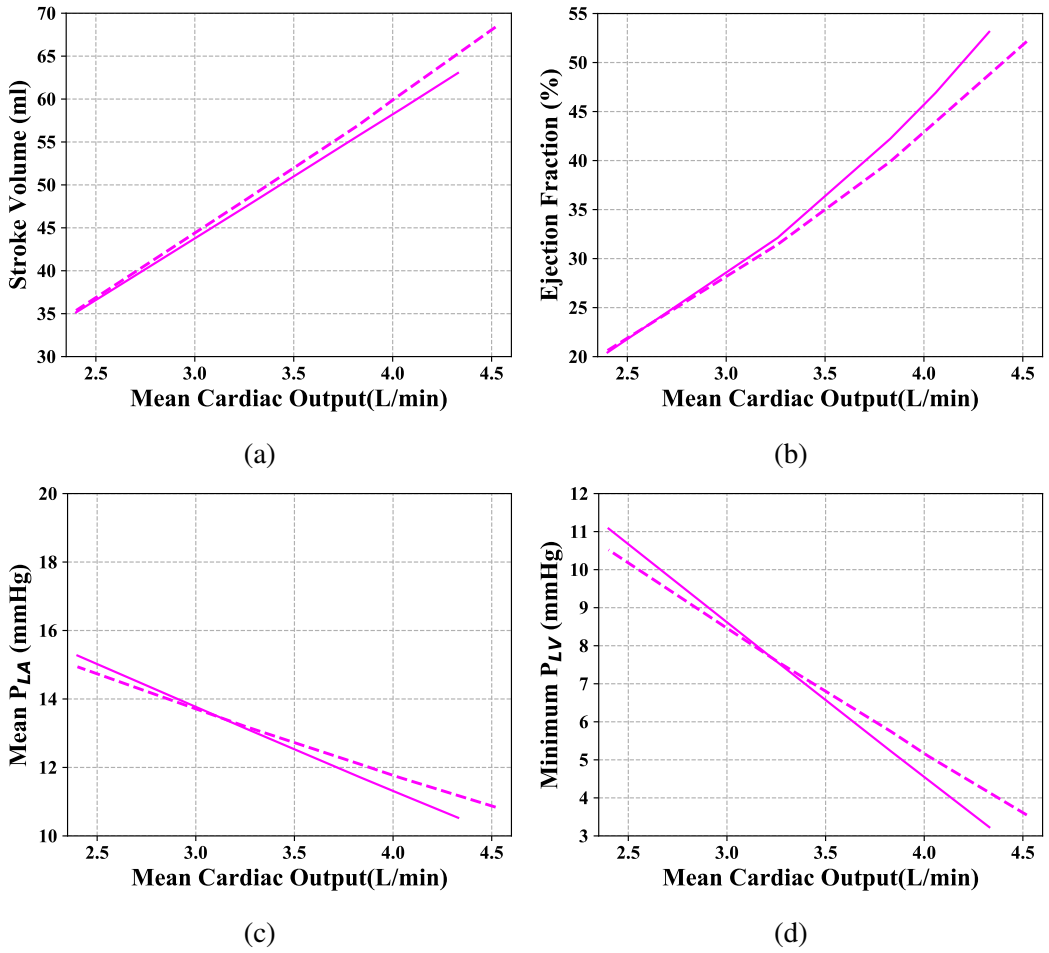

Fig. 6.5 Model outputs as function of mean CO in case of systolic heart failure using the E and full G models. (a) Stroke volume (b) ejection fraction (c) mean left atrial pressure (d) minimum left ventricular pressure. Solid line - the E mode, Dashed line - the full G model (see also Tables 6.3 and 6.4).

Figure 6.6 shows the PV loops in the four cardiac chambers using the E and full G models. There is a reduction in the stroke volumes of both the ventricles when the left ventricle has poor pumping function relative to normal conditions and this is true for both types of models. Also the filling pressure in both ventricles is rising under systolic heart failure conditions using the E and full G models. The maximum pressure in the left ventricle decreases under systolic heart failure and an opposite effect is observed in the right ventricle which experiences a slight increase in the maximum pressure under this abnormal condition using both types of models. The EDV of the left ventricle increases significantly, consequently the PV loops move towards the right using both models (see Figures 6.6a). These results of the PV loops agree well with the results of Mohammed et al. (2018) and Warriner et al. (2014). The PV loops of the right ventricle also shifts towards the right using both models. But this

shift is very small in comparison to the left ventricle. The PV loop of the left atrium shows an increase in both pressure and volume as we decrease the value of E_{maxLV} in the E model. While using the full G model the pressure rises and the volume decreases (see Figure 6.6c). In contrast, the pressure and volume in the right atrium decrease under systolic heart failure using the E model and the results are consistent with the full G model (see Figure 6.6d). The volumes distribution in the body and lung compartments are shown in Figures 6.7a and 6.7b respectively. The amount of blood in the pulmonary arteries and pulmonary veins is rising as a result of the systolic heart failure conditions using both types of models. In contrast, there is a reduction in the blood volume of the systemic arteries and systemic veins compartments. With regard to the mitral flow (Figure 6.7a) the ratio of E/A remains greater than 2 under systolic heart failure and small reduction in the DT is observed relative to normal conditions. The mean cardiac output as a function of heart rate is shown in Figure 6.7d. The mean CO plots of SHF become lower and flatten relative to normal conditions using both models.

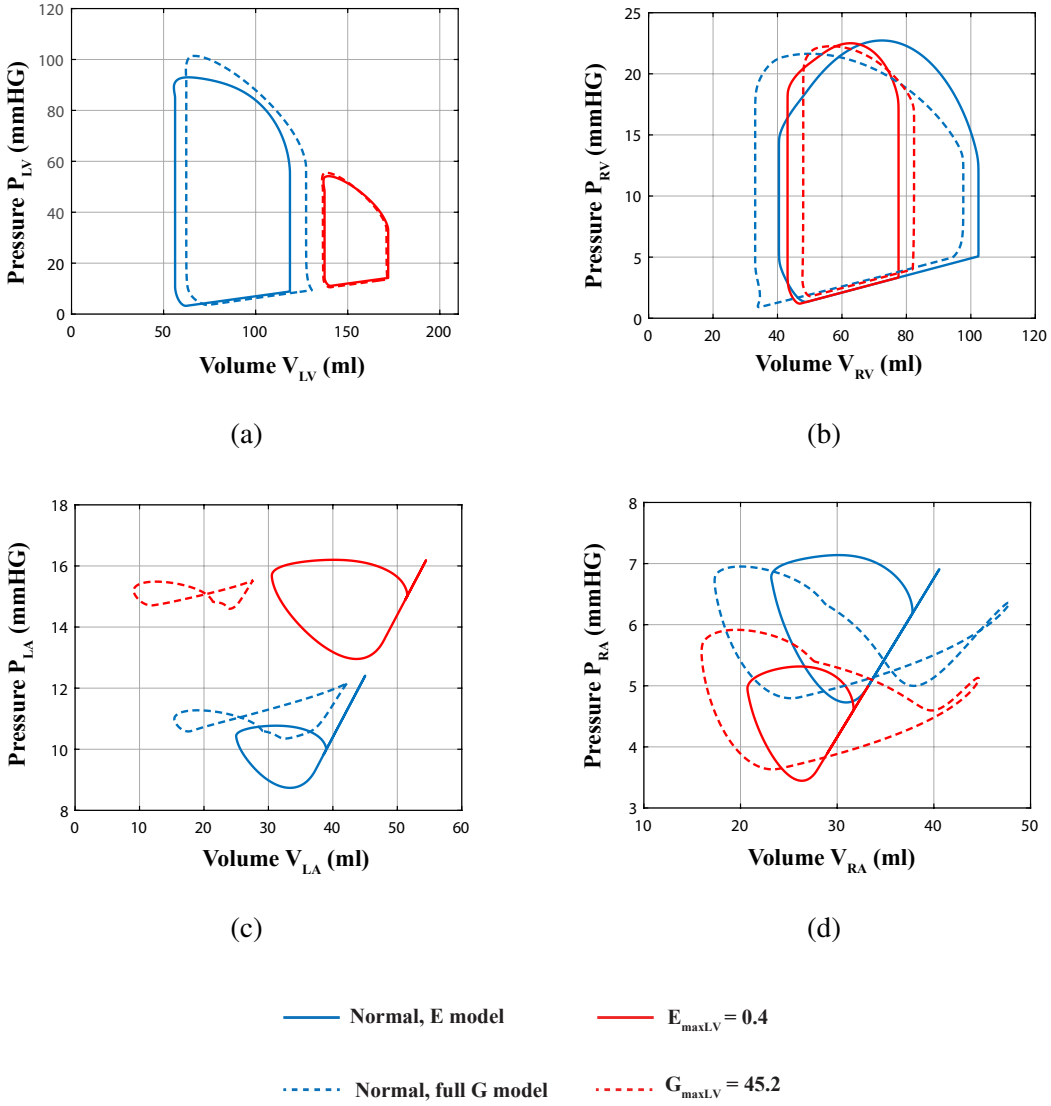

Fig. 6.6 Comparison of PV loops in a normal and a systolic heart failure at HR = 70 bpm (a) left ventricle (b) right ventricle (c) left atrium (d) right atrium. Solid line - the E model, Dashed line - the full G model.

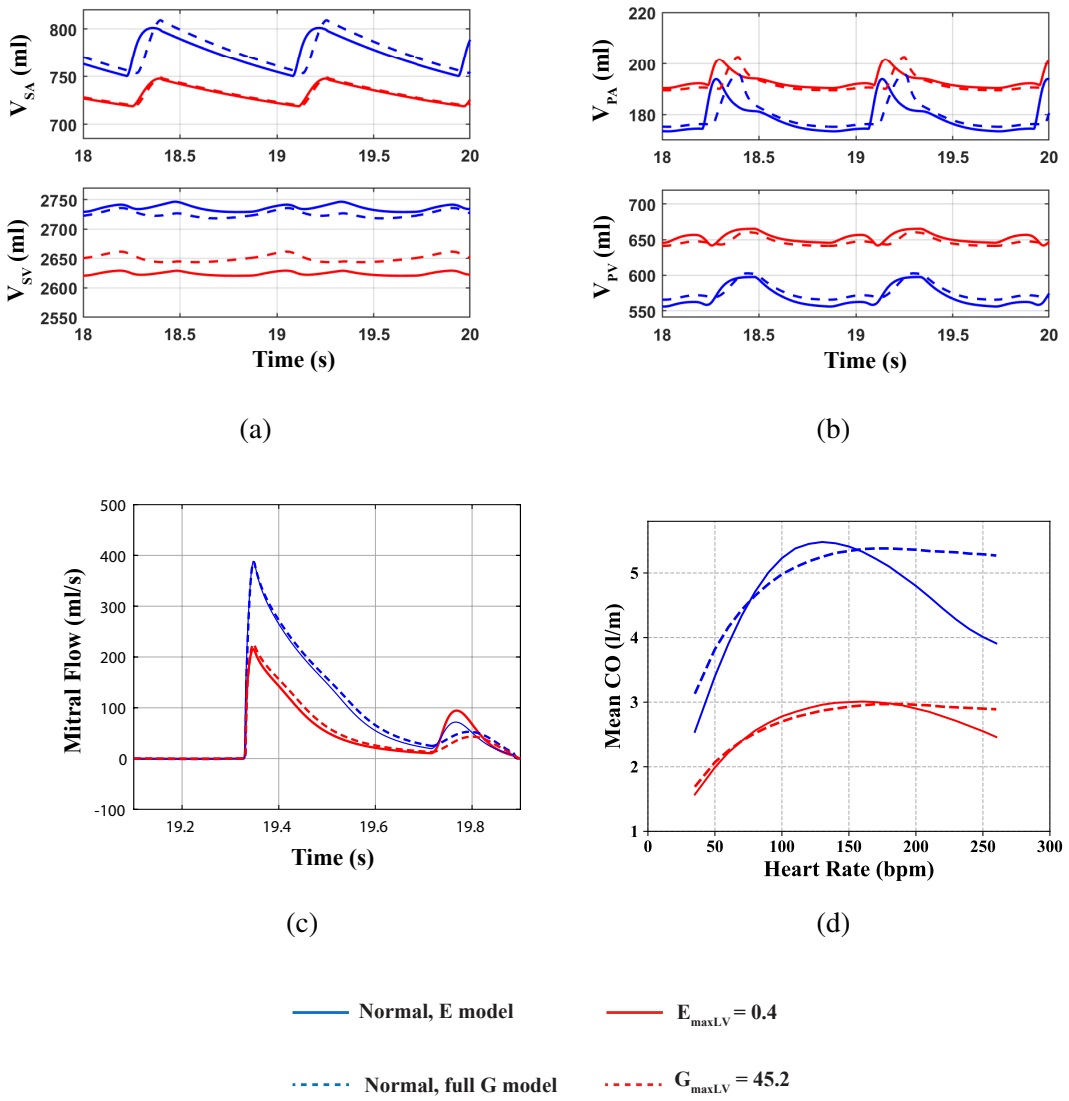

Fig. 6.7 (a) Comparison of volumes, blood flows and mean CO for normal and systolic heart failure at HR = 70 bpm: (a) blood volume in the systemic arteries (V_{SA}) and systemic veins (V_{SV}) (b) blood volume in the pulmonary arteries (V_{PA}) and pulmonary veins (V_{PV}) (c) mitral blood flow (d) mean cardiac output (CO) over a range of heart rates. Solid line - the E model, Dashed line - the full G model.

Chapter Summary

In this chapter, we simulated two conditions of heart failure by changing certain parameter values. We simulated the left-sided diastolic heart failure and systolic heart failure using

the E and full G models. The DHF was characterized by increasing the value of E_{minLV} in the E model and by changing the values of G_{maxLV} and E_{minLV} in the full G model. The SHF was simulated by changing the value of E_{maxLV} associated with the E model and the value of G_{maxLV} in the full G model. Our analysis using both models showed a decline in the mean CO and SV for both diastolic and systolic heart failure. In the case of diastolic heart failure, the ejection fraction remained within the normal physiological range even when the heart became 150% stiffer while in the case of systolic heart failure its value reduced rapidly. The left atrial and left ventricular filling pressures were elevated for both diastolic and systolic heart failure but that rise was more significant with the conditions of systolic heart failure. Since the left ventricle could not relax properly in the presence of diastolic heart failure, therefore a reduction in the end-diastolic volume was observed. In contrast, the end-diastolic volume in the left ventricle was high in the case of systolic heart failure. In the mitral flow, the DT was shorter than the normal value but the ratio of the E/A wave lay within the normal range when the left ventricle became stiffer. The E/A ratio was decreased and DT was relatively normal in the case of systolic heart failure. Both conditions of heart failure caused an accumulation of blood volume in the lung and left atrium compartments while in the systemic arteries and in the systemic veins the amount of blood was lower. Our results agreed with the biological findings and previous studies.

Chapter 7

Conclusions

Mathematical models and numerical simulations of the cardiovascular system are very beneficial for understanding the mechanism and physiological functions of this complex system. In this thesis, we developed a lumped-parameter mathematical model of the cardiovascular system capable of simulating the heart mechanics over a range of heart rates. In this final chapter, we discuss and summarize the main results and contributions of our work and suggest new directions for the future.

7.1 Summary and Contributions

In Chapters 2-3, we presented mathematical models of the cardiovascular system that can be used to simulate the dynamics of the system over a wide range of heart rates under normal, resting, conditions. The models include several new modelling features that were introduced progressively.

We used muscle force to generate pressure during contraction of the atria and the ventricles while keeping the elasticity constant. This is different from previously published models (see for example, Williams et al. (2013), Olufsen et al. (2004), Heldt et al. (2002)) in which muscles contraction was simulated using time-dependent elasticity. Using time-dependent force instead of time-dependent elasticity led to the occurrence of a maximum pressure in the PV loop at lower volumes in the isolated model of the ventricle (Chapter 2) which is more realistic. In the models of the closed circulation (Chapter 3) it led to higher cardiac outputs, higher stroke volumes and higher ejection fractions at high and low heart rates (see Figures 3.5a, 3.5b and 3.5d). There is also a difference in the PV loops of the four heart chambers at variable heart rates. The pressures in the left and right ventricles increase with high heart rate

more rapidly using time-dependent elasticity, while the movement of the left ventricular PV loops is more pronounced using the time-dependent force (see Figures 3.6c and 3.6d).

We introduced a new hypothesis about the mechanical contraction of the atria, assuming different elasticity properties during contraction and expansion and also that the rate of change of the atrial pressure is proportional to the volume as well as to the rate of change of volume. This enabled the production of realistic atrial PV loops (see for example, Pagel et al. (2003)). To the best of our knowledge, the only other model attempting to do this (with only partial success) is Pironet et al. (2013). The inclusion of the new hypothesis led to slightly higher cardiac outputs at high heart rates.

We modelled the inter-ventricular interaction. While this has been done previously (see for example, Hann et al. (2005), Smith et al. (2004), Santamore and Burkhoff (1991)), our mathematical derivation is different and provides a new mechanical analogy. The inclusion of the inter-ventricular interaction led to a very small decrease in the left ventricular stroke volume at low heart rates and a very small increase at high heart rates (see Figure 3.5b). There was a very small increase in the cardiac output at high heart rates (see Figure 3.5a). Such small effects of the inter-ventricular interaction under normal conditions is consistent with observations (Naeije and Badagliacca, 2017) suggesting that the inter-ventricular interaction may only have a role during exercise or in some diseases. The PV loops of the left and right ventricles had a slight bend when the inter-ventricular interaction was included which resembles the PV loops in Segers et al. (2001).

We suggested new formulas for the ventricular contractions and the atrial-ventricular (AV) delay times as a function of the RR-interval. The formulas fit ECG measurements of sheep and ensure that the model is valid up to 260 bpm (i.e. the sum of the contraction and delay times is lower than the heart period, see Figure 2.7b). This is better than other formulas suggested previously in the literature with which we compared our new formulas. Our formulas may not be accurate at very high or very low heart rates where ECG measurements were not available. They may also not be valid under exercise or disease conditions. Nevertheless, between the G and the E models, the mean cardiac output is captured well when compared with physiological data from Kumada et al. (1967) and we could see a drop in the mean cardiac outputs as well (see Figure 3.5a).

We modelled all the heart valves with pressure dependent resistance following Williams et al. (2013) but added hysteresis to the aortic valve resistance. This enabled us to model back flow through this valve.

A model that includes all the features mentioned above was simulated at a heart rate of 70 bpm (Chapter 3). Model parameters were taken from the literature or chosen such that the model outputs were within physiological range. We did not attempt to fit our model to a

specific experiment as is done for example in Marquis et al. (2018) because there could be a large variation between individuals. Rather, our aim is to understand the basic principles of how the cardiovascular system works. The model outputs agreed with a wide range of physiological measurements (see Table 3.1 and Figures 3.2, 3.3 and 3.4) though in most cases, the simulated values tended to be closer to the lower end of their respective physiological ranges.

In Chapter 3 we also analyzed models that included only some of the new modelling features and compared the PV loops of all the cardiac chambers over a range of heart rates. The effects of variable heart rates on the PV loops were not studied extensively in the literature. We are aware of one experiment in dogs (Maughan et al., 1985) which shows an increase in pressure and a shift to the right of the left ventricular PV loops as heart rate increases. The PV loops of the left ventricle generated by our models showed similar trends but there were some clear differences between the G and the E models as discussed above. The realistic eight-shape PV loops of the atria in our model preserved their form under most of the heart rates we simulated but shifted as well. More experiments showing how the PV loops of all the chambers change with heart rate are needed. It will also be beneficial to have more experiments showing how cardiac output, stroke volume and ejection fraction change with heart rate.

In Chapter 4, we described in detail how we found the parameter values. We provided two tables which consist of all parameters of the models developed in the previous chapters. Some of the parameters were based on the literature values, others were derived from the ECG, pressure and blood flow measurements and the rest of the parameters were estimated. We made comparison between the ECG's of sheep and humans by capturing timings of the key intervals and also proposed new formulas for the RT-interval of sheep and delay timings for both sheep and humans. In addition, we compared the newly suggested formulas for sheep with the already existing formulas in the literature. Moreover, we conducted a sensitivity analysis of the model by changing one parameter at a time. While this analysis is not complete (see for example, Saltelli et al. (2019), Marquis et al. (2018)), it does reveal the most influential parameters. Of particular concern in this model is its high sensitivity to small changes in the total blood volume.

In Chapter 5, we investigated the effects of RSA on mean cardiac output using the E, EVI, GNH and full G models. The EVI model was an extension of the E model in which the ventricular inter-dependence was included. We introduced two possible sources of RSA: periodicity of the HR which represents central control regulation and the periodicity of the resistance of the systemic veins which represents the effects of the pleural pressure (the pressure that drives respiration). Our simulations indicated that the mean cardiac output

did not change with RSA. The results were consistent with all the models mentioned above. Thereafter, we also generated the left and right stroke volumes, cardiac outputs, blood pressure and blood flows on the left and right sides of the heart to test the findings of (Elstad, 2012) that the left and right stroke volumes remain in opposite phase throughout the respiratory cycle. Our own simulations showed that the left and right stroke volume were in opposite phase at high heart rate while we used the EVI model. On the other hand, for the full G model the left and right stroke volumes were in opposite phase at low heart rate. In the presence of the respiratory-modulated HR the blood flows through the tricuspid valve and systemic veins exhibited more fluctuations in comparison with the other flows using both the EVI and full G models.

In Chapter 6, we simulated two conditions of heart failure: diastolic heart failure and systolic heart failure using the E and full G models. We characterised the diastolic and systolic heart failure conditions by changing certain parameters in our models which is similar to past studies (Luo et al., 2011, Mohammed et al., 2018), however, here we also used the full G model which is introduced in this thesis for first time. We compared the results for normal and heart failure conditions using both models. Both models showed reduction in the mean cardiac output and stroke volume for diastolic and systolic heart failure. The ejection fraction was reduced significantly for systolic heart failure while it stayed within the normal physiological range for diastolic heart failure. Both types of heart failure caused an accumulation of blood in the lung. Our model results agreed well with physiological findings and earlier investigations.

The normal ratio for the E/A lies between 1 and 1.5. In our simulated mitral blood flow, this ratio was 6.33 and 7.20 for the E and full G models, respectively, which is very high. Although this ratio is also acceptable from a physiological perspective, it usually happens in a case of super normal filling when the heart is very healthy (such as athletes and persons who do exercise routinely). Future studies could involve model modifications in which the ratio of the E/A lies between 1 and 1.5.

7.2 Directions for Future Research

The research presented in this thesis could be beneficial for further studies as we suggest below.

- Future theoretical studies could make G_{max} in Eq. (2.4) a function of heart period (in this study it is assumed to be constant).

- We added hysteresis in the aortic valve but we didn't study its effects. Future studies could explore the effects of hysteresis on the stroke volume and mean cardiac output.

- We modelled the inter-ventricular interaction and our analysis indicated that it did not affect the mean cardiac output and stroke volume significantly under normal conditions. Naeije and Badagliacca (2017) suggested that inter-ventricular interaction may have a role during exercise or in pulmonary artery disease. Mathematical models that can simulate the effects of exercise and diseases conditions could be helpful in the future to explore the precise role of ventricular inter-dependence. Moreover, future study could involve the inter-atrial interactions which has not been taken into account in this work.

- The sensitivity analysis which was performed in Chapter 4, addressed the issue of which parameters influenced particular outputs and suggested that the total blood volume is the most sensitive parameter. This sensitivity seems too high to be corrected by blood pressure control mechanisms alone (see for example, Ben-Tal et al. (2014)) and may suggest that the model is missing another important component, perhaps another volume unit in parallel that could act as a reservoir for blood volume. Such a parallel unit of volume could be added to the model in the future.

- It is reported by Elstad et al. (2018) that irregular breathing causes large pressure changes within the thorax which are transmitted to the heart and produce large variations in ventricular filling and ejection. These oscillations may further transfer to the systemic blood flow and can cause end organ damage. One of the possible functions of RSA is to serve as a counter measure to these fluctuations and stabilize the systemic blood flow. A mathematical model that can simulate the effects of arrhythmia / irregular heart beat will be helpful to test this important function of RSA that is underexplored.

- In recent studies, O'Callaghan et al. (2020) proposed that enhancing RSA increases cardiac output in rats with heart failure. The heart failure was induced by ligation (tying a blood vessel) of the left branch of the coronary artery. In Chapter 6, we have already simulated two conditions of heart failure. Further explorations could include a mathematical model of the coronary blood flow to investigate the role of RSA in the case of heart failure.

References

Abdullateef, S., Mariscal-Harana, J., Alastruey, J., Khir, A.W., 2018. A study on the characteristics influencing the pressure at the root of a distributed one-dimensional model of arterial blood flow. Computing 45, 1.

Alexander, J., Sunagawa, K., Chang, N., Sagawa, K., 1987. Instantaneous pressure-volume relation of the ejecting canine left atrium. Circulation Research 61, 209–219.

Anrep, G., Pascual, W., Rössler, R., 1936. Respiratory variations of the heart rate-II—the central mechanism of the respiratory arrhythmia and the inter-relations between the central and the reflex mechanisms. Proceedings of the Royal Society of London. Series B-Biological Sciences 119, 218–230.

Aoki, M., Okamoto, Y., Musha, T., Harumi, K.I., 1987. Three-dimensional simulation of the ventricular depolarization and repolarization processes and body surface potentials: Nornal heart and bundle branch block. IEEE transactions on biomedical engineering , 454–462.

Artiles, A.D., Heldt, T., Young, L.R., 2016. Effects of artificial gravity on the cardiovascular system: Computational approach. Acta Astronautica 126, 395–410.

Azzayani, A., 2020. A numerical model of elasticity for cardiovascular system that includes 2/3d displacements and deformations. International Journal for Simulation and Multidisciplinary Design Optimization 11, 20.

Balakrishnan, M., Chakravarthy, S., Guhathakurta, S., 2014. A simple 2d whole heart model for simulating electrocardiograms, in: Computing in Cardiology 2014, IEEE. pp. 517–520.

Batzel, J.J., Goswami, N., Lackner, H.K., Roessler, A., Bachar, M., Kappel, F., Hinghofer-Szalkay, H., 2009. Patterns of cardiovascular control during repeated tests of orthostatic loading. Cardiovascular Engineering 9, 134.

Batzel, J.J., Kappel, F., Schneditz, D., Tran, H.T., 2007. Cardiovascular and respiratory systems: modeling, analysis, and control. volume 34. SIAM.

Bauer, F., Jones, M., Shiota, T., Firstenberg, M.S., Qin, J.X., Tsujino, H., Kim, Y.J., Sitges, M., Cardon, L.A., Zetts, A.D., et al., 2002. Left ventricular outflow tract mean systolic acceleration as a surrogate for the slope of the left ventricular end-systolic pressure-volume relationship. Journal of the American College of Cardiology 40, 1320–1327.

Ben-Tal, A., Shamailov, S., Paton, J., 2012. Evaluating the physiological significance of respiratory sinus arrhythmia: looking beyond ventilation–perfusion efficiency. The Journal of physiology 590, 1989–2008.

Ben-Tal, A., Shamailov, S.S., Paton, J.F., 2014. Central regulation of heart rate and the appearance of respiratory sinus arrhythmia: New insights from mathematical modeling. Mathematical biosciences 255, 71–82.

Bozkurt, S., 2019. Mathematical modeling of cardiac function to evaluate clinical cases in adults and children. PloS one 14, e0224663.

Calderon, P.G.B., Habib, M., Kappel, F., Aurelio, A., 2017. Control aspects of the human cardiovascular-respiratory system under a nonconstant workload. Mathematical biosciences 289, 142–152.

Dernellis, J.M., Stefanadis, C.I., Zacharoulis, A.A., Toutouzas, P.K., 1998. Left atrial mechanical adaptation to long-standing hemodynamic loads based on pressure–volume relations. American Journal of Cardiology 81, 1138–1143.

DiVincenti Jr, L., Westcott, R., Lee, C., et al., 2014. Sheep (ovis aries) as a model for cardiovascular surgery and management before, during, and after cardiopulmonary bypass. Journal of the American Association for Laboratory Animal Science 53, 439–448.

Elstad, M., 2012. Respiratory variations in pulmonary and systemic blood flow in healthy humans. Acta Physiologica 205, 341–348.

Elstad, M., O'Callaghan, E.L., Smith, A.J., Ben-Tal, A., Ramchandra, R., 2018. Cardiorespiratory interactions in humans and animals: rhythms for life. American Journal of Physiology-Heart and Circulatory Physiology 315, H6–H17.

Elstad, M., Toska, K., Chon, K.H., Raeder, E.A., Cohen, R.J., 2001. Respiratory sinus arrhythmia: opposite effects on systolic and mean arterial pressure in supine humans. The Journal of physiology 536, 251–259.

Ferguson, J.J., Miller, M.J., Aroesty, J.M., Sahagian, P., Grossman, W., McKay, R.G., 1989. Assessment of right atrial pressure-volume relations in patients with and without an atrial septal defect. Journal of the American College of Cardiology 13, 630–636.

Fink, M., Batzel, J.J., Kappel, F., 2004. An optimal control approach to modeling the cardiovascular-respiratory system: An application to orthostatic stress. Cardiovascular Engineering: An International Journal 4, 27–38.

Formaggia, L., Quarteroni, A., Veneziani, A., 2010. Cardiovascular Mathematics: Modeling and simulation of the circulatory system. volume 1. Springer Science & Business Media.

Fox, J.G., 2015. Laboratory animal medicine. Elsevier.

Freudenberg, J., Schiemann, T., Tiede, U., Höhne, K.H., 2000. Simulation of cardiac excitation patterns in a three-dimensional anatomical heart atlas. Computers in biology and medicine 30, 191–205.

Funck-Brentano, C., Jaillon, P., 1993. Rate-corrected QT interval: techniques and limitations. The American journal of Cardiology 72, B17–B22.

Gelman, S., 2008. Venous function and central venous pressure a physiologic story. Anesthesiology: The Journal of the American Society of Anesthesiologists 108, 735–748.

Genain, M.A., Morlet, A., Herrtage, M., Muresian, H., Anselme, F., Latremouille, C., Laborde, F., Behr, L., Borenstein, N., 2018. Comparative anatomy and angiography of the cardiac coronary venous system in four species: human, ovine, porcine, and canine. Journal of Veterinary Cardiology 20, 33–44.

Grodins, F.S., 1959. Integrative cardiovascular physiology: a mathematical synthesis of cardiac and blood vessel hemodynamics. The Quarterly Review of Biology 34, 93–116.

Guyton, A.C., Coleman, T.G., Granger, H.J., 1972. Circulation: overall regulation. Annual review of physiology 34, 13–44.

Ha, R., Qian, J., Wang, D., Zwischenberger, J.B., Bidhani, A., Clark, J., 2004. A closed-loop model of the ovine cardiovascular system, in: Engineering in Medicine and Biology Society, 2004. IEMBS'04. 26th Annual International Conference of the IEEE, IEEE. pp. 3781–3784.

Hall, J.E., 2015. Guyton and Hall textbook of medical physiology e-Book. Elsevier Health Sciences.

Hann, C.E., Chase, J.G., Shaw, G.M., 2005. Efficient implementation of non-linear valve law and ventricular interaction dynamics in the minimal cardiac model. Computer methods and programs in biomedicine 80, 65–74.

Hayano, J., Yasuma, F., Okada, A., Mukai, S., Fujinami, T., 1996. Respiratory sinus arrhythmia: a phenomenon improving pulmonary gas exchange and circulatory efficiency. Circulation 94, 842–847.

Heldt, T., 2004. Computational models of cardiovascular response to orthostatic stress. Ph.D. thesis. Massachusetts Institute of Technology.

Heldt, T., Shim, E.B., Kamm, R.D., Mark, R.G., 2002. Computational modeling of cardiovascular response to orthostatic stress. Journal of applied physiology 92, 1239–1254.

van Heusden, K., Gisolf, J., Stok, W.J., Dijkstra, S., Karemaker, J.M., 2006. Mathematical modeling of gravitational effects on the circulation: importance of the time course of venous pooling and blood volume changes in the lungs. American Journal of Physiology-Heart and Circulatory Physiology 291, H2152–H2165.

Jung, E., Lee, W., 2006. Lumped parameter models of cardiovascular circulation in normal and arrhythmia cases. Journal of the Korean Mathematical Society 43, 885–897.

Kappel, F., Peer, R.O., 1993. A mathematical model for fundamental regulation processes in the cardiovascular system. Journal of mathematical biology 31, 611–631.

Karaaslan, F., Denizhan, Y., Kayserilioglu, A., Gulcur, H.O., 2005. Long-term mathematical model involving renal sympathetic nerve activity, arterial pressure, and sodium excretion. Annals of biomedical engineering 33, 1607–1630.

Katz, A.M., Konstam, M.A., 2012. Heart failure: pathophysiology, molecular biology, and clinical management. Lippincott Williams & Wilkins.

Kossaify, A., Nasr, M., 2019. Diastolic dysfunction and the new recommendations for echocardiographic assessment of left ventricular diastolic function: Summary of guidelines and novelties in diagnosis and grading. Journal of Diagnostic Medical Sonography 35, 317–325.

Kotani, K., Struzik, Z.R., Takamasu, K., Stanley, H.E., Yamamoto, Y., 2005. Model for complex heart rate dynamics in health and diseases. Physical Review E 72, 041904.

Kumada, M., Azuma, T., Matsuda, K., 1967. The cardiac output-heart rate relationship under different conditions. The Japanese journal of physiology 17, 538–555.

Lau, V., Sagawa, K., Suga, H., 1979. Instantaneous pressure-volume relationship of right atrium during isovolumic contraction in canine heart. American Journal of Physiology-Heart and Circulatory Physiology 236, H672–H679.

Lim, E., Chan, G.S., Dokos, S., Ng, S.C., Latif, L.A., Vandenberghe, S., Karunanithi, M., Lovell, N.H., 2013. A cardiovascular mathematical model of graded head-up tilt. PloS one 8, e77357.

Litwin, S.E., Grossman, W., 1993. Diastolic dysfunction as a cause of heart failure. Journal of the American College of Cardiology 22, A49–A55.

Luo, C., Ramachandran, D., Ware, D.L., Ma, T.S., Clark, J.W., 2011. Modeling left ventricular diastolic dysfunction: classification and key indicators. Theoretical Biology and Medical Modelling 8, 1–46.

Maeder, M.T., Kaye, D.M., 2009. Heart failure with normal left ventricular ejection fraction. Journal of the American College of Cardiology 53, 905–918.

Malatos, S., Raptis, A., Xenos, M., 2016. Advances in low-dimensional mathematical modeling of the human cardiovascular system. J Hypertens Manag 2, 1–10.

Marquis, A.D., Arnold, A., Dean-Bernhoft, C., Carlson, B.E., Olufsen, M.S., 2018. Practical identifiability and uncertainty quantification of a pulsatile cardiovascular model. Mathematical biosciences 304, 9–24.

Maughan, W.L., Sunagawa, K., Burkhoff, D., Graves Jr, W.L., Hunter, W.C., Sagawa, K., 1985. Effect of heart rate on the canine end-systolic pressure-volume relationship. Circulation 72, 654–659.

Melchior, F., Srinivasan, R.S., Thullier, P.H., Clere, J.M., 1994. Simulation of cardiovascular response to lower body negative pressure from 0 to -40 mmhg. Journal of Applied Physiology 77, 630–640.

Mohammed, F.H., Shafei, E.M., El-Garhy, A.M., El-Dosoky, M.A., 2018. Modeling of the effect of dilated cardiomyopathy on the behavior of the heart, in: 2018 9th Cairo International Biomedical Engineering Conference (CIBEC), IEEE. pp. 17–20.

Mozaffarian, D., Benjamin, E.J., Go, A.S., Arnett, D.K., Blaha, M.J., Cushman, M., De Ferranti, S., Després, J.P., Fullerton, H.J., Howard, V.J., et al., 2015. Heart disease and stroke statistics - 2015 update: A report from the american heart association. circulation 131, e29 – e322.

Naeije, R., Badagliacca, R., 2017. The overloaded right heart and ventricular interdependence. Cardiovascular research 113, 1474–1485.

Nguyen, L.D., Leger, C., 2002. Four-dimensional reconstruction of the left ventricle using a fast rotating classical phased array scan head: preliminary results. Journal of the American Society of Echocardiography 15, 593–600.

O'Callaghan, E.L., Lataro, R.M., Roloff, E.L., Chauhan, A.S., Salgado, H.C., Duncan, E., Nogaret, A., Paton, J.F., 2020. Enhancing respiratory sinus arrhythmia increases cardiac output in rats with left ventricular dysfunction. The Journal of physiology 598, 455–471.

Olansen, J.B., Clark, J., Khoury, D., Ghorbel, F., Bidani, A., 2000. A closed-loop model of the canine cardiovascular system that includes ventricular interaction. Computers and biomedical research 33, 260–295.

Olufsen, M., Tran, H., Ottesen, J., 2004. Modeling cerebral blood flow control during posture change from sitting to standing. Cardiovascular engineering: an international journal 4, 47–58.

Olufsen, M.S., Ottesen, J.T., Tran, H.T., Ellwein, L.M., Lipsitz, L.A., Novak, V., 2005. Blood pressure and blood flow variation during postural change from sitting to standing: model development and validation. Journal of Applied Physiology 99, 1523–1537.

Pagel, P.S., Kehl, F., Gare, M., Hettrick, D.A., Kersten, J.R., Warltier, D.C., 2003. Mechanical function of the left atrium new insights based on analysis of pressure–volume relations and doppler echocardiography. Anesthesiology: The Journal of the American Society of Anesthesiologists 98, 975–994.

Paton, J.F., Nalivaiko, E., Boscan, P., Pickering, A.E., 2006. Reflexly evoked coactivation of cardiac vagal and sympathetic motor outflows: observations and functional implications. Clinical and experimental pharmacology and physiology 33, 1245–1250.

Pilla, J.J., Blom, A.S., Brockman, D.J., Ferrari, V.A., Yuan, Q., Acker, M.A., 2003. Passive ventricular constraint to improve left ventricular function and mechanics in an ovine model of heart failure secondary to acute myocardial infarction. The Journal of thoracic and cardiovascular surgery 126, 1467–1475.

Pironet, A., Dauby, P.C., Paeme, S., Kosta, S., Chase, J.G., Desaive, T., 2013. Simulation of left atrial function using a multi-scale model of the cardiovascular system. PloS one 8, e65146.

Qian, J., Clark, J., Lu, K., Ghorbel, F., Zwischenberger, J., Bidani, A., 2002. A closed-loop model of the ovine cardiovascular system, in: Engineering in Medicine and Biology, 2002. 24th Annual Conference and the Annual Fall Meeting of the Biomedical Engineering Society EMBS/BMES Conference, 2002. Proceedings of the Second Joint, IEEE. pp. 1585–1586.

Ratcliffe, M.B., Wallace, A.W., Salahieh, A., Hong, J., Ruch, S., Hall, T.S., 2000. Ventricular volume, chamber stiffness, and function after anteroapical aneurysm application in the sheep. The Journal of thoracic and cardiovascular surgery 119, 115–124.

Rodriguez, D.A.A., Durand, E., De Rochefort, L., Boudjemline, Y., Mousseaux, E., 2015. Simultaneous pressure–volume measurements using optical sensors and MRI for left ventricle function assessment during animal experiment. Medical Engineering and Physics 37, 100–108.

Saltelli, A., Aleksankina, K., Becker, W., Fennell, P., Ferretti, F., Holst, N., Li, S., Wu, Q., 2019. Why so many published sensitivity analyses are false: A systematic review of sensitivity analysis practices. Environmental Modelling & Software 114, 29–39.

Santamore, W.P., Burkhoff, D., 1991. Hemodynamic consequences of ventricular interaction as assessed by model analysis. American Journal of Physiology-Heart and Circulatory Physiology 260, H146–H157.

Segers, P., Steendijk, P., Stergiopulos, N., Westerhof, N., 2001. Predicting systolic and diastolic aortic blood pressure and stroke volume in the intact sheep. Journal of Biomechanics 34, 41–50.

Senzaki, H., Chen, C.H., Kass, D.A., 1996. Single-beat estimation of end-systolic pressure-volume relation in humans: a new method with the potential for noninvasive application. Circulation 94, 2497–2506.

Shi, Y., Lawford, P., Hose, R., 2011. Review of zero-d and 1-d models of blood flow in the cardiovascular system. Biomedical engineering online 10, 33.

Smith, B.W., Chase, J.G., Nokes, R.I., Shaw, G.M., Wake, G., 2004. Minimal haemodynamic system model including ventricular interaction and valve dynamics. Medical engineering & physics 26, 131–139.

Taha, B.H., Simon, P., Dempsey, J., Skatrud, J., Iber, C., 1995. Respiratory sinus arrhythmia in humans: an obligatory role for vagal feedback from the lungs. Journal of Applied Physiology 78, 638–645.

Tan, C.O., Taylor, J.A., 2010. Does respiratory sinus arrhythmia serve a buffering role for diastolic pressure fluctuations? American Journal of Physiology-Heart and Circulatory Physiology 298, H1492–H1498.

Taylor, J.A., Eckberg, D.L., 1996. Fundamental relations between short-term RR interval and arterial pressure oscillations in humans. Circulation 93, 1527–1532.

Timischl, S., 1998. A global model of the cardiovascular and respiratory system. Karl-Franzens-Universität Graz, Austria .

Toska, K., Eriksen, M., 1993. Respiration-synchronous fluctuations in stroke volume, heart rate and arterial pressure in humans. The Journal of Physiology 472, 501–512.

Trunk, P., Mocnik, J., Trobec, R., Gersak, B., 2007. 3d heart model for computer simulations in cardiac surgery. Computers in Biology and Medicine 37, 1398–1403.

Tsuruta, H., Sato, T., Shirataka, M., Ikeda, N., 1994. Mathematical model of cardiovascular mechanics for diagnostic analysis and treatment of heart failure: Part 1 model description and theoretical analysis. Medical & biological engineering & computing 32, 3–11.

Van de Vooren, H., Gademan, M.G., Swenne, C.A., TenVoorde, B.J., Schalij, M.J., Van der Wall, E.E., 2007. Baroreflex sensitivity, blood pressure buffering, and resonance: what are the links? Computer simulation of healthy subjects and heart failure patients. Journal of Applied Physiology 102, 1348–1356.

Vovkodav, O., Pasichnyk, R., 2014. The method of identification of a mathematical model for the cardiovascular system response dynamics to exercise stress. Journal of Applied Computer Science 22, 91–99.

Warriner, D.R., Brown, A.G., Varma, S., Sheridan, P.J., Lawford, P., Hose, D.R., Al-Mohammad, A., Shi, Y., 2014. Closing the loop: modelling of heart failure progression from health to end-stage using a meta-analysis of left ventricular pressure-volume loops. PLoS One 9, e114153.

Williams, N.D., Wind-Willassen, Ø., Wright, A.A., Program, R., Mehlsen, J., Ottesen, J.T., Olufsen, M.S., 2013. Patient-specific modelling of head-up tilt. Mathematical medicine and biology: a journal of the IMA 31, 365–392.

Wolfensohn, S., Lloyd, M., 2003. Conduct of minor procedures. Handbook of Laboratory Animal Management and Welfare, 3rd ed.; Wolfensohn, S., Lloyd, M., Eds , 150–181.

Yerebakan, C., Klopsch, C., Prietz, S., Boltze, J., Vollmar, B., Liebold, A., Steinhoff, G., Sandica, E., 2009. Pressure-volume loops: feasible for the evaluation of right ventricular function in an experimental model of acute pulmonary regurgitation? Interactive cardiovascular and thoracic surgery 9, 163–168.

Yin, M., Yazdani, A., Karniadakis, G.E., 2019. One-dimensional modeling of fractional flow reserve in coronary artery disease: Uncertainty quantification and bayesian optimization. Computer Methods in Applied Mechanics and Engineering 353, 66–85.

Zakeri, R., Moulay, G., Chai, Q., Ogut, O., Hussain, S., Takahama, H., Lu, T., Wang, X.L., Linke, W.A., Lee, H.C., et al., 2016. Left atrial remodeling and atrioventricular coupling in a canine model of early heart failure with preserved ejection fraction. Circulation: Heart Failure 9, e003238.

Zimik, S., Pandit, R., 2017. Reentry via high-frequency pacing in a mathematical model for human-ventricular cardiac tissue with a localized fibrotic region. Scientific reports 7, 1–14.

Appendix A

Matlab Programs

A.1 Matlab program for the detection of key intervals from ECG

```
data=readtable('Sheep 1.xlsx');
T=data.Time;
Ecg1=data.ECG;
Ecg = Ecg1./100;
id=0;
i=1;
R0=0.5;
R1=0.03;
j=1;
Finding R points
while i<length(Ecg)
while id==0i<length(Ecg)
if Ecg(i)<R0
i=i+1;
else
n1(j)=i;
id=1;
end
end
while id==1i<length(Ecg)
if Ecg(i+1)>Ecg(i)
```

```
i=i+1;
else
nR(j)=i;
id=2;
end
end
if i<length(Ecg)
R(j)=T(nR(j));
Rv(j)=Ecg(nR(j));
end
while id==2i<length(Ecg)
if Ecg(i+1)<Ecg(i)
i=i+1;
else
n2(j)=i;
id=3;
end
end
if i<length(Ecg)
R1(j)=T(n2(j));
R1v(j)=Ecg(n2(j));
end
while id==3i<length(Ecg)
if Ecg(i+1)>Ecg(i)
i=i+1;
else
n3(j)=i;
id=4;
end
end
if i<length(Ecg)
R2(j)=T(n3(j));
R2v(j)=Ecg(n3(j));
end
while id==4i<length(Ecg)
if Ecg(i+1)-Ecg(i)<0.15
```

```
i=i+1;
else
n4(j)=i;
id=5;
end
end
if i<length(Ecg)
R3(j)=T(n4(j));
R3v(j)=Ecg(n4(j));
end
id=0;
j=j+1;
end
Finding RR-intervals
for i=1:length(R3)-1
RRint(i)=R3(i+1)-R3(i);
end
RRint
for k=1:length(n4)
i=n4(k);
while id==0
if Ecg(i-1)>=Ecg(i)
i=i-1;
else
nQ(k)=i;
id=6;
end
end
TQ(k)=T(nQ(k));
Qv(k)=Ecg(nQ(k));
id=0;
k=k+1;
end
for k=1:length(n4)
i=n4(k);
while id==0
```

```
if Ecg(i+1)>Ecg(i)
i=i+1;
else
nS(k)=i;
id=7;
end
end
TS(k)=T(nS(k));
Sv(k)=Ecg(nS(k));
TQRS(k)=TS(k)-TQ(k);
id=0;
k=k+1;
end
TQRS
Finding QT-Interval
for k=2:length(nR)
i=nR(k);
while id==0
if Ecg(i+1)<Ecg(i)
i=i+1;
else
nt(k)=i;
id=8;
end
end
TT(k)=T(nt(k));
eTv(k)=Ecg(nt(k));
Tqt(k)=TT(k)-TQ(k-1);
id=0;
k=k+1;
end
Tqt
finding the RT-interval
for k=1:length(R3)
TRt(k)=TT(k+1)-R3(k);
end
```

```
TRt
finding the p-wave
for k=1:length(nQ)
i=nQ(k);
while id==0
if Ecg(i-1)<Ecg(i)
i=i-1;
else
np(k)=i;
id=9;
end
end
Tp1(k) = T(np(k));
Tp1v(k)=Ecg(np(k));
id = 0;
k=k+1;
end
for k=1:length(R3)-1
Tp(k)=Tp1(k)-R1(k);
end
Tp
for k=1:length(R3)-1
Td(k)=R3(k)-R1(k);
end
Td
plot(T,Ecg,'b', R,Rv,'*r', TS,Sv,'*g', TQ, Qv,'*k', TT, eTv, '*m' )
```

A.2 Matlab program of the full G model

Main full G model.m

global G_{maxRV} G_{maxLV} G_{maxRA} G_{maxLA} V_{una}V$_{unlv}$ V_{unrv} C_{SA} C_{SV} C_{PA} C_{PV} R_{SA} R_{SV} R_{PA} R_{PV} V_{unsa} V_{unsv} V_{unpa} V_{unpv} global HRf tstartB TL Vtotal LstrokeV RstrokeV LcardiacOutput RcardiacOutput blood flow

global T V_{LA} V_{LV} V_{SA} V_{SV}V$_{RA}$V$_{RV}$ V_{PA} V_{PV} $delG_{LA}$ $delG_{LV}$ $delG_{RA}$ $delG_{RV}$ P_{LA} P_{LV} P_{SA} P_{SV} P_{RA} P_{RV} P_{PA} P_{PV} global Rmv Rav Rtv Rpv delPmv delPav delPtv delPpv RRint FB meanLCOP

global filepath meanLcardOutp meanRcardOutp G_{LV} G_{RV}

global e_{LA} e_{LV} e_{Ra} e_{RV} R_{opmv} R_{opav} R_{optv} R_{oppv} buffer $G_{minLA}$$G_{minLV}$$G_{minRA}$ G_{minRV} f aC f aO Es a

f aC= 0;f aO =1; idT = readtable(strcat(filepath,'Plot Filesfor Plot.xlsx')); reads the specified excel file

id = 3; 1 = plot at initial point, 2+ plot from last point, 3 = plot from last point (t=0)

file param = char(idT.Values(2));

file IC = char(idT.Values(3));

read parameters file

paramT = readtable(file param);

RSA_{amp} = paramT.Values(1);

mHR = paramT.Values(2);

FB = paramT.Values(3);

len sim =100;

t_{inc} = paramT.Values(5);

E_{minLA} = paramT.Values(6);

E_{maxLA} = paramT.Values(7);

E_{minLV} = paramT.Values(8);

E_{maxLV} = paramT.Values(9);

E_{minRA} = paramT.Values(10);

E_{maxRA} = paramT.Values(11);

E_{minRV} = paramT.Values(12);

E_{maxRV} = paramT.Values(13);

V_{total} = paramT.Values(14);

V_{una} = paramT.Values(15);

V_{unlv} = paramT.Values(16);

V_{unrv} = paramT.Values(17);

V_{unpa} = paramT.Values(18);

V_{unpv} = paramT.Values(19);
V_{unsa} = paramT.Values(20);
V_{unsv} = paramT.Values(21);
C_{SA} = paramT.Values(22);
C_{SV} = paramT.Values(23);
C_{PA} = paramT.Values(24);
C_{PV} = paramT.Values(25);
R_{SA} = paramT.Values(26);
R_{SV} = paramT.Values(27);
R_{PA} = paramT.Values(28);
R_{PV} = paramT.Values(29);
R_{opmv} = paramT.Values(30);
R_{opav} = paramT.Values(31);
R_{optv} = paramT.Values(32);
R_{oppv} = paramT.Values(33);
buffer = paramT.Values(34);
e_{LA} = paramT.Values(35);
e_{LV} = paramT.Values(36);
e_{RA} = paramT.Values(37);
e_{RV} = paramT.Values(38);
E_{minLAG} = paramT.Values(39);
E_{minLVG} = paramT.Values(40);
E_{minRAG} = paramT.Values(41);
E_{minRVG} = paramT.Values(42);
E_{maxLAG} = paramT.Values(43);
E_{maxLVG} = paramT.Values(44);
E_{maxRAG} = paramT.Values(45);
E_{maxRVG} = paramT.Values(46);

w = (2*pi/60)*FB; breathing frequency in radians/sec
HRf = @(x) 60./(mnHR -(RSA_{amp}/2)*cos(w*x)); heart rate function
IC withdelp nonlinear,tstartB
=readFromFile withdelp nonlinear(id,file IC);
initialises initial conditions and time to start beat
tstartB init = tstartB;
tend = tstartB + len sim;
TL = HRf(tstartB);

options = odeset('AbsTol', 1e-8, 'RelTol', 1e-8);
LCO=[]; RCO=[]; EDV =[]; ESV=[]; SVL = []; SVR = []; EF = []; TL1 = []; LCO2=[];
RCO2=[]; mCOPr=[]; Q1=[]; QL = []; Q1R=[]; Qr = []; AP = []; minPSa = []; maxPSa = [];
tinc 1 = round(TL/t inc);
while 1
tend s = tstartB + TL;
TT = [TT;tend s];
tvec = (tstartB: (TL/tinc 1): tend s);
if tstartB == tstartB init
$[T,Y]$ = ode45(equations, tvec, IC, options);
else
$[T,Y]$ = ode45(@equations, tvec, Ylast, options);
end
Ylast = Y(length(Y),:);
V_{LA} = Y(:,1);
P_{LA} = Y(:,2);
P_{LV} = Y(:,3);
V_{SA} = Y(:,4);
V_{RA} = Y(:,5);
P_{RA} = Y(:,6);
P_{RV} = Y(:,7);
V_{PA} = Y(:,8);
V_{PV} = Y(:,9);
$g = 4/a * (1 + e^{-a*(PLv-PRv))} - (2/a)$;
G_{LV} = Gv(tvec,EminLvG,EmaxLvG);
G_{RV} = GvR(tvec,EminRvG,EmaxRvG);
$delG_{LA}$ = delGa(tvec,EminLaG,EmaxLaG);
$delG_{LV}$ = delGv(tvec,EminLvG,EmaxLvG);
$delG_{RA}$ = delGa(tvec,EminRaG,EmaxRaG);
$delG_{RV}$ = delGv(tvec,EminRvG,EmaxRvG);
$V_{LV} = ((PLv - G_{LV})/e_{LV}) + V_{unlv}$+(1/Es)*g ;
$V_{RV} = ((P_{RV} - G_{RV})/e_{RV}) + V_{unrv}$-(1/Es)*g;
V_{SV} = Vtotal - $(V_{LA} + V_{LV} + V_{RA} + V_{RV} + V_{SA} + V_{PA} + V_{PV})$;
$P_{SA} = (V_{SA} - V_{unsa})/C_{SA}$;
$P_{SV} = (V_{SV} - V_{unsv})/C_{SV}$;
$P_{PA} = (V_{PA} - V_{unpa})/C_{PA}$;

$P_{PV} = (V_{PV} - V_{unpv})/C_{PV}$;
Resistances of the valves
for i=1:length(tvec)
Rmv(i,1) = res valve A($P_{LA}(i), P_{LV}(i)$,R_{opmv}); mitral valve
Rav(i,1) = res valve V($P_{LV}(i), P_{SA}(i)$,R_{opav}); aortic valve
Rtv(i,1) = res valve V($P_{RA}(i), P_{RV}(i)$,R_{optv}); tricuspid valve
Rpv(i,1) = res valve V($P_{RV}(i), P_{PA}(i)$,R_{oppv}); pulmonary valve
end change in pressure of the valves
delPmv = delP(P_{LA}, P_{LV}); delPav = delP(P_{LV}, P_{SA}); delPtv = delP(P_{RA}, P_{RV}); delPpv = delP(P_{RV}, P_{PA});
RRint=HRf(T); RR interval
HR=60./RRint; Heart rate
mAP = (1/3)*(2*min(PSa)+max(PSa));
AP = [AP;mAP];
minPSa =[minPSa;min(PSa)];
maxPSa = [maxPSa;max(PSa)];
blood flows
LstrokeV=(max(V_{LV})-min(V_{LV}));
RstrokeV=(max(V_{RV})-min(V_{RV}));
SVL = [SVL;LstrokeV];
SVR = [SVR;RstrokeV];
EDV = [EDV;max(V_{LV})];
ESV = [ESV;min(V_{LV})];
EF = (LstrokeV/max(V_{LV}))*100;
LcardiacOutput=(60/1000)*LstrokeV/TL;
RcardiacOutput=(60/1000)*RstrokeV/TL;
LCO=[LCO;LcardiacOutput];
RCO=[RCO;RcardiacOutput];
meanLcardOutp=(60/1000)*sum(LCO2)/sum(TL1);
meanRcardOutp=(60/1000)*sum(RCO2)/sum(TL1);
$\text{blood}_f low = ((PLv - PSa)./Rav)$;
$trp = 0$;
$fork = 2 : (length(bloodflow) - 1)$
$trp = trp + bloodflow(k)$;
end
$Q = ((TL/tinc1)/2) * (bloodflow(1) + bloodflow(length(bloodflow)) + 2 * trp)$;
$Q1 = [Q1; Q]$;

$QL = [QL; (Q/TL) * (60/1000)];$
$mnCOP = (60/1000) * sum(Q1)/sum(TL1);$
$bloodflowR = ((\mathrm{P}_{RV} - P_{PA})./\mathrm{Rpv});$
trp1 = 0;
for k=2:(length(blood flow R)-1)
trp1 = trp1+blood flow R(k);
end
QR = ((TL/tinc 1)/2)*(blood$_f lowR(1) + bloodflowR(length(bloodflowR)) + 2 * trp1);$
$Q1R = [Q1R; QR];$
$Qr = [Qr; (QR/TL) * (60/1000)];$
$mnCOPR = (60/1000) * sum(Q1R)/sum(TL1);$
$subplot(2,1,1)$
$plot(T,\mathrm{V}_{SA},$'–b');drawnow limitrate;hold on; grid on
subplot(2,1,2)
plot(T,V_{SV},'–b');drawnow limitrate;hold on; grid on
tstartB = tend$_s$;
$TL = HRf(tstartB);$
$iftends >= tend$
$break$
end
end
$writeToFile(Ylast, tends);$
equations.m
$functiondy = equations(t, y)$
$dy = zeros(9,1);$
global$_{LA}$ e_{LV} Es TL e_{RA} e_{RV} G_{minLA} G_{minLV} G_{minRA} G_{minRV} C_{SA} C_{SV} C_{PA} C_{PV} Vtotal R_{SA} Rmv Rav V_{unlv} V_{unrv}
global V_{unsa} V_{unsv} V_{unpa} V_{unpv} R_{opmv} R_{opav} R_{optv} R_{oppv} Rtv Rpv G_{maxLA} G_{maxLV} G_{maxRA} G_{maxRV} G_{LV} G_{RV}
Es = 1; a = 0.4;
V_{LA} = y(1); Left Atrium volume
P_{LA} = y(2); Left Atrium pressure
P_{LV} = y(3); Left Ventricle volume
V_{SA} = y(4); Systemic arteries volume
V_{RA} = y(5); Right Atrium volume
P_{RA} = y(6); Right Atrium pressure

P_{RV} = y(7); Right Ventricle volume
V_{PA} = y(8); Pulmonary arteries volume
V_{PV} = y(9); Pulmonary veins volume
G_{LV} = Gv(t,G_{minLV},G_{maxLV});
G_{RV} = Gv(t,G_{minRV},G_{maxRV});
$delG_{LA}$ = delGa(t,G_{minLA},G_{maxLA});
$delG_{LV}$ = delGv(t,G_{minLV},G_{maxLV});
$delG_{RA}$ = delGa(t,G_{minRA},G_{maxRA});
$delG_{RV}$ = delGv(t,G_{minRV},G_{maxRV});
pressuers (note that these are also defined in main.m)
g = 4/a*(1+exp(-a*($P_{LV} - P_{RV}$)))-(2/a);
g1 = exp(-a*($P_{LV} - P_{RV}$));
S = (1/Es)*(4*g1)/((1+g1)^2);
$B = (1/S) * (S + (1/e_{RV}))$*(S+(1/$e_{LV}$))-S;
$V_{LV} = ((P_{LV} - G_{LV})/e_{LV)+V_{unlv}}$+(1/Es)*g;
$V_{RV} = ((P_{RV} - G_{RV})/e_{RV}) + V_{unrv}$-(1/Es)*g;
V_{SV} = Vtotal - ($V_{LA} + V_{LV} + V_{RA} + V_{RV} + V_{SA} + V_{PA} + V_{PV}$);
$P_{SA} = (V_{SA} - V_{unsa})/C_{SA}$;
$P_{SV} = (V_{SV} - V_{unsv})/C_{SV}$;
$P_{PA} = (V_{PA} - V_{unpa})/C_{PA}$;
$P_{PV} = (V_{PV} - V_{unpv})/C_{PV}$;
resistances (note that these are also defined in main.m)
Rmv = res valve A(P_{LA},P_{LV},R_{opmv}); mitral valve
Rav = res valve V(P_{LV},P_{SA},R_{opav}); aortic valve
Rtv = res valve At(P_{RA},P_{RV},R_{optv}); tricuspid valve
Rpv = res valve Vp(P_{RV},P_{PA},R_{oppv}); pulmonary valve
Differential equations
$dy(1) = (\mathrm{P}_{PV} - P_{LA})./R_{PV} - (P_{LA} - P_{LV})./Rmv$;
if $((P_{PV} - P_{LA})/R_{PV} - (P_{LA} - P_{LV})/Rmv)$<0
$dy(2) = 1 * e_{LA} * dy(1) + 1 * delG_{LA} + 0.5 * (V_{LA} - V_{una})$;
else
$dy(2) = 0.1 * e_{LA} * dy(1) + 0.1 * delG_{LA} + 0.2 * (V_{LA} - V_{una})$;
end
$dy(3) = (1/B) * (((P_{RA} - P_{RV})/Rtv$ - $(P_{RV} - P_{PA})/Rpv) + (1/S) * (S + (1/e_{RV})) * ((1/e_{LV}) *$
$delG_{LV} + (P_{LA} - P_{LV})/Rmv - (P_{LV} - P_{SA})/Rav) + (1/e_{RV}) * delG_{RV})$;
$dy(4) = (P_{LV} - P_{SA})./Rav - (P_{SA} - P_{SV})./R_{SA}$;

$dy(5) = (P_{SV} - P_{RA})./R_{SV1}(t) - (P_{RA} - P_{RV})./Rtv;$
if $((P_{SV} - P_{RA})/R_{SV1}(t) - (P_{RA} - P_{RV})/Rtv) < 0$
$dy(6) = 1 * e_{RA} * dy(5) + 1 * delG_{RA} + 0.6 * (V_{RA} - V_{una});$
else
$dy(6) = 0.1 * e_{RA} * dy(5) + 0.92 * delG_{RA} + 0.18 * (V_{RA} - V_{una});$
end
dy(7)= (1/B)*(((P$_{LA} - P_{LV})/Rmv - (P_{LV} - P_{SA})/Rav) + (1/S) * (S + (1/e_{LV})) * ((1/e_{RV}) *$
$delG_{RV} + (P_{RA} - P_{RV})/Rtv - (P_{RV} - P_{PA})/Rpv) + (1/e_{LV}) * delG_{LV});$
$dy(8) = (P_{RV} - P_{PA})./Rpv - (P_{PA} - P_{PV})./R_{PA};$
$dy(9) = (P_{PA} - P_{PV})./R_{PA} - (P_{Pv} - P_{LA})./R_{PV};$
end

Gv.m

```
function y = Gv(t,Emin,Emax)
global tstartB TL
y = zeros(size(t));
TM =TMv(TL); TR =1*TRv(TL); d = delay(TL);
for k=1:length(t)
tdiff = t(k) - tstartB;
if (tdiff <= d)
y(k) = Emin;
elseif (tdiff >= d)  (tdiff <= (TM+d))
y(k) = Emin + (Emax - Emin)/2*( 1 - cos((pi)*(tdiff-d)/TM) );
elseif (tdiff >= (d+TM))  (tdiff <= (d+TM+TR))
y(k) = Emin + (Emax- Emin)/2*( 1 + cos(pi*(tdiff-(d+TM))/TR) );
else
y(k) = Emin;
end
end
y = y(:);
end
```

Ga.m

```
function y = Ga(t,Emin,Emax)
global tstartB TL
y = zeros(size(t));
TM,TR=atrium contraction timing(TL);
for k=1:length(t)
```

```
tdiff = t(k) - tstartB;
if tdiff <= TM
y(k) = Emin + (Emax - Emin)/2*( 1 - cos(pi*tdiff/TM) );
elseif (tdiff >= TM)  (tdiff <= (TM + TR) )
y(k) = Emin+ (Emax - Emin)/2*( 1 + cos(pi*(tdiff-TM)/TR) );
else
y(k) = Emin;
end
end
y = y(:);
end
res valve V.m
function y = res valve V(Pin,Pout,Rop)
global f aC f aO
Rcl =100;
V1=7;V2=-30;
if (f aC==1) (f aO==0)
This is the function for opening the valve
beta =4;
hys=0;
y = Rcl - (Rcl-Rop)./(1+exp(-beta*((Pin-Pout)-hys)));
if (Pin-Pout)>V1
f aC=0;
f aO=1;
end
end
if (f aC==0) (f aO==1)
This is the function for closing the valve
beta =4;
hys=-4.5;
y = Rcl - (Rcl-Rop)./(1+exp(-beta*((Pin-Pout)-hys)));
if (Pin-Pout)<V2
f aC=1;
f aO=0;
end
end
```

```
end
res valve A.m
function y = res valve A(Pin,Pout,Rop)
Rcl =100;
beta =4;
y = Rcl - (Rcl-Rop)./(1+exp(-beta*(Pin-Pout)));
end
```